INTEGRATED STUDY ON NUMERICAL MODELING OF COOLING RATE IN A LABORATORY SCALE RUN OUT TABLE BASED ON EXPERIMENTAL DATA

Thesis submitted by

PRABIR BISWAS

Doctor of Philosophy (Engineering)

DEPARTMENT OF MECHANICAL ENGINEERING
FACULTY COUNCIL OF ENGINEERING & TECHNOLOGY
JADAVPUR UNIVERSITY
KOLKATA-700032, INDIA

2026

JADAVPUR UNIVERSITY
FACULTY OF ENGINEERING AND TECHNOLOGY

1. **Title of the Thesis:** **Integrated Study on Numerical Modeling of Cooling Rate in a Laboratory Scale Run Out Table Based on Experimental Data**

2. **Name, Designation & Institution of the Supervisor:**
   Dr. Pranibesh Mandal
   Assistant Professor
   Mechanical Engineering Department
   Jadavpur University, Kolkata

3. **Publications from International Conference:**
   1. Biswas, P., Mondal, S., Mookherjee, S., & Mandal, P. (2020). Modelling of Artificial Neural Network to control the cooling rate of a Laboratory Scale Run-Out Table. MATEC Web of Conferences, 306, 03004. https://doi.org/10.1051/matecconf/202030603004.
   2. Biswas, P., Chakraborty, K., Raha, P. K., & Mandal, P. (2023). Modelling of artificial neural network to validate the experimental data of a laboratory scale ROT. Journal of Graphic Era University. https://doi.org/10.13052/jgeu0975-1416.1126.

4. **List of Publications in Journal**
   1. Biswas, P., & Mandal, P. (2023). An optimization study of cooling rate of a laboratory scale ROT based on experimental results. Journal of the Institution of Engineers (India): Series D. https://doi.org/10.1007/s40033-023-00575-7.

5. **List of Patent:** NIL

JADAVPUR UNIVERSITY
FACULTY OF ENGINEERING AND TECHNOLOGY

List of Presentations in National/International/Conferences/Workshops:

i. The 6th International Conference on Mechatronics and Mechanical Engineering (ICMME 2019) , Osaka, Japan on November 27-30, 2019

ii. 3rd International Conference on Emerging Developments in Engineering & Technology (ICEDET-2022), 22nd-23rd April, 2022, Department of Mechanical and Computer Science Engineering, Shivalik College of Engineering, Dehradun.

JADAVPUR UNIVERSITY
FACULTY OF ENGINEERING AND TECHNOLOGY

PROFORMA-I

STATEMENT OF ORIGINALITY

I, Prabir Biswas, registered on 14th May 2018, do hereby declare that this thesis entitled **"Integrated Study on Numerical Modeling of Cooling Rate in a Laboratory Scale Run Out Table Based on Experimental Data"** contains literature survey and original research work done by the undersigned candidate as part of the Doctoral studies.

All information in this thesis has been obtained and presented in accordance with existing academic rules and ethical conduct. As required by these rules and conduct, I declare that I have fully cited and referred all materials and results that are not original to this work.

I also declare that I have checked this thesis as per the Policy of Anti-Plagiarism, Jadavpur University, 2019, and the level of similarity as checked by iThenticate software is 4%.

Signature of the candidate: Prabir Biswas

Date: 01.07.26

Certified by Supervisor:
(Signature with Date, Seal)

1. Prasanta Mandal 01.07.25

Assistant Professor
Dept. of Mechanical Engineering
Jadavpur University, Kolkata-32

JADAVPUR UNIVERSITY
FACULTY OF ENGINEERING AND TECHNOLOGY

PROFORMA-II

CERTIFICATE FROM THE SUPERVISOR

This is to certify that the thesis entitled **"Integrated Study on Numerical Modeling of Cooling Rate in a Laboratory Scale Run Out Table Based on Experimental Data"** submitted by Sri Prabir Biswas who got his name registered on 14.05.2018 for the award of Ph.D. (Engineering) degree of Jadavpur University, is absolutely based upon his own work under the supervision of Dr. PRANIBESH MANDAL and that neither his thesis nor any part of the thesis has been submitted for any degree/diploma or any other academic award anywhere before.

Pranibesh Mandal 01.07.18

(Dr. Pranibesh Mandal)
Signature of the Supervisor
and date with Official Seal

Assistant Professor
Dept. of Mechanical Engineering
Jadavpur University, Kolkata-32

ACKNOWLEDGMENT

Jadavpur University has given me an incredible education over the last few years. It has stretched me academically and personally. To complete this task of writing this thesis was never easy for me and it would have not been completed without the noble contribution of the people around me. The long association with the people in the Mechanical Engineering Department and Hydraulic Laboratory was the most quality time of my academic life and I have got enough inspiration for breathing in the future. The dedication, sincerity, and caring I found in all the teachers for the scholars, I will probably never find elsewhere. I am very grateful to the people who have been with me to share this whole experience.

I cannot start without acknowledging Dr. Pranibesh Mandal. I want to thank my supervisor for his advice, guidance, help, time, and enthusiasm. There cannot be any match to describe the role he played in completing this thesis. I am inspired by his dedication during the moments I have spent with him. He had spared his precious time on my every need during the whole work of my thesis. His simplified method of describing problems and presenting them easily and nicely will always be my pathfinder during my academic career.

I am also very thankful to Professor Saikat Mookherjee for his valuable guidance and all professors, staff of the Department of Mechanical Engineering, Jadavpur University for extending all facilities to carry out the present research.

I am deeply thankful to my colleagues, Prahar Sarkar and Abhyuday Aditya for their steady support in conducting the experiments and helping me gather the necessary data. I sincerely thank my friends and batchmates at Jadavpur University for their constant support throughout my research journey.

Finally, I would like to express my gratitude to my parents and wife for their unconditional support, love, and affection. Their encouragement and never-ending kindness made everything easier to achieve.

Dept. of Mechanical Engineering
Jadavpur University, Kolkata, India

[PRABIR BISWAS]

Dedicated to

My Parents & My Beloved Wife

CONTENTS

ABSTRACT

Run-out Tables, or ROTs, have been used by several sectors for an extended period to achieve diverse microstructures of steel. One of the key factors affecting the final microstructure is the cooling rate, which is controlled by several parameters associated with the Run-out Tables. However, a significant portion of previous studies has focused on various aspects, such as the metallurgical behavior, stress development within the strip, and temperature distribution during the cooling process on the Run-out Table. The aim of this research is to establish a concrete connection between the cooling rate of the hot strip and other independent experimental variables that can be adjusted. This understanding will facilitate the regulation and enhancement of the cooling rate on the Run-out Table.

Experiments were carried out on the Laboratory Scale Run Out table as part of the first phase of this research project. The aim of these experiments was to investigate the nature of the interrelationships among the various experimental parameters. In the second part of this dissertation, two distinct datasets have been selected from the observed data. Each of these datasets has a different combination of factors not seen in the other datasets. In order to checking the consistency of the experimental data, an Artificial Neural Network (ANN) was used before proceeding with the process of establishing the correlation. Two distinct sets of experimental data, including dependent and independent variables, have been used to verify the consistency of the experimental configuration. Both sets of data show great consistency throughout the process, demonstrating substantial progress in this research, particularly in connecting the dependent and independent parameters in the final phase. The experimental data has been used to analyze the cooling rate of the specimen in the third portion of this research.

Three regression models were used to determine the relationship between two verified data sets using regression analysis in the final step of this study. Each of three models shows good agreement for both sets of data. Out of the three models, linear regression model analysis is prioritized above nonlinear regression analysis owing to the fact that it is easier to use and provides more accurate results. According to the findings of this research, for the first and second data sets, the independent variables account for 94% and 95% of the dependent variable, respectively. The effect of every independent parameter on the cooling are highlighted.

ABBREVIATIONS

ROTs	Run-Out Tables
HSM	Hot Strip Mill
TMCP	Thermo-Mechanically Controlled Processed
ANN	Artificial Neural Network
TiC	Titanium Carbides
R22	Chlorodifluoromethane (Refrigerant)
CHF	Critical Heat Flux
CFD	Computational Fluid Dynamics
UFC	Ultra-Fast Cooling
AHSS	Advanced High-Strength Steel
EHAS	Electro-Hydraulic Actuation System
PID	Proportional-Integral-Derivative
BV	Ball valve
FM	Flow Meter
GV	Globe Valve
SV	Solenoid Valve
PV	Proportional Valve
PRV	Pressure Relief Valve
LVDT	Linear Variable Differential Transformer
VCC	Valve-Control Card
MS	Mild Steel
RTS	Real-Time System
VI	Virtual Instrument
MSE	Mean Squared Error
ReLU	Rectified linear activation function
R	Correlation coefficient
SD	Standard deviation
c	Constant for regression analysis
b	Coefficient for regression analysis

NOMENCLETURE

$\dot{v}$	Volume flow rate (m^3/h)
T	Temperature (^oC)
T_{avg}	Average plate temperature (^oC)
T_{in}	Starting temperature of the plate (^oC)
du	Distance between the upper nozzle bank and the plate (mm)
dl	Distance between the lower nozzle bank and the plate (mm)
h	Heat transfer coefficient ($W/m^2.K$)
T_∞	Ambient temperature(^oC)
m	Mass of the plate (kg)
C_p	Specific heat (kJ/kg.K)
t	Time (Sec)
q	Cooling rate(°C/Sec)
A	Surface area (m^2)
ρ	Density(kg/m^3)
Þ	Thermodynamics parameter (^oC.Sec)

LIST OF FIGURES

LIST OF TABLES

INTRODUCTION

Run-Out Tables, also known as ROTs, have been used by many industries for a significant amount of time in order to obtain various microstructures of steel. The cooling rate, which is one of the most important factors in determining the steel's final microstructure, is controlled by a number of various Run-Out Tables (ROTs) parameters. Nevertheless, the majority of previous research has focused on diverse topics, such as metallurgical behaviour, the temperature distribution of the strip during cooling at the run-out table, stress development in the hot strip and many others. The intent of this research is to establish an empirical correlation between the cooling rate of the hot strip and the various independent experimental factors in order to regulate the cooling rate of the hot strip at the run-out table which is one of the research gaps in this area. This chapter serves as an introduction to the study by first discussing the history of the topic and the context in which it was conducted. Next, the research problem, the research aims and the objectives are presented, followed by a discussion of the significance of the study and finally, the limitations.

Using a slab with known dimensions and chemical characteristics, the hot strip mill is used to produce coils with the specified gauge and qualities. A typical contemporary conventional hot strip mill includes a reheating furnace, descaling units, roughing and finishing stands, run-out tables and down coilers which is usually comes after a continuous casting facility. Modern material processing technology must now be able to produce goods at a cheap cost, with great productivity and of higher quality which is an immense challenge. Steel is made through a lengthy and remote manufacturing process. Slap goods are routed through a number of equipment, such as a roughing mill and a finishing rolling mill, to obtain the proper size of product. The steel strip type is established at this point after the rolling stand has finished.

Temperature is one of the key elements used to manage the mechanical and physical characteristics of steel strip in order to achieve the required product quality. Because impingement cooling enables extremely fine control of the cooling rate, it has become useful in a variety of metallurgical and electronic sectors. Along the run-out table, controlled water cooling systems are applied to manage the phase transition process and flatness; precipitation strengthening happens mostly during the cooling and cooling after cooling processes. A significant amount of work has been done over the course of the past few decades all over the world in an attempt to quantify the thermo mechanical and metallurgical phenomena that occur during controlled hot rolling. This has been accomplished with the assistance of mathematical models that are more fundamentally based and relatively limited experimental data. It has been brought to attention that the regulated cooling of the run-out table, which occurs in hot strip mills, is an essential component in the management of the mechanical properties of steel strips.

ROTs are critically important in steel industry and many studies are being conducted on ROTs over the previous several decades. The cooling mechanism, phase transition of steel and prediction of residual stress in hot rolled steel strips during run-out table cooling have become key study subjects.

This research, however, has usually concentrated on the aforementioned aspects of the issue where the cooling process must be controlled more precisely to achieve the appropriate steel grade based on current market demand.

Yet, the steel's microstructure may alter unfavorably as a result of under cooling or overcooling. As a result, it's necessary to regulate the ROT's various experimental variables in order to manage the cooling rate. An artificial neural network has been employed to verify the consistency of multiple sets of independent experimental data alongside the corresponding cooling rates, with the aim of regulating the cooling rate effectively. To investigate the cooling rate of hot strips on the run-out tables (ROTs), a generation-wise iterative technique was employed, supported by rigorously verified experimental data. The cooling rate or the thermodynamics parameters that will determine the cooling rate have been empirically related to the observed data using multiple regression analysis. Establishing the relationship between cooling rate or thermodynamic parameter as the dependent variable and various independent parameters in this research will contribute to achieving the desired steel quality. The correlation established through this study will support the steel industry in achieving the required steel grade and will also serve as a useful reference for future research in the academic field.

The study's background has been introduced in the first chapter. It has been identified what the research aims are and the value of such a study.

In chapter two, the current literature will be evaluated to identify critical methods and strategies for skills development within the context of rapidly changing sectors, particularly technology-intensive industries.

In Chapter three, both the experimental setup and the methodology for conducting the experiment are addressed in detail.

The methodologies for doing the study are explained in great depth in chapter four.

A more in-depth discussion of the study's findings and interpretation may be found in Chapter five.

The conclusion, limits and future scope of this study have been presented in the last chapter.

LITERATURE REVIEW

The inclusion of a literature review chapter is an essential aspect of any research undertaking, as it furnishes a thorough and extensive examination of preexisting information and research discoveries pertaining to the particular subject matter under investigation. Within the scope of this investigation, the primary emphasis is placed on the "Run Out Table," a critical component within the steel production procedure. The Run Out Table (ROT), often referred to as the ROT, is of paramount importance in maintaining the integrity and physical characteristics of the ultimate steel output. This chapter aims to comprehensively examine the substantial corpus of literature pertaining to the Run Out Table, including its historical evolution, operational principles, technical progress and its relevance within the steel industry. This chapter aims to establish a solid foundation for the subsequent analysis and discussion of the role of the Run-Out Table in steel manufacturing processes through a comprehensive review and synthesis of existing literature.

2.1 Basic Overview

Run Out Tables (ROTs) have long been used in industries to achieve various microstructures in steel. The microstructure of the material is mostly influenced by the rate at which it is cooled. This cooling rate, in turn, is determined by many elements such as the velocity of the plate, the distance between the nozzle bank, the flow rate of the coolant and several other parameters of the ROTs. The cooling process of steel involves a thermo-metallurgical phase change, where the desirable mechanical characteristics of the steel are influenced by the cooling rate. Mukhopadhyay et al. (2005) created an internet-based mathematical model for a hot strip mill (HSM) in order to enhance comprehension of the coiling temperature at the run-out table. Experimental trials conducted on different steel grades and thicknesses confirmed the model's accuracy in forecasting coiling temperature. Furthermore, the model was used to calculate cooling rates at various strip segments, providing valuable information on the development of microstructure and mechanical properties. The technical study conducted by Padhy et al. (2018) emphasises the importance of steel in many sectors and the need for it to have certain mechanical and material characteristics. It highlights the labor-intensive process of producing steel sheets in rolling mills. The research aims to investigate the cooling processes used in the run-out table (ROT) of the rolling mill. Furthermore, it emphasises the intricacy caused by the need for certain material characteristics, which in turn requires meticulous steel processing techniques. Moreover, the article highlights that the pace at which the material is cooled not only affects important material characteristics but also has an effect on the duration of the run-out table. The magnitude of heat transfer also has major consequences in this domain.

Horský et al. (1998) highlight the need of precise data on the degree of spray cooling in the hot rolling method used for flat and long products. To effectively design and control cooling sections, it is crucial to understand the magnitude of heat transfer, which is influenced by surface temperature, coolant pressure and velocity. The authors suggest that the cooling process may be represented by using a linear high-speed stand to derive the relevant functions.

A finite element-based, integrated process model is a helpful tool for researchers and engineers involved in the area of hot strip rolling. The capacity to precisely model and forecast the behaviour of strips on the run-out table has extensive implications for optimising processes, enhancing product quality and advancing computational materials research [Sun et al.,2002].

The study of Suebsomran et al. (2013) is a noteworthy addition to the area of numerical heat transfer analysis, specifically in the realm of steel manufacture. Their methodology presents a structured framework for simulating the transient heat conduction in strip steel cooling processes, yielding useful insights into temperature distributions and thermal dynamics. Three variables, namely strip velocity, external fluid velocity and cooling water temperature are used to generate the cooling conditions at the ROT and investigate the influential cooling factors. Furthermore, their use of sophisticated numerical methodologies emphasises the significance of computational approaches in addressing practical engineering obstacles. ROT is crucial in the hot rolling process of dual-phase steel that is alloyed with carbon, aluminium, chromium, manganese and silicon. This specific area of study falls within the domain of the sciences of materials and metallurgical engineering.

Suwanpinij et al. (2012) demonstrates a multidisciplinary methodology for comprehending and enhancing the hot rolling process of dual-phase steel. This methodology integrates experimental methodologies, mathematical models and industrial-scale confirmation. The results of this study add to the existing knowledge on materials processing and have consequences for the creation of high-performance steels for various applications.

The finite element-based comprehensive process model is a valuable addition to the area of materials processing. The capability to analyse the thermal and metallurgical characteristics of strips during hot strip rolling provides useful information for optimizing the process, controlling quality and designing products. The model's proven efficacy in elucidating the impacts of various process factors underscores its significance in furthering the comprehension and optimisation of industrial processes [Sun et al., 2002].

Through the creation of a three-dimensional numerical model, Cho et al. (2014) make a significant contribution to the understanding and prediction of edge wave behaviour in hot-rolled steel during run-out table cooling. This is a very important contribution. Through the identification of strain gradients as a significant component that contributes to the production of edge waves and the examination of the impacts of process parameters, this work contributes to the advancement of our understanding of edge wave processes and offers practical recommendations for reducing edge wave defects in industrial practice. By conducting this study, a substantial step has been taken towards improving strip flatness control and strengthening the quality of goods made from hot-rolled steel. For the purpose of achieving the necessary quality in accordance with the requirements of the industry, cooling temperature control also becomes an important issue of study in this sector.

Guo et al. (2013) used ANSYS to create a mathematical model for H-beams under controlled cooling to analyse temperature fields and their impact on morphological and mechanical characteristics. The study provides insights into the thermal behaviour of H-beams under varying cooling settings by analyzing patterns of temperature throughout regulated cooling and air cooling. The microstructural investigation shows the existence of ferrite and pearlite in various sections of the H-beam, along with noticeable differences in grain size.

A pioneering strategy to enhancing coiling temperature prediction and control in hot strip rolling is presented by Xie et al. (2006). This approach makes use of data mining techniques to achieve the desired results. The research provides a complete framework for the development of sophisticated control models. This is accomplished by using online information processing technologies and merging regression analysis with neural networks. There are implications for improving product quality, optimizing production processes and increasing the competitiveness of the hot strip rolling business as a result of this study, which marks a major development in the area. Researchers, engineers and industry experts who are engaged in the fabrication of steel and the optimization of the process might benefit greatly from the acceleration of the cooling rate on ROT.

The article by Guemo et al. (2018) offers a detailed review of rapid cooling on the run out table for the manufacturing of thermo-mechanically controlled processed (TMCP) steel. The authors highlight the significance of modelling, the value of understanding water cooling processes and the necessity of solving issues in transition boils. The study highlights the collaborative efforts that are required to foster innovation in the steel industry.

Nayak et al. (2016) studied how changing spray variables such as mass flux, input pressure, flow rate, nozzle tip to target distance and plate thickness, affected heat flux. A broad variety of air and water pressures were adjusted to thoroughly evaluate the heat transfer properties under various spray situations. This work enhances knowledge of heat transfer mechanisms when spray impacts hot steel surfaces, providing practical insights for improving heat flux in industrial processes like steel fabrication.

The work that was done by Serajzadeh et al. (2004) is a major addition to the area of steel fabrication. They achieved this by establishing a mathematical model that can predict temperature history as well as changes in microstructure that occur throughout the cooling process. Our knowledge of the behaviour of steel during cooling and the development of its microstructure is improved as a consequence of this work since it takes into account a variety of characteristics and validates the modelling findings via experimental observations. The findings of this study not only contribute to the advancement of the current state of the art in steel manufacture, but they also provide useful insights that can be used to optimize cooling operations and improve product quality.

Regression analysis is a powerful and widely adopted statistical tool used in research to explain and quantify relationships among variables (Jang et al., 2013; Atici et al., 2011). By modeling the interaction between dependent and independent variables, researchers can predict outcomes, assess the strength of associations, and identify patterns within complex datasets. This approach not only facilitates hypothesis testing but also enhances the interpretability of data, thereby supporting evidence-based decision-making. In various fields, including engineering, regression analysis plays a pivotal role in understanding the influence of specific variables on outcomes, contributing to the advancement of knowledge and the formulation of data-driven policies.

As research continues to evolve, regression methods remain central to both exploratory and confirmatory analyses. For instance, Golhar et al. (2021) introduced an innovative approach to estimate aluminum content in samples using ultrasonic properties such as hardness, velocity, attenuation, and elastic modulus. Their study utilized linear regression via SPSS to objectively correlate these ultrasonic features with aluminum percentages, demonstrating the value of statistical modeling in enhancing non-destructive testing (NDT) accuracy.

Similarly, Pavlenko et al. (2022) proposed a novel framework that integrates normalization, probability theory, and matrix-based linear regression to evaluate material properties while accounting for supplier variability. This structured analytical method empowers manufacturers to better predict material behavior and select optimal solutions.

Wiranto et al. (2020) applied multiple linear regression to investigate the effects of welding parameters—such as material dimensions, voltage, and timing—on shear strength. Their findings highlight the critical importance of parameter precision and present a systematic strategy for quantifying their influence on weld quality.

Additionally, Ozden et al. (2020) employed both multiple linear regression and tree-based regression techniques to explore the intricate relationship between laser process parameters and material properties. Their work not only enhances understanding of laser-material interactions but also supports the optimization of manufacturing processes and lays the groundwork for future research on laser-based material property evaluation.

2.2 Temperature variation and Thermal Stress

The monitored cooling of steel products plays a crucial role in planning rolling programs due to the strong influence of austenite transition kinetics on the resulting microstructures and mechanical characteristics. Therefore, the accurate forecasting of temperature patterns on the run-out table has significant importance for researchers and mill designers.

By constructing a thorough mathematical model for calculating temperature distribution on the run-out table, the work that was done by Serajzadeh et al. (2006) marks a major addition to the area of steel manufacture. A robust framework for forecasting the development of temperature throughout the cooling process is provided. This framework is achieved by resolving numerical instabilities, applying sophisticated numerical methods and adding phase transition kinetics. Using this model not only helps to improve the knowledge of thermal behaviour in the steel production process, but it also contributes to the improvement of product quality and the efficiency of the process. Zhou et al. (2003) performed a computational analysis that gives useful insights into the formation of residual stresses in thinner hot-rolled steel strips throughout the process of cooling on the run-out table. These developments were seen throughout the process of cooling. Our comprehension of the elements that influence the production of residual stress is improved as a result of this work since it makes use of the analysis of finite elements and takes under consideration the transformation of steel. The results provide insight on the role of temperature gradients in determining patterns of residual stress and provide information that may be used to optimise cooling systems in order to reduce residual stresses and enhance product quality. Wang et al. (2008) provides significant contributions to the understanding and management of the change in strip flatness that occurs throughout the cooling process on the run-out table in hot rolling operations. The research contributes to the advancement of our understanding of the processes that govern form control by drawing attention to the relevance of strip flatness in quality control and by studying the underlying causes of flatness problems. Wang et al. present a detailed study of thermal stresses and provide practical techniques for eliminating flatness faults. As a result, they improve the efficiency and quality of hot rolling operations. This is accomplished via the use of finite element analysis.

Through their exhaustive numerical analysis, Weisz-Patrault et al. (2018) make a contribution to the knowledge of the development of residual stress and flatness flaws in thin strips while they are being cooled on the run-out table. The research offers vital insights into the

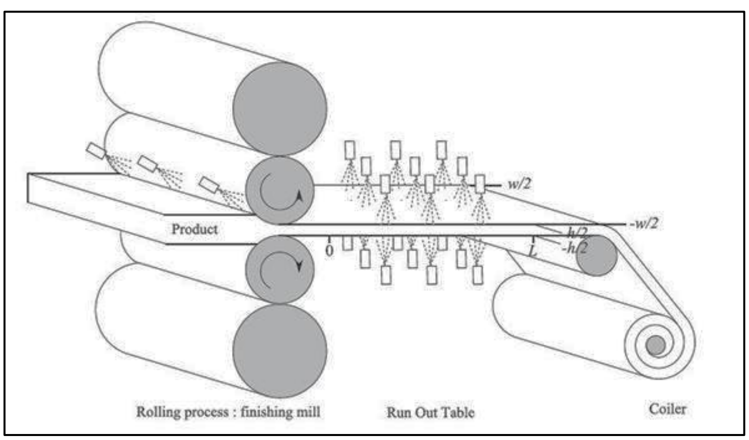

Fig. 2.2.1 Chain hot forming process on Run Out table [Weisz-Patrault et al., 2018]

intricate multiphysics processes that are involved in strip cooling. These insights are obtained via the use of a multi-step numerical technique and the execution of rigorous post-processing studies. Our knowledge of the mechanisms behind the production of flatness defects and residual stress has been advanced as a result of this study, which has potentially important consequences for the optimisation of processes and quality control in the steel manufacturing industry.

The combination of phase change analysis with thermo-elastic analysis modelling that was done by Nasab et al. (2015) is an effective method for determining the course of austenite breakdown and thermal stresses that occur during hot strip rolling processes. The suggested model allows researchers to optimize rolling processes and confidently anticipate material characteristics. This is accomplished via the use of thermo-mechanical finite element simulation and the consideration of the impacts of process factors. The findings of this study contribute to the development of hot strip rolling technology, which in turn improves the effectiveness and quality of the processes involved in the manufacturing of steel. When it comes to understanding the behaviour of steel strips on the ROT in hot strip mills, the numerical model that was created by Han et al. (2002) represents a considerable development. Through the incorporation of thermal, mechanical and metallurgical concerns, the model provides a complete framework for the simulation of the behaviour of deformation, temperature and phase transition. This study not only improves our knowledge of the parameters that influence strip behaviour during cooling, but it also gives useful insights that can be used to optimize hot strip rolling operations and improve product quality. The study conducted by Yuasa et al. (1990) illustrates the influence of improvements in temperature control systems on the operations of hot strip mills, specifically in meeting the increasing requirements of the industry for high-strength steel and thick strip manufacturing. The introduction and execution of a novel temperature regulation system at NKK's Keihin Works signify a notable advancement in attaining accurate temperature profiles and required mechanical characteristics in steel strips.

Spray cooling technique has been shown to be successful in lowering temperature differences inside H-beams [Qin et al., 2016]. To be more specific, they find considerable reductions in temperature variations between the web and the flange, as well as in the height direction. This information highlights the potential of this strategy for enhancing the uniformity and quality of H-beam products. Practical elements such as particular nozzle configurations are also taken into consideration in this research to produce the best possible cooling effects. These configurations include the angle between the nozzle center outside the R angle and the inner surface of the flange, as well as the distance between the two.

The study conducted by Wang et al. (2012) makes significant contributions to the comprehension and reduction of flatness faults in steel strips during the process of run out table cooling. The work examines the unevenness of temperature distribution and develops elasto-plastic constitutive equations to understand the intricate relationship between thermal, mechanical and microstructural elements that contribute to flatness faults. Wang et al. (2013) provide useful insights into the difficulties presented by flatness faults in hot-rolled steel strips and give viable solutions to alleviate these problems. The study makes a significant contribution to the field of online shape control models and the enhancement of flatness characteristics of hot rolled steel strips. This is achieved by identifying the root causes of flatness defects, creating an elastoplasticity constitutive model and suggesting a shape compensation control strategy.

The study conducted by Serajzadeh (2003) on mathematical modelling of temperature distribution and phase transition behaviour during hot strip rolling offers significant insights into the fundamental phenomena and their implications for optimizing the operation. The work improves our comprehension of hot strip rolling processes and provides practical ideas for enhancing product quality and efficiency by integrating numerical simulations with validation through experimentation. This research investigates the heat transmission and phase change that occur on the run-out table during the continuous hot strip rolling process of a low carbon steel in a commercial setting. The Scheil additivity rule and the Avrami-type equation are used to forecast the phase transition and temperature fluctuations in the strip, specifically for the ferrite and pearlite transformations. Lim et al. (2018) offers useful insights into the comparative comparison of heat transfer models and artificial neural network (ANN) approaches for predicting the final cooling temperature in accelerated control cooling procedures. The research showcases the higher precision and efficiency of ANN, emphasizing the promise of modern computational approaches in improving predictive capacities and optimizing industrial processes.

Wu et al. (2022) adds to the continuous progress in the field of flatness control technology in hot rolling operations. The work offers new insights into the processes that cause flatness flaws in steel strips by examining stress development and flatness throughout run-out table cooling employing an extensively coupled finite element model. These observations provide possibilities for upgrading the technology used to regulate flatness, optimizing the parameters of the production process, and improving the quality of products in the steel sector. The flatness of strip management throughout the cooling process is crucial in the steel industry as producers strive to enhance efficiency and quality. The strip flatness and crown control approach outlined in the main words signifies a notable advance in the realm of automated strip form regulation. This model provides a high level of accuracy and suitability for a wide range of mill setups by taking into account metal transverse flows and inter-stand deformation. The fact that it is successfully used in industrial settings highlights its efficacy in strengthening strip shape control and quality of the product in hot strip mills [Hai-jun LI et al., 2010].

Zhao et al. (2017) performed a research that offers a thorough comprehension of the microstructure, mechanical characteristics and hydrogen permeation behaviour of hot rolled enamel steel. The work provides significant insights to the area of materials science and engineering by examining the impact of coiling temperature on the development of TiC precipitates and the resulting material performance. The results have consequences for optimizing the production conditions and creating enamel steel with customized characteristics for various industrial uses.

Mohapatra et al. (2012) performed research that highlights the significance of ultra-fast cooling methods in steel production and their influence on the development of microstructure and mechanical qualities. The research offers useful insights for process optimization and management by examining various cooling techniques and categorising ultra-fast cooling kinds. Further study is needed to improve the efficiency and efficacy of ultra-fast cooling methods in order to produce high-quality steel products for various industrial uses.

2.3 Cooling Medium

The choice of cooling medium in the Run Out table cooling process is crucial in the steel industry as it directly impacts the required qualities, dimensions and quality of the finished steel product. The selection of the cooling medium used in this process is crucial in influencing the ultimate quality, microstructure and mechanical characteristics of the steel product. The cooling medium functions as a thermal reservoir, extracting heat from the high-temperature steel product and enabling fast cooling. Various cooling media, including water, air, or a mix of both (mist cooling), provide different rates of heat transfer, enabling manufacturers to customise the cooling process to accomplish specified cooling rates and microstructural alterations. Manufacturers may optimise the mechanical qualities and performance of steel by manipulating the transition kinetics of austenite to other phases, such as ferrite, pearlite, or martensite, by management of the cooling medium. Appropriate choice and control of the cooling medium aid in mitigating surface and interior flaws in the steel product, such as fissures, distortion, or residual strains. The cooling medium achieves constant characteristics throughout the material by evenly cooling the steel surface and minimizing thermal gradients.

Ravikumar et al.(2014) performed an experiment to assess the effectiveness of a water-based polymer addition in improving the spray-cooling efficiency of heated steel plates. The researchers sought to enhance heat transfer efficiency and achieve rapid cooling rates necessary for the manufacturing of high-strength steel by dissolving polyvinylpyrrolidone (PVP) in water within concentration ranges of 10-150 ppm. Precise regulation of cooling rates is necessary for the production of high-strength steel grades in order to attain certain microstructures, such as fine-grained ferrite and martensite. These microstructures are crucial for enhancing mechanical qualities, including strength and toughness. The researchers collected temporary temperature data throughout the cooling process using thermocouples placed underneath the surface. They then used a commercially available programme called INTEMP to estimate the history of surface temperature and heat flow. The cooling process achieved a maximum cooling rate of 253 °C/s and a critical heat flow of 4.212 MW/m^2, which is the upper limit of a 'Ultrafast cooling' method. The results emphasize the effectiveness of the water-based polymer addition in improving the efficiency of heat transmission and facilitating quick cooling, thereby presenting encouraging opportunities for the manufacturing of high-strength steel.

Ravikumar et al. (2015) conducted a study on the usage of nanofluids as a cooling medium in air-atomized spray cooling. The research examines the use of nanofluids to optimize cooling efficiency, optimize heat transfer rates and tackle issues related to high heat flux applications. The work seeks to enhance cooling rates and key heat fluxes in industrial applications by integrating nanofluids into the cooling process, which is crucial for effective heat dissipation. The research utilizes the INTEMP programme for inverse heat conduction analysis of surface heat flow and temperatures. This is done by using internal temperature histories received from thermocouples throughout the cooling process. The work achieves a thorough comprehension of heat transfer dynamics in air-atomized spray cooling using nanofluids by combining experimental data with computer simulations. The research investigates the use of nanofluids in air-atomized spray cooling to improve heat transfer efficiency and address constraints of conventional cooling techniques.

Dhua et al. (2013) signified a notable progress in the advancement and characterisation of ultrafine grained steel for future applications via the use of air cooling. The work showcases the possibility of creating ultrafine grained steels with outstanding mechanical characteristics by using exact control over composition and processing parameters in laboratory-scale manufacturing procedures.

The study conducted by Hou et al. (2013) is to investigate the performance of a cooling system that makes use of R22 as the coolant. The heat transfer coefficient, cooling surface temperature and critical heat flux (CHF) were some of the major characteristics that were taken into consideration throughout the design and construction of the system, which was particularly built and manufactured for the purpose of experimental assessment. Notably, the pressure at the input of the nozzle was changed between 0.6 and 1.0 MPa in order to evaluate the effect that it had on the efficiency of the cooling process.

Ravikumar, et al. (2014) emphasise the effectiveness of air-atomized spray cooling, a process in which compressed air is used to break down water into small droplets. This method provides accurate manipulation of cooling rates and enables efficient dissipation of heat from the stainless steel plate, resulting in increased metallurgical characteristics and improved overall performance. The research highlights the substantial impact of run-out table cooling rates, particularly in the temperature range between 900–600 °C, on the metallurgical characteristics of stainless steel. Swift cooling within this crucial temperature range is vital for attaining the appropriate microstructures and mechanical qualities, making it a central focus of the study. The objective of this study is to enhance the cooling efficiency by using ethanol-water combinations and ethanol-water-surfactant mixes. The experimental results demonstrate that the ethanol-water combination attains an optimal cooling rate of 183 °C/s, but the ethanol-water-surfactant mixture obtains a greater cooling rate of 235 °C/s. Cho et al. (2008) provide significant insights into the cooling effectiveness of impacting water jets in ROT processing, clarifying the intricate fluid flow phenomena and their impact on the creation of water pools and pressure distributions. The proven computational fluid dynamics (CFD) model provides a robust tool for optimizing cooling techniques and improving the quality of steel strips manufactured in industrial settings.

The research done by Nobari et al. (2016) highlights the significance of cooling patterns on the rate of transformation (ROT) in determining the ultimate characteristics of hot-rolled steel. The study makes a significant contribution to our knowledge of cooling processes during steel manufacturing by presenting a new model that takes into account boiling heat transfer mechanisms. The findings from this research have implications for improving cooling procedures in industrial environments, which may eventually result in the manufacturing of hot-rolled steel products with improved microstructure and mechanical qualities.

Gomez et al. (2020) emphasise the constraints of prior experimental investigations, which have been unsuccessful in faithfully replicating ROT circumstances. In order to fill this deficiency, they propose a novel experimental configuration that can rapidly cool steel surfaces at velocities ranging from 0 to 8 m/s, accurately simulating the operational circumstances of real-world rapid oil quenching processes. The study sheds insight on the intricate dynamics of quench cooling on the ROT, emphasizing the need of taking into account surface speed and water jet temperature for developing efficient cooling solutions. Their discoveries aid in the advancement of optimizing quench cooling procedures in steel production, which has consequences for attaining desired material characteristics.

The study conducted by Aamir et al. (2014) provides useful insights into the effect of spray parameters, notably intake pressure, on cooling performance when water is used as the coolant. This work improves our knowledge of the thermal behaviour of water-based cooling systems by conducting a systematic investigation of cooling time and rate across a variety of sample geometries and operating circumstances. The findings of this study have implications for enhanced design and efficiency in a variety of industrial contexts.

The study undertaken by Sharma et al. (2019) enhances our comprehension of the temporary cooling circumstances on stainless steel foil via the use of thermal imaging methods. Their research emphasises the impact of factors such as Reynolds number and plate speed on the dynamics of heat transfer during the process of transient cooling. The Reynolds number is adjusted within the range of 2500 to 10000, while the speed of the plate test specimen is varied from 0 to 40 mm/s. The work provides useful information for optimizing cooling operations in steel fabrication process.

2.4 Ultra-Fast Cooling

The use of ultra-fast cooling in the run-out table cooling process has many benefits, including as higher control over the microstructure, improved mechanical characteristics, decreased residual stresses and heightened energy efficiency. Through the use of UFC, steel makers may create top-notch steel products that possess exceptional performance attributes, hence satisfying the requirements of many industrial sectors. Ultra-fast cooling (UFC) is an essential procedure in steel production that involves quickly chilling heated steel products to attain precise microstructural traits and mechanical attributes.

Padhy, Mishra, et al. (2018) performed tests to enhance the initial UFC process in the ROT. They manipulate parameters such as the nozzle count, the quantity of air-assisted water and the spacing between the nozzles while maintaining other influential aspects at a constant level. The researchers use sophisticated tools to examine the cooling profiles of the strips and ascertain the efficacy of heat flux elimination, coolant distribution and cooling capacity. Bhattacharya et al. (2009) conduct a thorough analysis to determine the duration it takes for a solitary droplet to evaporate when it comes into contact with a heated carbon steel strip surface. Their study is grounded on basic principles of heat transfer and takes into account a spray that consists of several liquid droplets arranged in an array, with a low density of spray flux. The researchers investigate the feasibility of using spray evaporative cooling instead of traditional laminar jet impingement cooling to achieve rapid cooling rates, such as 300 °C/s, for a 4 mm thick carbon steel strip in the run out table (ROT) of the hot strip mill. In addition, the researchers formulated a comprehensive mathematical equation to predict the minimum size of droplets necessary to accomplish rapid cooling, based on the thickness of the steel strip.

Chen et al. (1992) compare their results with conventional boiling heat transfer research, emphasizing characteristics including heat fluxes, heat transfer coefficients, spray rate and cooling efficiency. This comparison study is used to compare their findings with current literature and acquire insights into the distinctiveness of cooling procedures in the steel sector. This method enhances comprehension of the distinct difficulties and possibilities in steel mill cooling applications by emphasizing similarities and distinctions.

Ravikumar et al. (2013) examined how the inclination angle of the nozzle, which varied from 0° to 60°, influenced the rapid cooling process. The trials used an average mass flow of water of 510 kg/m^2s. Two kinds of coolants were employed, namely pure water and cationic water with a concentration of 600 ppm. The stainless steel plate was initially held at a temperature of 900 °C, which accurately reflects the conditions seen on the run-out table in the steel sector. The inverse heat solver used observed temperature input data to predict the transient surface heat flow and temperature histories. At the same year Ravikumar et al. (2013) provides valuable insights into the correlation between carbon content, cooling rate and mechanical characteristics of steel. Steel samples with greater levels of carbon need increased water flow rates in order to achieve ultrafast cooling speeds above 140°C/s. These findings indicate that the amount of carbon present in steel significantly influences its cooling characteristics during rapid cooling procedures. Furthermore, the examination of the microstructure, tensile strength and hardness revealed that an augmentation in carbon content not only impacted the pace at which the steel samples cooled but also had an effect on the ensuing microstructure and mechanical characteristics. More precisely, the end products displayed properties that were in line with advanced high-strength steel (AHSS) grades. These properties included a high martensite phase composition ranging from 65% to 95%, as well as notable tensile strength and hardness.

The experimental results demonstrate [Mohapatra et al., 2013] significant findings regarding the efficacy of salt-infused air atomized spray in augmenting cooling rates during UFC. The use of air atomized spray containing MgSO4 salt results in a notably greater cooling rate in comparison to atomized spray consisting of pure water, with an enhancement factor of 1.5. Conversely, when using air-atomized spray with NaCl salt, there is a somewhat lower enhancement factor of 1.2. The accumulation of salt during the transition boiling phase is recognized as a crucial factor that contributes to the increased rate of heat transfer by conduction. Furthermore, the research emphasises the impact of surface tension on the instability of vapour film, where higher surface tension results in greater instability and enhanced cooling effectiveness.

The comparison research emphasizes [Jha et al., 2015] the significance of choosing suitable cooling methods and surfactant levels to get the most favourable cooling rates for surfaces that are either stationary or in motion. The results enhance the comprehension of rapid cooling processes and provide practical recommendations for optimizing cooling systems in industrial applications. Additional study in this field might investigate supplementary aspects that affect cooling efficiency and devise inventive cooling methods to address changing industrial requirements. Jha et al. (2015) performed a research to investigate the heat transfer kinetics of alumina nanofluid-based air atomized spray impingement on hot-moving steel plates with beginning temperatures above the Leidenfrost threshold. The research provides insights into the efficacy of using alumina nanofluid-based air atomized spray impingement as a feasible cooling method for high-temperature steel plates in motion. The use of surfactants enhances the heat transfer efficiency of the nanofluid, creating opportunities for the advancement of cooling systems in several industrial sectors. Further investigation in this field has the potential to enhance our comprehension of heat transfer mechanisms and stimulate advancements in ultrafast cooling technologies. The application of innovative cooling systems on the run-out table (ROT) has attracted considerable attention due to the market's demanding criteria and the need to minimize production costs while maintaining high quality. Liu et al. (2012) offer a comprehensive explanation of the control methods and models used in UFC and LC. These systems have a crucial function in managing cooling parameters, such as temperature, flow rate and pressure. They provide accurate control over the cooling process to obtain the required qualities of steel. The study conducted by Cai et al. (2014) on the three-stage cooling process for DP steels using prepositional UFC equipment is an innovative technique to steel manufacturing. Researchers utilize a combination of experimental observations and predictive modelling to gain valuable insights into the intricate relationships among cooling conditions, microstructure evolution, and mechanical properties. This enables the development of optimized steel manufacturing processes and improved product performance.

2.5 Research Gap

A review of the existing literature reveals that the majority of previous research has primarily concentrated on various aspects of the run-out table cooling process, such as metallurgical behavior, phase transformation characteristics, and the temperature distribution of steel strips during cooling. Several studies have also addressed the influence of process parameters on cooling efficiency and final material properties. However, very limited attention has been given to the development of a cooling control methodology based on real-time experimental temperature data. In particular, no significant investigation has been reported in which the cooling rate is dynamically controlled and optimized using continuously measured temperature feedback during the actual cooling process. This gap highlights the need for an experimental and numerical approach that integrates real-time temperature monitoring with cooling rate control to improve process accuracy and product quality.

2.6 Objective

Research in this field focuses on the cooling technique used on the Run Out Table (ROT) to achieve the desired quality of steel. The effectiveness of this technique depends on factors such as the cooling medium, temperature distribution and nozzle position, as well as the flow rate of the coolant. Understanding and applying advanced cooling techniques in the steel industry relies on studying these essential elements. The focus of this work was on the ways in which an empirical link may be built among the experimental data obtained from the Laboratory Scale Run Out table. This relation can be used for controlling the rate at which the cooling occurs. There is a degree of uncertainty about the results of the experiments, which have also been complied. Ultimately, checking the consistency between experimental findings and computational results is fundamental to formulating a feasible and simplified relationship, thereby guiding the direction of subsequent investigations in this study.

SYSTEM DESCRIPTION AND FINDING

This chapter provides a concise overview of the experimental setup, namely the Laboratory Scale Run-Out Table and its corresponding methodology for obtaining results. A comprehensive explanation is provided for the various components of the experimental setup. This section also provides descriptions of the software applications or tools that were used.

3.1 Experimental Set-up

The laboratory configuration comprises several components, including a furnace, two sets of nozzles, an air supply line and a water supply line for the nozzles. Additionally, there is an electro-hydraulic actuation system (EHAS) responsible for providing reciprocating motion to the specimen plate. Fixtures are also present to secure the specimen on the cooling bay, which is equipped with roller-fitted rails. Furthermore, a mechanical handling zone is situated between the cooling bay and the furnace.

3.1.1 Furnace

The furnace used in this study is of the chamber type, equipped with a total of 18 Kanthal GLOBAR SD Silicon Carbide heating elements. These elements are strategically positioned along the two inner side walls of the furnace chamber. The furnace has a maximum heating rate of 15 degrees Celsius per minute. The installation of the furnace's control panel is conducted as a distinct and independent process. On the control panel, there are indications for both the voltage and the current. There is a safety controller that places a cap on the highest temperature that can be reached. The device allows for the selection of various temperature values, expressed in degrees Celsius, using an adjustable dial. The heating elements will not exceed the specified temperature setting. With the assistance of an Automatic PID type programmable temperature indicating controller, the operator has the ability to exercise control over the heating process. The acronym PID stands for Proportional-Integral-Derivative controller. The aforementioned feedback control system is extensively used in engineering and industrial contexts for the purpose of regulating and controlling diverse processes. The PID controller is specifically designed to autonomously regulate a control variable, such as the position of a valve, the speed of a motor, or the temperature of a system, in accordance with a predetermined set point or reference value. A limit switch is installed in order to guarantee the deactivation of the heaters upon the opening of the furnace door. The operation of the furnace door is of the vertical raising type and is performed manually.

Table 3.1 Furnace Specifications

Sl. No.	Description	Specification
1.	Made	Kanthal, Sandvik Asia Ltd.
2.	Serial number	SF-074
3.	Working Chamber Dimensions	Depth:800mm,Width:800mm, Height:300mm
4.	Maximum Furnace Temperature	1200^{o}C
5.	Power Rating	21kW
6.	Power Supply	415±10%V, 50±5%Hz, 3-phase AC supply
7.	Temperature Controller	Make:Eurotherm,Model:2416

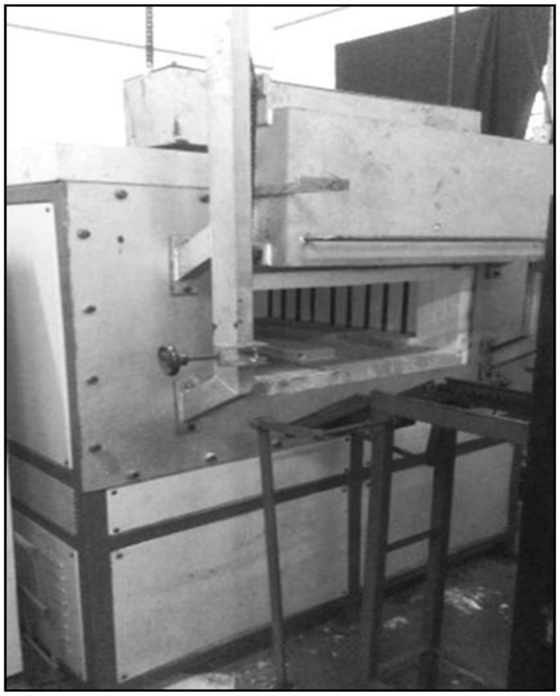

Fig. 3.1.1 Closed Chamber Type Furnace

Fig. 3.1.2 Furnace Control Panel

3.1.2 Nozzle Bank

There are two distinct categories of nozzles, the first category includes long, round cross-section nozzles that are designed to disperse water and are often referred to as full cone hydraulic nozzles. The second category comprises rectangular cross-section nozzles that are specifically engineered to emit a combination of air and water are commonly known as air mist nozzles. According to the details shown in Figure 3.1.3 and 3.1.4, it is evident that the plate is equipped with a configuration of hydraulic nozzles. Specifically, there are two rows of nozzles, with five nozzles in each row, positioned symmetrically on both sides of the plate. Consequently, the total number of hydraulic nozzles on the plate equals to 20. In a similar manner, the plate is equipped with two rows of air mist nozzles, with five nozzles positioned in each row on both sides, resulting in a total of twenty nozzles. The cooling bay is equipped with two banks of nozzles, with each bank including twenty individual nozzle units. These nozzle banks are positioned on both sides of the cooling bay, allowing for simultaneous spraying of both the upper and downward surfaces of the specimen plate. The air mist and hydraulic nozzles are organized in alternating rows. In the case of either air atomizing or hydraulic nozzles, a total of four nozzles situated at the four terminal locations of the two rows are linked to a shared header. The other six nozzles are connected to individual headers, with each header corresponding to a certain nozzle bank. As seen in Figure 3.3. The air atomizing nozzles are characterized by headers with a square cross section, whereas the hydraulic nozzles include headers with a circular cross section. The vertical positions of the nozzle banks may be regulated by the use of a simple screw and nut system. The distance between the nozzle banks and the specimen plate may be adjusted in order to achieve varying cooling speeds. A 45mm clearance is maintained between the nozzle bank and the specimen plate on all sides when the nozzle bank is positioned at the zero point on the attached scale. The spacing between the nozzle banks may be adjusted within the range of 0-140mm on the given scale. Table 3.2 presents the specifications that are involved. The cooling bay receives water from a shared pump, which is then distributed to the headers on both sides. The compressed air originating from a compressor is directed towards the square header, which serves as the conduit for the mist spraying nozzles. Supplied air and water, when subjected to high pressure, undergo full mixing inside the square header and are then emitted as mist via the nozzles. In this study, it was observed that when the water supply line to the mist spraying nozzles is stopped, these nozzles may be repurposed for air spraying. Consequently, the cooling process can be accomplished only by the use of air, as shown in this research. In the current study, just air cooling has been used.

Fig.3.1.3 Nozzle Bank and Cooling Bay

Fig. 3.1.4 Nozzle Bank Setup

3.1.3 Air Circuit

The air is first pressured inside a centrifugal compressor, which is powered by a 3-phase induction motor. Subsequently, the pressurized air is delivered to the nozzle banks through a straightforward circuit. This circuit is linked to the upstream compressor line by means of a ball valve (BV). The circuit consists of an air filter that has a regulator that is manually regulated, a vortex flow meter (FM) and a pressure gauge that is linked to a needle valve in order to control the pressure setting. The regulator on the air filter is what allows the user to manually adjust the pressure. As can be seen in Figure 3.1.5, the line is equipped with a globe valve (GV) measuring 1 inch to regulate the flow of air. The amount of air that is allowed to pass through is controlled by a pilot-operated solenoid valve of the diaphragm type that is ordinarily closed. Prior to reaching the mist spraying nozzles, the air supply line undergoes bifurcation into two separate branches.

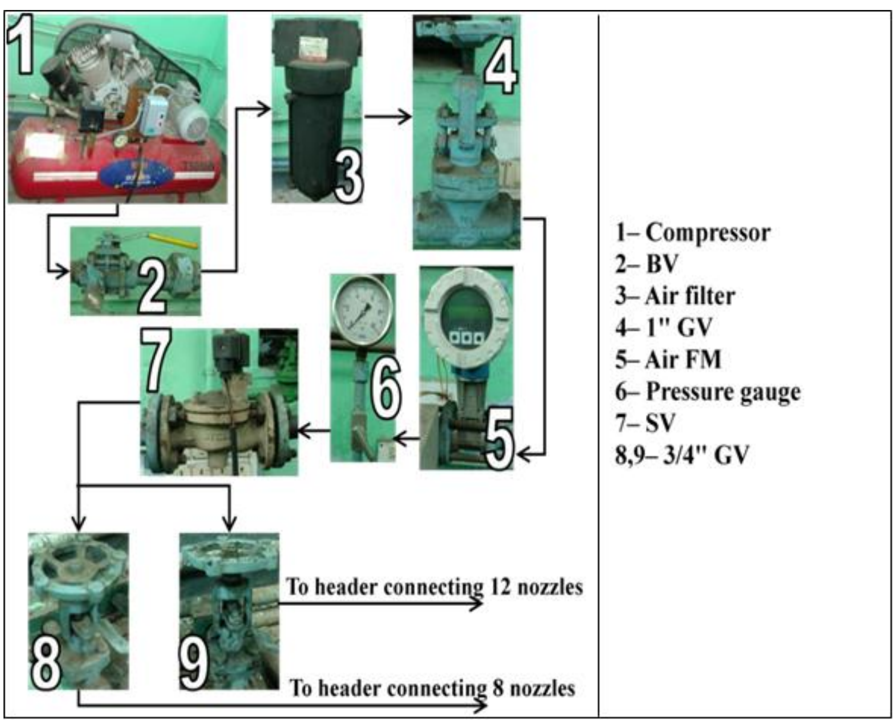

Fig.3.1.5 Air Circuit

One branch of the system is responsible for supplying air to the headers that link to a total of 8 nozzles, while the other branch supplies air to the headers that connect to a total of 12 nozzles. Each branch is equipped with individual ¾" globe valves. Table 3.3 displays the technical specifications of the air circuit components.

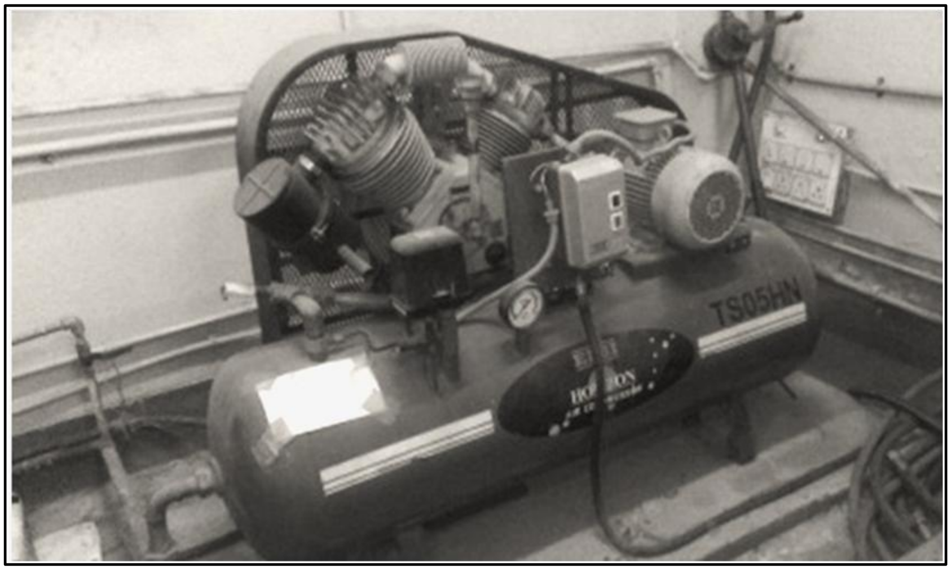

Fig.3.1.6 Air Compressor

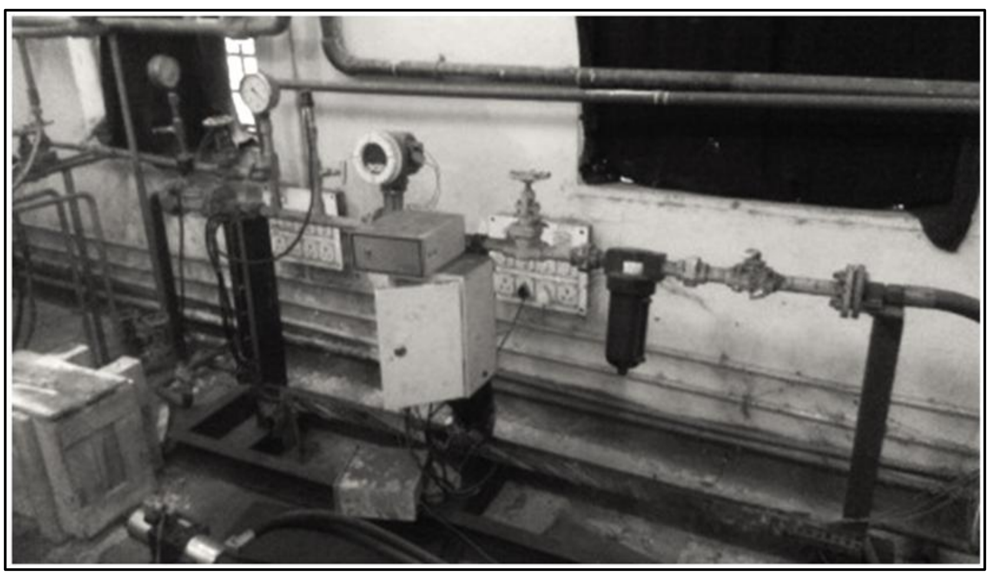

Fig. 3.1.7 Compressed air flow circuit with digital flow meter

Table.3.2 Airline component specifications

Component	Qty.	Make	Model	Specification
Compressor	1	ELGI Equipments Ltd.	TS05120 H	UnitRPM:925 Max. Working Pressure:12kgf/cm^2 Air Receiver Capacity: 220L MotorUsed:ELGImade,5.5hp,1450rpm,50Hz
Ball Valve (BV)	1	Mevada Engineering Works(P)Ltd.	BL-30-F-W-A3	Size and Rating:1",S.W.600#
Air Filter	1	ShavoNorgen	SF17-800-M8DC	Size and Rating:1", BSP(F)800# Max. Inlet Pressure:17.5kgf/cm^2
Vortex Flow Meter	1	Endress +Hauser	PROWIRL 72W25	Size:1",150#,FLGD Max. Flow: 10m^3/h Max. Pressure: 8barSupply:24VDC
Pressure Gauge	1	Wika	EN837-1	Range:0-10bar Size:½"BSP(M)
Needle Valve	1	Expo Engineering Enterprises	E8-NVFN	Size and Rating:½”,BSP(F), 800#(TH)
Solenoid Valve (SV)	1	Avcon	9160K25/CI/S4/BN/A1	Size and Rating:1",FLGD,150# Supply:24VDC
Globe Valve(GV)	1	Mevada Engineering Works(P)Ltd.	GB-1-R-W-A4	Size and Rating:1",S.W.800#
	2			Size and Rating:¾",S.W.800#

3.1.4 Water Circuit

The water supply is sourced from an elevated tank and first passes through a simplex basket filter through a backwash valve (BV). Subsequently, a vertical inline multistage centrifugal pump is used to increase the pressure of the water, which is then transported via a pressure gauge equipped with a needle valve. After the first division, the line was then branches into a bypass line and a main line. The bypass line is equipped with a pilot-operated diaphragm type solenoid valve that is generally open, along with a 1" globe valve, which is used to regulate and control the flow of water. Figure 3.1.8 illustrates the division of the main line into two branches subsequent to an additional filtering process. Each of the lines is equipped with a normally closed solenoid valve (SV) and a flow meter. The line with a greater diameter is connected to the mist spraying nozzles, while the other line is connected to the water spraying nozzles. Both lines are equipped with a gas volume (GV) and a pressure gauge. In accordance with Figure 3.8, the water supply to the headers, which are connected to 8 and 12 nozzles respectively, is facilitated by the division of each line into two distinct lines. In each line leading up to the headers, there is a globe valve installed for controlling the flow of liquid. The particulars of the requirements are included in the table.3.4.

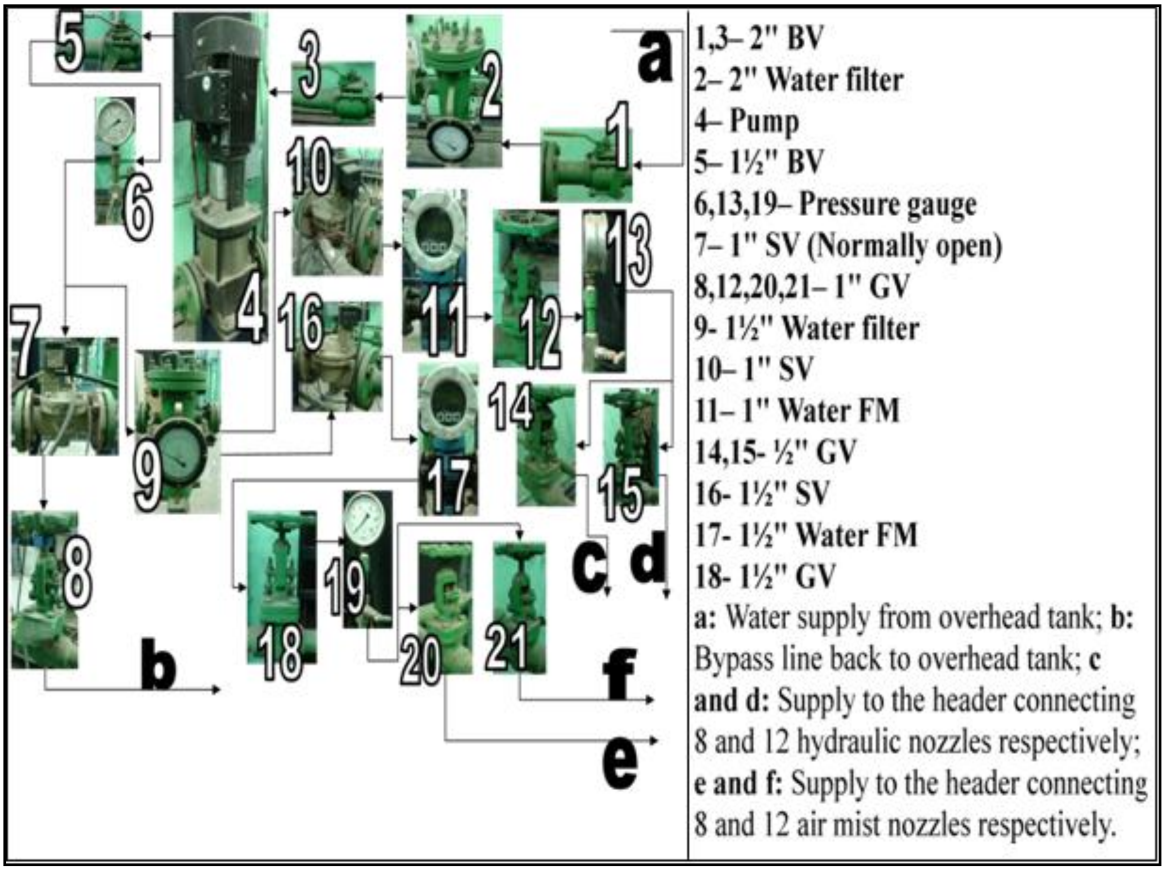

Fig. 3.1.8 Water Circuit Details

Fig. 3.1.9 Water Flow Circuit

Table.3.3 Water line component specifications

Component	Qty.	Make	Model	Specification
Water Filter	2	Filtration Engineers India Pvt.Ltd.	FR-244450NB	Size and Rating:2", ANSIFLGD,150# Mesh:200µ Max. Pressure:2bar
			FR-244440NB	Size and Rating:1½",ANSIFLGD,150# Mesh:100µ Max. Pressure:5bar
Ball Valve(BV)	2	Mevada Engineering Works(P)Ltd.	BL-30-F-W-A3	Size and Rating:2",S.W.600#
	1			Size and Rating:1½",S.W.600#
Pump	1	Grundfos	CR10-4-A-FJ-A-E-HQQE	RPM:2896 Max. Flow: 10m^3/h Shut offHead:40.8m Motors used: (a)Grundfosmade,1.5kW,50Hz, 2890-2910rpm (b)Grundfosmade,1.5kW,60Hz,3470-3530rpm
Pressure Gauge	3	Wika	EN837-1	Size:½",BSP(M) Range:0-10bar
Needle Valve	3	Expo Engineering Enterprises	E8-NVFN	Size and Rating:½",BSP(F),800#(TH)
Solenoid Valve(SV)	1	Avcon	9162K25/CI/S4/BN/A1	Size and Rating:1",FLGD,150# Supply:24VDC
	1		9160K25/C1/S4/BN/A1	
	1		9160K35/C1/S4/BN/A1	Size and Rating:1½",FLGD,150# Supply:24VDC
Electromagnetic Flow Meter	2	Endress +Hauser	PROMAG10P 25	Size:1",FLGD,150# Max. Flow: 10m^3/h Max Pressure: 10bar Supply:220VAC50Hz
				Size:1½",FLGD,150# Max. Flow: 10m^3/h MaxPressure:10bar Supply:220V AC50Hz
Globe Valve(GV)	4	Mevada Engineering Works(P) Ltd.	GB-1-R-W-A4	Size and Rating:1",S.W.800#
	1			Size and Rating:1 ½",S.W.800#
	2			Size and Rating:½",S.W.800#

3.1.5 Electro-Hydraulic Actuation System

A power pack, also known as a proportional valve (PV), and a hydraulic actuator are the three components that make up the electro-hydraulic actuation system. The hydraulic oil that is utilized is of the grade Servo system HLP 68. The flow of oil starts at the reservoir and is directed towards a swash plate-type axial piston pump, which is powered by a 3-phase induction motor. Prior to entering the pump, the oil passes through an oil filter. A pressure relief valve (PRV), which is linked to the line, serves to restrict the upper limit of the line pressure. The oil is then sent to the PV, which is a solenoid-operated, four-way, three-position direction control valve. As illustrated in Figure 3.2.1, this valve operates a single-acting actuator that is hinged to a mechanical link and attached to a rod that extends from the holding tray. Because of the pin

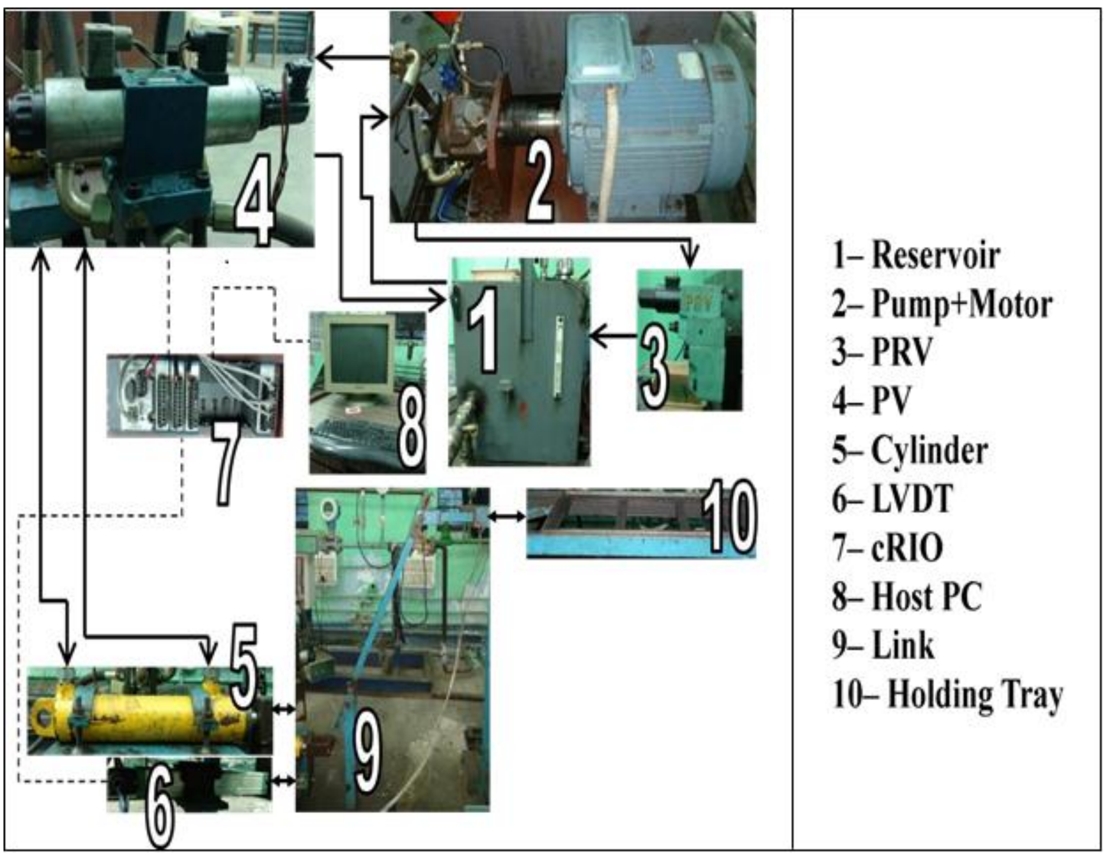

Fig.3.2.1 Electro-Hydraulic Actuation System (EHAS)

Table.3.4 EHAS component specifications

Component	Qty.	Make	ModelNo.	Specification
Pump	1	Rexroth	A10VSO 45DR/31R-PPAI2NOO	Nominal Pressure:280bar Flow:60Lpm Motor Used: ABB made,30kW,50Hz,1470rpm
PRV	1	Yuken	EBG-03-H-11	Max. Pressure:245bar
Oil Filter	1	Hydac	DFBN/HC110G10 B 1.1	Max. Pressure:420bar
PV	1	Rexroth	4WRE10 E1-50-21/G24K4/V	Flow: 50Lpm Supply: 24V DC Dead band:±1.5V Solenoid Resistance: 4.1ΩSolenoid InputCurrent:2.6A
Actuator	1		---	Type: Single actingBore:50mm Stroke length:200mm
LVDT	1	Gefran	LT-M-0200S-XL02020000X000 X 00	Stroke Length:200mm Linearity:±0.05% Repeatability:0.01mm
Real-time serial processor	1	National Instruments	NI-cRIO-9102	16-bit,1kHzsamplingrate, Accuracy: ±100ppm(max)
Input Module	2	National Instruments	NI-cRIO-9215	4-Ch ±10V 16 bit simultaneous analog input Max. Gain Error:0.2%
			NI-cRIO-9211	4-Ch±80mV24bit thermocouple input Max. Gain Error:0.05%at 25°C
Output Module	1	National Instruments	NI-cRIO-9263	4-Ch±10V16 bit analog output Max Gain Error:0.35%

joint that is located at the fulcrum point of the link, it is divided in a ratio of 1:4 from the rod end to the actuator end. As a result, the speed of the plate is four times that of the actuator speed. Both the cylinder and the plate have stroke lengths that are proportional to one another in the same way. The real-time system receives feedback of the actuator displacement via the use of a Linear Variable Differential Transformer (LVDT). The cRIO RTS is a compact and reconfigurable system used for real-time input and output. It consists of several components, including a 16-bit NI-cRIO 9102 real-time serial processor with digital to analog and analog to digital signal converters, NI-cRIO 9004 real-time controller, NI-cRIO 9215 input module and NI-cRIO 9263 output module. This system serves as a data acquisition system and is connected to a Host PC. The Host PC sends signals to a valve-control card (VCC) with a gain error of 0.04% through the output module of the RTS. The command voltage is sent to the PV in turn via the VCC. Because the data collection system includes both an NI-cRIO 9211 input module for temperature input and an NI-cRIO 9211 input module for time input, it is possible to utilize either one of these modules to determine the temperature of the heated plate. Table.3.4 provides the specifics of the requirements in further detail.

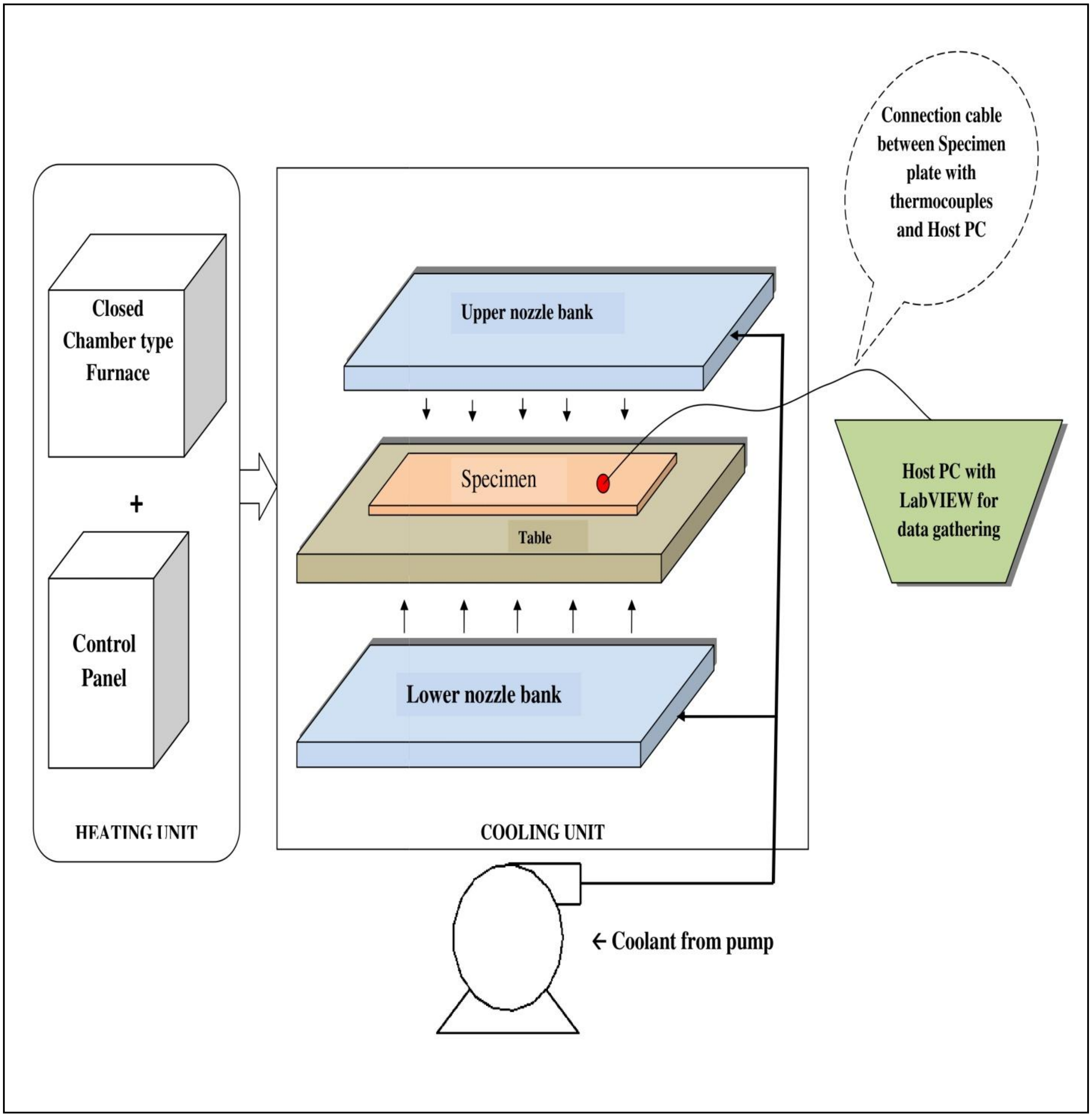

Fig. 3.2.2 Schematic diagram of the experimental apparatus

Fig. 3.2.3 Experimental setup

3.1.6 Holding Tray

The sample plate is placed in two holding trays: one is used throughout the heating process in the furnace, while the other is utilized for reciprocation. The second tray is linked to the actuator by a mechanical connection. In order to serve as representative samples, experimental analyses have been carried out using mild steel (MS) plates characterized by dimensions of 597 mm in length, 202 mm in width and 10 mm in thickness. The necessary perforations have been drilled in the provided sample plates and four K-type thermocouples have been securely attached to these locations shown in figure 3.2.4.

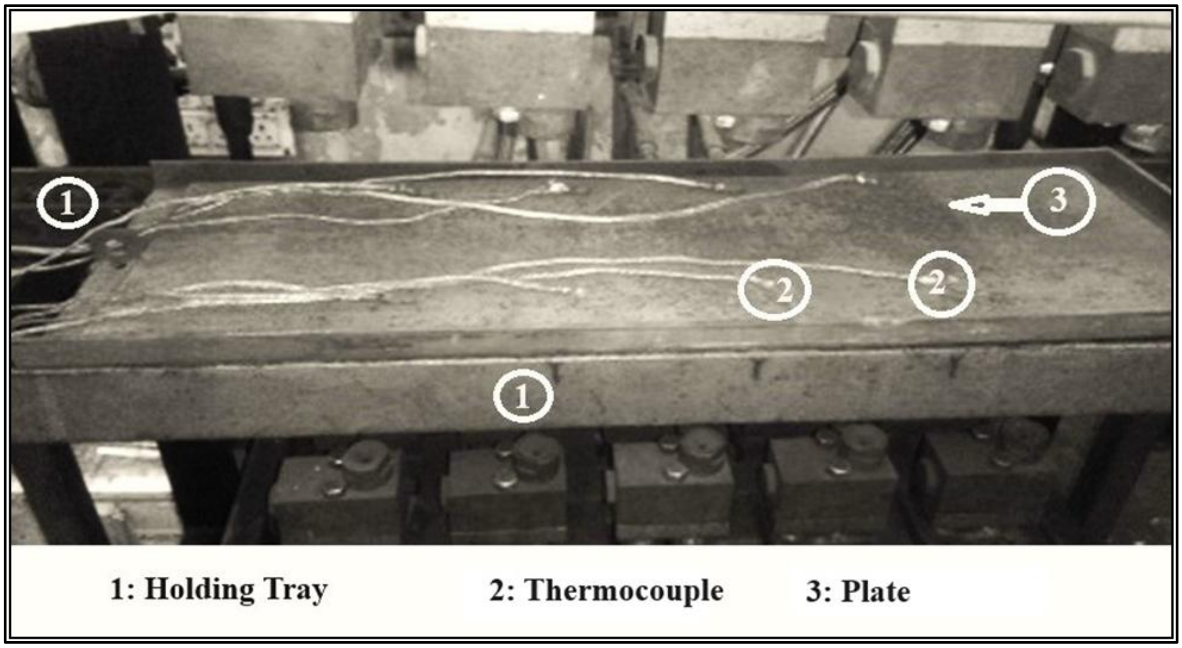

Fig. 3.2.4 Holding Tray and Plate with Thermocouple

3.2 Finding and Assumption

K-type thermocouples have been affixed to four distinct positions on the sample MS plate. Initially, the sample plate is subjected to heating inside the furnace until it reaches the designated temperature, often referred to as the target temperature. The PID controller has been used to regulate the desired temperature, resulting in the automated cessation of the heater upon attaining the target temperature. The hot plate is manually extracted from the furnace and thereafter transported to the cooling bay by use of roller-fitted rails. The ball valve of the airline is opened prior to the initiation of the compressor. The two ¾" gate valves (GVs), which provide direct access to the nozzle bank headers, have been uniformly adjusted to maintain consistent airflow velocity through each of the nozzles. The primary control valve with a 1" nominal bore is adjusted incrementally to either open or shut, in order to either raise or decrease the rate of air flow ($\dot{v}$) as needed. The reading of the flow meter has been monitored and the control valve (GV) has been adjusted to achieve the required flow rate. During the heating process of the plate,

Fig.3.2.5 NIcRIO Modules

the adjustment wheel is used to position the nozzle banks at the required distance (D) from the cooling bay. In addition to the solenoid valve being powered to open and let air flow through it, the data gathering process has also been initiated simultaneously by executing the VI on LabVIEW in the Host PC. This has caused both processes to begin simultaneously. The temperatures ($\boldsymbol{T}$) at four specific points on the plate were measured using the Real-Time System (RTS) at a time interval of 0.01 seconds during the whole cooling process. The average temperature of the four sites was calculated to get the average plate temperature ($\boldsymbol{T_{avg}}$).The data collecting is halted and the compressor is switched off when the temperature of the plate exceeds the standard room temperature of 30°C. Process is repeated with different values for the flow rate ($\dot{\boldsymbol{v}}$), the starting temperature of the plate ($\boldsymbol{T_{in}}$) and the distance between the banks of nozzles (***dl)***. The real-time analysis of the cooling properties of the sample plate has been conducted utilizing the aforementioned technology. The study examines the cooling behaviour of a plate under various situations by varying three parameters: the air flow rate ($\dot{v}$) from the nozzles, the initial temperature of the sample plate (T_{in}) and the distance (***dl***) between the nozzle bank and the plate.

Table.3.5 Ranges and base values of the parameters

Parameter	Range	Base Value
Flow Rate ($\dot{v}$)	5-7m^3/h	6m^3/h
Initial Temperature of the plate (T_{in})	100ºC-700ºC	30ºC
Nozzle bank distance (*dl*)	45-185mm	115mm

During each run, one of the three parameters listed above was considered as a variable, while the other two were maintained at a constant value chosen as the base value. As an example, throughout the investigation of the impact of altering $\dot{v}$ the cooling process of the plate, the values of T_{in} and ***dl*** have remained constant at their initial levels. The table 3.5 provides the specified ranges and initial values for the parameters. The base value for each parameter has been selected approximately at the middle of the range. The heat transfer coefficient (h) has been determined by applying the convection equation to the plate, taking into account certain assumptions to streamline the calculation process. Based on the physical characteristics of the plate, it can be concluded that convection is the primary method of heat transmission throughout the cooling process. The impact of radiation and conduction may be disregarded in comparison. Additionally, it is believed that the plate is thin, resulting in little heat loss from all surfaces except for those immediately exposed to the air jet. The collected data indicate that there is little geographic variation in temperature throughout the plate. Therefore, the plate is considered to be a lumped system, with the assumption that the temperature is consistent over the whole plate. Given the aforementioned assumptions, the calculation of $\boldsymbol{h}$ may be readily derived from the convection equation, which simplifies to the following concise form as a result of those assumptions:

$$\boldsymbol{hA(T - T_{\infty}) = mC_p\left(\frac{dT}{dt}\right)} \tag{3.1}$$

Where, A= Surface Area (the total area of the two surfaces under air jet)

$\boldsymbol{T_{\infty}}$= Ambient Temperature (taken to be 30°C)

$\boldsymbol{m}$ = mass of the plate

$\boldsymbol{C_p}$= specific heat of Mild Steel

The temperature gradient, denoted as $\boldsymbol{\frac{dT}{dt}}$, is the rate at which the temperature decreases and may be determined based on the $\boldsymbol{T}$ values. The density (**ρ**) of mild steel has been considered to be 7850kg/m^3 and the specific heat ($\boldsymbol{C_p}$) has been assumed to be 510.7896 J/kg-°C. Graphs depicting the mean temperature ($\boldsymbol{T_{avg}}$), the rate of cooling ($\boldsymbol{q}$) and the coefficient of heat transfer ($\boldsymbol{h}$) as functions of time ($\boldsymbol{t}$) have been acquired under various circumstances.

3.3 Cooling Methodology

The cooling methodology of the working specimen on the Run-Out Table (ROT) was designed to replicate the industrial accelerated cooling process of hot steel plates under controlled laboratory conditions. The experimental arrangement included a heating furnace, a cooling bay equipped with nozzle banks, air and water supply systems, an Electro-Hydraulic Actuation System (EHAS) and a real-time data acquisition system for continuous temperature monitoring.

Initially, a mild steel (MS) specimen plate of dimensions 597mm × 202mm × 10 mm was prepared by drilling holes at the required positions for the installation of four K-type thermocouples. These thermocouples were fixed at predetermined locations on the plate to monitor temperature variations throughout the cooling process.

The specimen plate was first placed on the holding tray inside the chamber-type furnace and heated to the desired target temperature. The furnace was fitted with 18 Kanthal GLOBAR SD Silicon Carbide heating elements mounted along the inner side walls, providing a maximum heating rate of 15°C/min. Heating was controlled using an automatic PID-type programmable temperature controller to ensure accurate attainment of the target temperature. In addition, a safety controller was installed to prevent the temperature from exceeding the preset limit.

Once the target temperature was reached, the heated specimen was manually removed from the furnace and transferred to the cooling bay through roller-fitted rails positioned between the furnace and the ROT system. The specimen was then placed on the holding tray connected to the Electro-Hydraulic Actuation System (EHAS). However, in the present study, the reciprocating motion of the EHAS remained inactive during the cooling process.

The cooling bay consisted of two nozzle banks positioned on both sides of the specimen to allow simultaneous cooling of both the upper and lower surfaces. Each nozzle bank contained 20 nozzles arranged in alternating rows of hydraulic nozzles and air-mist nozzles. For the present investigation, only air cooling was used by shutting off the water supply line to the mist nozzles, thereby allowing them to function solely as air-spraying nozzles.

Compressed air required for cooling was supplied by a centrifugal compressor driven by a 3-phase induction motor. The air passed through an air filter, pressure regulator, vortex flow meter, pressure gauge, globe valves and a solenoid valve before entering the nozzle headers. The air flow rate (Q) was regulated by adjusting the main 1-inch globe valve, while the two ¾ inch globe valves were opened equally to maintain uniform air velocity through all nozzles.

The distance between the nozzle banks and the specimen plate (D) was adjusted using a screw and nut mechanism. At the zero-scale position, the initial clearance was 45 mm, and the nozzle distance could be varied up to 140 mm depending on the required cooling intensity.

Before the cooling process began, the nozzle banks were set at the required distance and the desired air flow rate was established. At the same time, the solenoid valve was energized to permit airflow, and the data acquisition system was started using LabVIEW interfaced with the compact reconfigurable input-output real-time system (cRIO RTS).

Although the EHAS is capable of providing reciprocating motion to simulate the movement of steel plates on an industrial Run-Out Table, this feature was not utilized in the present work. Therefore, the specimen remained stationary during the cooling process while being subjected to air jets from both nozzle banks.

Cooling continued until the specimen temperature reached room temperature (approximately 30°C), after which the compressor and the data acquisition system were switched off.

The experiments were repeated by varying three important process parameters i.e.; initial plate temperature (T_{in}), air flow rate (Q), and nozzle bank distance (D). This methodology enabled a systematic investigation of the cooling characteristics of the specimen under controlled air-cooling conditions using the laboratory-scale Run-Out Table system.

METHODOLOGY

The comprehensive strategy for conducting the study delineates the precise methodologies and approaches employed to address the research inquiries or hypotheses, which are thoroughly elucidated in the methodology chapter. This section explores the complexities of the study's design, the process of selecting participants, the methods used for data collecting and the analytical approaches employed. This chapter seeks to establish the validity, dependability and integrity of the research process by providing a thorough explanation of the processes followed and the reasoning behind each decision. By thoroughly examining the methodology, readers acquire understanding of how the study was carried out, allowing them to assess the strength of the findings and the reliability of the conclusions made.

4.0 Research Design

Run Out Tables (ROTs) have long been used in industries to get various microstructures in steel. The microstructure is mostly influenced by the cooling rate, which is determined by many elements such as plate velocity, nozzle bank distance, coolant flow rate and other parameters of the Run Out Tables (ROTs). The cooling process induces thermo-metallurgical phase transition, making the cooling rate a crucial factor in achieving the appropriate mechanical characteristics of steel. Ultra-Fast Cooling (UFC) in ROT involves the application of high flow rates of coolants, such as air, water, air-water mist, etc., over a surface area that is evenly dispersed and in motion. The observed data is being used to determine the cooling rate, a crucial element for attaining desirable characteristics of steel. The inverse problem is of great importance since it seeks to determine the appropriate output parameter for a given input cooling rate. The inverse issue poses a significant challenge due to the acquisition of multidimensional data from the experiment. Modeling the inverse problem specifically, establishing a correlation between the cooling rate as an independent variable and other experimentally observed parameters is fundamental to effectively controlling the cooling process.

The initial phase of this study involved conducting a series of controlled experiments on a Laboratory-Scale Run-Out Table to generate the data required for formulating the inverse problem. This process aimed to determine key numerical relationships such as regression coefficients and functional correlations linking the cooling rate to various experimental parameters, thereby enabling the development of a predictive model for cooling rate regulation.

In the second phase of this research, an Artificial Neural Network (ANN) was implemented to assess the consistency and reliability of multiple sets of independent experimental parameters in relation to their corresponding cooling rates. The primary objective of this approach was to enhance the predictive accuracy of the cooling rate model and to facilitate more effective control of the cooling process.

In the third phase of this research, a generation-wise iterative technique was utilized to investigate the cooling behavior of specimens on the Run-Out Tables (ROTs). This analytical approach was grounded in rigorously verified experimental data and aimed to refine the understanding of the cooling rate under varying process conditions.

In the final stage of this research, multiple regression analysis was employed to empirically establish the relationship between the cooling rate or the thermodynamic parameters influencing it and the independent experimental variables. This statistical approach enabled the quantification of the influence of each experimental factor on the cooling behavior, thereby contributing to the development of a robust predictive model for controlling the cooling rate with greater precision.

4.1 Data Collection

Data has been collected through experiment on the Laboratory Scale Run Out Table which consists of many components, including a furnace, two sets of nozzles, an air supply line and a water supply line for the nozzles. Furthermore, there exists an electro-hydraulic actuation system (EHAS) which is accountable for delivering back-and-forth movement to the specimen plate though in this work specimen plat remains static. Fixtures are provided to secure the specimen on the cooling bay, which is furnished with rails connected with rollers. Additionally, there is a mechanical handling area located between the furnace and the cooling bay. Four separate spots on the sample MS plate have been equipped with K-type thermocouples. Firstly, the sample plate is heated inside the furnace until it attains the specified temperature, often known as the target temperature. The PID controller has been used to regulate the required temperature, leading to the automatic termination of the heater once the goal temperature is reached. The hot plate is physically removed from the furnace and then transferred to the cooling chamber using rails equipped with rollers. The airline's ball valve is opened before starting the compressor. The two ¾" gate valves (GVs) have been equally calibrated to provide a constant airflow velocity through each of the nozzles by providing direct access to the nozzle bank headers. The main control valve, which has a nominal bore of 1 inch, is adjusted gradually to either open or close, in order to increase or decrease the rate of air flow ($\dot{v}$) as required. The flow metre reading has been checked and the control valve (GV) has been adjusted to get the desired flow rate. While heating the plate, the adjustment wheel is used to precisely place the nozzle banks at the desired distance (***dl***) from the cooling bay. Furthermore, as the solenoid valve is being energised to allow the passage of air, the data collection procedure is concurrently activated by running the Virtual Instrument (VI) on LabVIEW on the Host PC. As a result, both procedures have started concurrently. The temperatures ($\boldsymbol{T}$) at four specified spots on the plate were monitored using the Real-Time System (RTS) at a time interval of 0.01 seconds over the whole cooling process. The mean plate temperature ($\boldsymbol{T_{avg}}$) was determined by calculating the mean temperature of the four locations. Data collection ceases and the compressor is off when the plate temperature above the specified ambient temperature of 30 degrees Celsius. The procedure is iterated using varying values for the volume flow rate of coolant ($\dot{\boldsymbol{v}}$), the initial temperature of the plate ($\boldsymbol{T_{in}}$) and the spacing between the rows of nozzles ($\boldsymbol{dl}$).

The system described above consists of several interdependent components that are very sensitive to external disruptions. For example, any variations in the speed of the compressor have a significant impact on the flow rate in the air circuit. It is important to use caution while handling thermocouples during readings, since even the slightest movement might result in fluctuations in the recorded values. The experiment begins by establishing the air or water circuit, as needed. Only air is used as a coolant in this work. The air circuit is initiated by activating the air compressor and regulating the airflow through the nozzle banks using the globe valve connected to the air circuit. The flow meter registers a fluctuating flow rate within a certain range. The desired condition for stabilizing the flow rate is to minimize the range and ensure its consistency during the measurement. The ball valve located next to the above water tank controls the water flow towards the centrifugal pump in the water circuit. The included digital flow meters are used for the purpose of monitoring the rate at which water flows, which then proceeds to the nozzle banks via distinct globe valves. Priming should be performed if necessary and the flow rate in the water circuit may be adjusted by manipulating the globe valve in the bypass line.

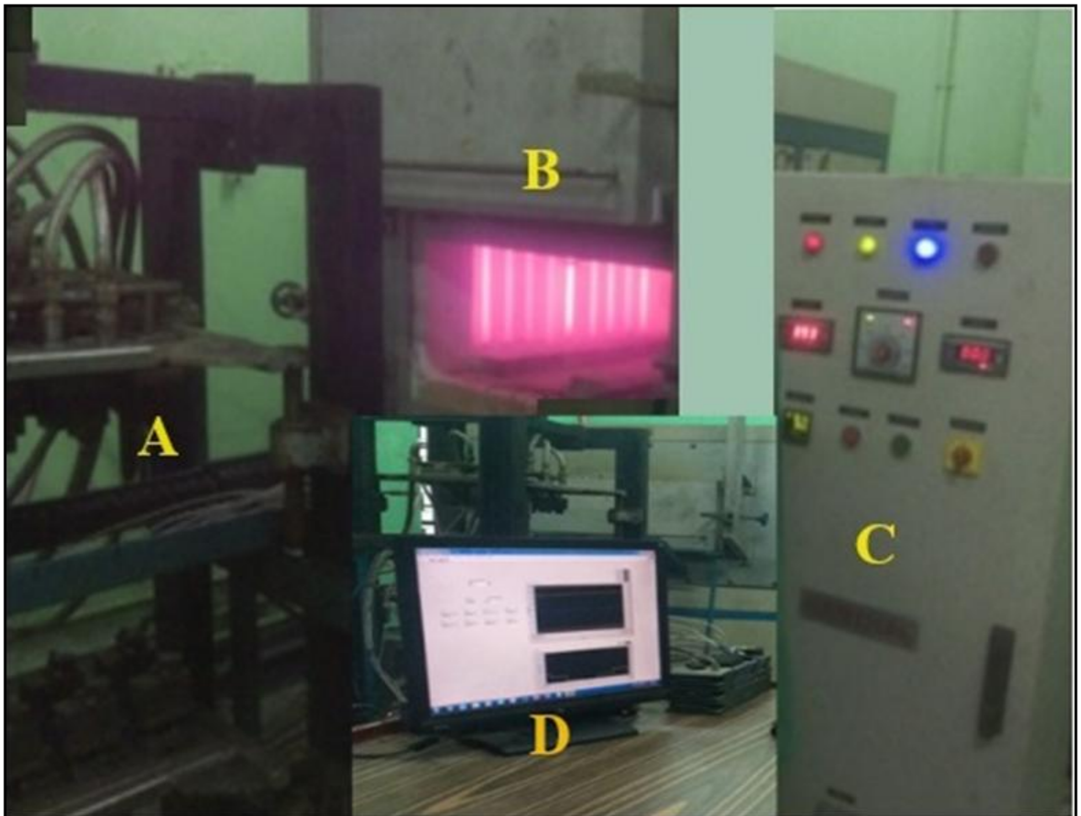

A: The Nozzle Bank setup B: The Furnace with heating elements
C: The Furnace Control Panel D: Host PC running LabView

Fig. 4.1 Experimental Set-up

Next, the nozzle banks are precisely positioned at the correct distance (*dl*) from the plate by using the hand wheel connected to each of the nozzle banks. The plate's ultimate distance is manually verified using a 30cm measuring scale. Special attention is given to consider and correct for any parallax inaccuracies. The process of achieving a stable flow rate requires a substantial duration. The plate remains stationary during the whole experimental process, with simply an air jet being used. Up to a maximum operating temperature of 1200 degrees Celsius, the heating boiler that is included in the arrangement may be heated. Keeping this in mind, as well as making an effort to complete each measurement within a reasonable amount of time, all of the readings in this research have been taken beginning at an average temperature of 600°C to

605°C and then cooled to an average plate temperature that is close to 99°C. To acquire the temperature data in real time on a computer, a NIcRIO is used to transport the thermocouple data into the computer. This allows the data to be obtained in real time. For the purpose of acquiring this data, the software platform that is used on the computer is LabVIEW. LabVIEW is used to depict fluctuations in temperature over time in real time and at the same time, the data is concurrently put into a Microsoft Excel file. The mean temperature (T_{avg}) variation has also been incorporated into the readings. This helps to keep track of the average plate temperature at the most crucial periods, such as when the reading begins at an approximate average plate temperature of 600 degrees Celsius and ends at an average plate temperature that is close to 100 degrees Celsius. This is made possible by the fact that data from eight different thermocouples is simultaneously available on LabVIEW.

The data extracted from the Excel file is shown as discrete time points, beginning at zero and increasing in increments of 0.01 seconds. The data includes the temperatures recorded by thermocouples as well as the average temperature, which are organized in adjacent columns.

For the purpose of checking the consistency of the data that was obtained, an Artificial Neural Network (ANN) was used as the tool. After checking the consistency of the experimental data were used to construct a relation that allows for the control the cooling rate via the method of regression analysis.

4.2 Data Analysis

Two distinct datasets, each with unique combinations, have been selected from the observed data. During the initial stage of this selection process, 29 samples of upper nozzle distance (***du***), lower nozzle distance (***dl***) and volume flow rate of air ($\dot{\boldsymbol{v}}$) are used as inputs.

These inputs are paired with an equal number of samples of $\int_0^t T dt$ i.e.; a thermodynamic parameter Þ, which serve as the target values that define the network outputs. Secondly several experimental data, including the convective heat transfer coefficient (h), the volume flow rate of coolant ($\dot{v}$) and the mean specimen temperature (T_{mf}), were utilized as input parameters, with the rate of cooling (q) serving as the output parameter.

4.2.1 Consistency Checking of Experimental Data

An Artificial Neural Network built in MATLAB has been used in order to check the consistency and tested for dependability of the data that has been observed. The use of artificial neural networks in research activity has been a beneficial technique for a considerable amount of time. Overall, Xie et al. (2007) demonstrate the efficacy of Artificial Neural Networks in analysing heat transport in shell-and-tube heat exchangers. The research showcases the effectiveness of Artificial Neural Networks (ANNs) in properly predicting outlet temperature differences and total heat transfer rates by using the Back-Propagation technique and experimenting with various network topologies. The results emphasise the capability of artificial neural network (ANN) methods in optimizing thermal systems and enhancing energy efficiency in engineering applications. Ermiş et al. (2007) have shown that Artificial Neural Networks are useful in analyzing heat transmission in finned-tube latent heat thermal energy storage systems. The paper offers useful insights into the thermal behaviour of such devices under various operating situations by introducing an ANN algorithm and performing a numerical examination. The results emphasize the need of using ANN-based methods to optimize thermal energy storage devices for real-world use. Artificial Neural Networks (ANN) are often used in the research sector to effectively address problems caused by a lack of appropriate observable data. The study conducted by Pacheco-Vega et al. (2001) highlights the significance of accuracy concerns while estimating heat rates for refrigerated heat exchangers using Artificial Neural Networks. The paper offers useful insights into the problems and approaches for enhancing the accuracy of ANN models by using restricted experimental measurements and examining the influence of training data on network performance. The use of cross-validation methods presents a viable method for discovering data shortcomings and improving the reliability of heat rate predictions based on neural networks. Islamoglu (2003) uses the back-propagation method and ANNs to estimate heat transfer rates in heat exchangers. The work proves ANN-based modelling techniques' dependability and accuracy by matching experimental outcomes with ANN predictions. ANNs allow heat engineers to quickly analyse heat transfer rates and evaluate heat exchanger performance after engineering adjustments due to their simplicity of modelling. Jambunathan et al. (1996) emphasise the importance of liquid crystal thermography and neural networks in convective heat transfer coefficient assessment. This complete technique improves convective heat transfer comprehension and prediction, optimizing engineering systems that use heat transfer processes. Hassan et al. (2009) provide evidence of the effectiveness of feed-forward back propagation neural networks in accurately forecasting the physical characteristics and hardness of aluminum-copper/silicon carbide composites that were synthesised using the composting process. Artificial Neural Networks (ANN) is the preferred choice due to its ability to provide excellent outcomes while keeping costs and testing time low. Tan et al. (2009) provide evidence of the efficacy of artificial neural networks in modeling the thermal performance and monitoring the state of fin-tube heat exchangers. Artificial neural networks (ANNs) provide significant tools for optimizing heat exchanger operation and maintenance in diverse engineering applications by precisely forecasting heat transfer rates and spotting performance deterioration. The research conducted by Patel et al. (2017) offers significant insights into the use of neural networks for the purpose of quality optimization in the processes of squeeze casting.

An Artificial Neural Network (ANN) is a component of Artificial Intelligence. A neural network is a computer system that consists of artificial neurons designed to mimic a human nervous system. It utilizes modern computing methods to data varification and address intricate and nonlinear connections between input and output variables. The algorithm expresses the output signals of the neurons as a function of the input signals. In this process, the input vectors **'p_i'** are multiplied by their respective weights **'w_i'** and then sent through a summing function. The bias value **'b'** is added to the result, producing the net input **'n'**.

i.e., $\boldsymbol{n} = \sum_{i=1}^{R}(\boldsymbol{p}_i\boldsymbol{w}_i + \boldsymbol{b}), \forall \boldsymbol{i} = \mathbf{1}(\mathbf{1})\boldsymbol{R}$ (4.1)

The net input is fed to the transfer function to generate the output. i.e., a = *f*(n).

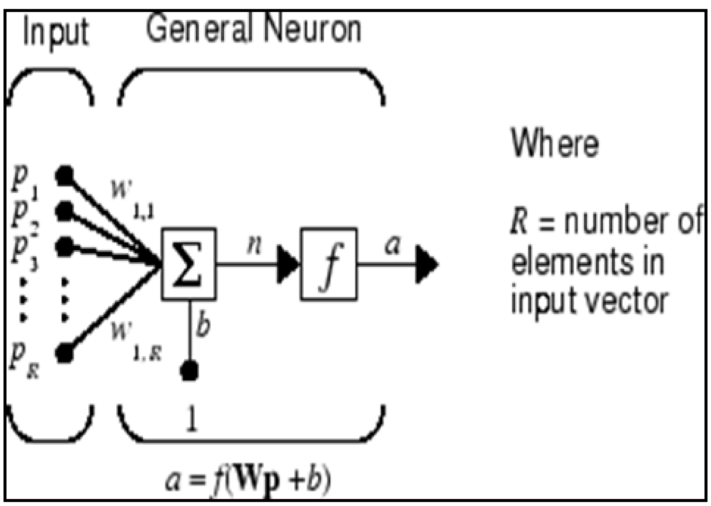

Fig. 4.2 A typical neuron of Artificial Neural Network

Artificial Neural Networks use several forms of Transfer Functions, with the Log-Sigmoid Transfer Function ('logsig'), Tan Sigmoid Transfer Function ('tansig') and Linear Transfer Function ('purelin') being the most often utilized. Once the bias and weights have been initialized, the network is prepared for training. This process involves adjusting the values of the biases and weights to optimize the performance of the network. Performance functions exist for the purpose of analyzing network performance. The default performance function used is Mean Square Error (MSE), which is specified below.

$$mse = \frac{1}{N}\sum_{i=1}^{N}(e_i)^2 = \frac{1}{N}\sum_{i=1}^{N}(t_i - a_i)^2 \tag{4.2}$$

Where, e_i = error, t_i = Target, a_i= output.

Checking consistency of two distinct sets of experimental data using ANN included the careful consideration of the following stages and selection criteria.

4.2.1.1 Consistency Checking of Data Set 1

A multilayer feed-forward neural network is developed to fit the first set of data. This neural network consists of an input layer, a single hidden layer and an output layer. It aims to establish a relationship between a numeric dataset of inputs and a dataset of outputs. The inputs' weights and biases are changed using a conventional backpropagation learning technique. The Neural Network Fitting Tool was used to determine the optimal mix of hidden neurons, training function and transfer function. The modelling of ANN involves the following steps:

Step 1. Selection of Data

At the beginning of this selection procedure, 29 samples of upper nozzle distance (du), lower nozzle distance (dl) and volume flow rate of air ($\dot{v}$) are used as inputs. The inputs are associated with an equivalent number of $\int_0^t T dt$ samples, which represent the goal values defining the network outputs for a thermodynamic parameter **Ƀ**. The input is a matrix with dimensions of 29 rows and 3 columns, while the aim is to get a matrix with dimensions of 29 rows and 1 column.

Step 2. Division of Data

The input vectors and target vectors are partitioned into three distinct data sets in the following manner- (i) Training: The purpose of using this data is to provide the necessary training for the network. (ii) Verification: These data will be used to authenticate the generalization of the Network. (iii) Testing: This data will be used for a totally separate evaluation of network generalization. Various permutations of this split have been experimented with and it has been determined that the 60%-20%-20% division yields the most precise outcome accordingly.

Step3.Creation of Network

Various configurations of hidden neurons and transfer functions have been used in constructing the network structure. The most optimal outcome was achieved while using the sigmoid transfer function ('tansig') in the hidden layer and the linear transfer function ('purelin') in the output layer, with a hidden layer size of 20.

Step 4.Training Network

Various techniques were evaluated and the Levenberg-Marquardt training algorithm of MATLAB (‘trainlm’) was determined to be the most precise when using the Mean Squared Error (MSE) as the performance function. The training halted after six iterations when the validation error got up.

Step 5. Evaluation

The Mean Squared Error (MSE) serves as the performance metric. Performance charts, regression plots and histogram plots are used to verify and assess the network performance.

4.2.1.2 Consistency Checking of Data Set 2

The input parameters for the experiment were the convective heat transfer coefficient ($\boldsymbol{h}$), the volume flow rate of coolant ($\dot{\boldsymbol{v}}$) and the mean specimen temperature ($\boldsymbol{T_{mf}}$). The output parameter measured was the rate of cooling. Three unique artificial neural network training procedures were used to check the consistency of the experimental findings, aiming to verify the effectiveness of the experimental setup in monitoring the cooling rate. For second set of data varification, three separate Neural Network approaches (Network 1, 2 and 3) have been used to train the experimental data. These strategies include different combinations of training, adaptation and performance functions. In both Network-1 and Network-3, the network type, training function, performance function, properties for layer-1 and properties for layer-2 have been respectively specified as 'Feed-forward back-propagation', 'RAINLM', 'MSE', 'TANSIG' and 'PURELIN'. The adaptation function 'LEARNGD' has been used for Network-1, whereas 'LEARNGDM' has been employed for Network-3. The rectified linear activation function (ReLU) has been used in Network 2, specifically with three hidden layers.

The ANN models Network-1 and Network-3 consist of a single input layer, a single hidden layer and a single output layer. Each layer has twenty neurons in the hidden layer and one neuron in the output layer. The input matrix X, with dimensions 3×1, represents the feature values for convective heat transfer coefficient, mean film temperature and volume flow rate of cooling air. Define W_1 as the matrix representing the weights and B1 as the matrix representing the biases of the hidden layer. The matrix W_1 has dimensions of 20×3. Therefore, the multiplication of W_1 and X results in a matrix of dimensions 20 × 1. B_1 is a matrix with dimensions 20 × 1. The intermediate output of the hidden layer may be represented as a matrix.

$$Z_1 = W_1X + B_1 \tag{4.3}$$

The intermediate output undergoes a TANSIG function and is converted to:

$$O_1 = F_1(Z_1) = F_1(W_1X + B_1) \tag{4.4}$$

The weight matrix in the output layer is denoted as W_2 with dimensions of 1×20, whereas the bias matrix is represented by B_2 with dimensions of 1×1. The intermediate result is computed as follows:

$$Z_2 = W_2O_1 + B_2 \tag{4.5}$$

The equation undergoes further transformation using the PURELIN Transfer function, resulting in the final relation:

$$O_2 = F_2(Z_2) = F_2(W_2O_1 + B_2) \tag{4.6}$$

$$O_2 = F_2[W_2F_1(W_1X + B_1) + B_2] \tag{4.7}$$

The network's output, in the form of the cooling rate that has been taught or forecasted, may be expressed as:

$$q = O_2 = F_2[W_2F_1(W_1X + B_1) + B_2] \tag{4.8}$$

Network-2 consists of an input layer, three hidden layers and an output layer. The input layer consists of three parameters i.e., convective heat transfer coefficient, mean film temperature and volume flow rate of air. An activation function is responsible for transforming the combined weighted input of a node into its corresponding activation or output. The inputs undergo a multiplication operation with their respective weights inside a certain node and the results are then summed together. Subsequently, this value undergoes a transformation via an activation function. The Rectified Linear Unit (ReLU) is a function that is linear at different intervals and outputs the input directly if it is positive, else its outputs zero. The ReLU function is defined as f(x) = max(0, x).

An analysis has been conducted on the performance of the networks indicated above, using the correlation coefficient (R) as a crucial performance assessor. The Mean Square Error (MSE) is a crucial metric for evaluating the performance error of networks.

4.3 Cooling Rate Study

In this section of this study, a generation-wise iterative methodology was adopted to investigate the cooling rate, utilizing experimental data as the basis for analysis. Critical thermal and flow parameters namely the heat transfer coefficient ($\boldsymbol{h}$), the mean plate temperature ($\boldsymbol{T_{mf}}$), the volumetric flow rate of the coolant ($\dot{\boldsymbol{v}}$), upper nozzle distance ($\boldsymbol{du}$) and lower distance($\boldsymbol{dl}$) were systematically varied during the simulation process. This approach aimed to assess the impact of these parameters on the cooling rate ($\boldsymbol{q}$), thereby providing insights into the thermal performance of the cooling system from a mechanical engineering perspective.

4.4 Modeling of Correlation

Statistical analysis techniques were employed to evaluate both the strength and direction of the correlation between two continuous quantitative variables. This analysis aimed to quantify how variations in one variable correspond to changes in another, with the broader objective of identifying factors that can enhance the cooling rate. Experimental data served as the foundation for this investigation. Multiple regression models were developed and assessed using SPSS software to determine the most robust values for the correlation coefficient (R) and the coefficient of determination (R-square). Among the models tested, linear regression was found to yield the highest R and R-square values, indicating a strong empirical relationship between the variables. The preference for the linear regression model is attributed to its computational simplicity and efficiency, making it the most suitable method for this analysis.

RESULTS AND DISCUSSION

This crucial chapter presents the findings of a comprehensive investigation, delving into the conclusions derived from rigorous data analysis and their subsequent interpretation. This section offers a thorough examination of the empirical data obtained from research endeavors, expanding on the theoretical framework established in previous chapters. Through meticulous examination of quantitative data and subjective observations, an attempt has been made to uncover the intricate nuances that underpin the objectives and assumptions of this study.

This chapter is an essential phase in the process of collecting and interpreting data to integrate knowledge, emphasizing the importance of the findings in the broader academic discourse. The results will be examined in relation to prior studies and theoretical frameworks in order to comprehend the significance of the research contributions and their possible impact on theory, practice and future research endeavours. The objective is to unearth significant insights by carefully analyzing and reflecting on material, while also recognizing the complexities, limitations and possibilities for additional exploration.

This chapter comprises three main stages of investigation. The first stage focuses on verifying the consistency, accuracy, and reliability of the collected data. In the second stage, the cooling rate of the specimen on ROTs is analyzed in detail. The final stage explores the correlation between the cooling rate (***q***) or associated thermodynamic parameters (**Þ**= $\int_0^T Tdt$) and various experimental factors, providing a comprehensive understanding of the underlying phenomena. Where in the thermodynamic parameter, ***T*** denotes temperature and ***dt*** represents an infinitesimal time interval; therefore, the parameter **Þ** corresponds to the time-integrated temperature history during the cooling process. This parameter reflects the cumulative thermal exposure of the material, indicating the duration for which it remains at elevated temperatures, and is useful for interpreting cooling behavior, thermal history effects, and the resulting changes in material properties.

5.1 Consistency Checking of Experimental Data

Two separate datasets have been selected to check the consistency of the experimental data before using them in regression analysis to determine correlations between the thermodynamic parameter (Þ) or cooling rate ($\boldsymbol{q}$) and independent observed data from the experimental setup.

5.1.1 Consistency Analysis of Data Set 1

The dataset consists of 29 samples of upper nozzle distance ($\boldsymbol{du}$), lower nozzle distance ($\boldsymbol{dl}$) and volume flow rate of coolant ($\dot{\boldsymbol{v}}$), which are used as input variables. The goal values for the neural network outputs are defined by the same number of samples $\int_0^T \boldsymbol{T}d\boldsymbol{t}$, which represents a thermodynamic parameter **Þ**. The number of neurons in the hidden layer is adjusted to determine the ideal size of the hidden layer. The performance index is selected as the mean squared error (MSE) and the correlation coefficient (R). The Table 5.1.1.1 displays the Mean Square Error (MSE), Overall Correlation Coefficient (R) and the hidden layer size of the networks. The MSE (Mean Squared Error) measurements quantify the average of the squared differences between the actual and projected values. Smaller numbers suggest better performance in terms of model accuracy. The correlation coefficient provides a quantitative estimate of the magnitude and direction of a linear association between the observed and expected values. A score approaching 1 indicates a robust positive correlation, while a value approaching -1 signifies a strong negative correlation. A number close to 0 shows the absence of a linear association. According to Table 5.1.1.1, the correlation coefficient (R) value of 3-20-1 model is 0.7929, which suggests a robust positive association between the actual and anticipated values. Overall, the 3-20-1 model has superior performance compared to the other models presented. This is evident from its highest correlation coefficient of 0.7929 and the lowest mean squared error (MSE) value of 9.97×10^{-23}, which signifies excellent predictive capabilities shown in Fig. (5.1.1.1).

Table 5.1.1.1 Comparison of Neural Structure

ANN	Structure-I	Structure-II	Structure-III	Structure-IV
Structure	3-15-1	3-20-1	3-25-1	3-30-1
MSE	4.89×10^{-16}	9.97×10^{-23}	9.97×10^{-23}	9.97×10^{-23}
Overall Correlation Coefficient (R)	0.1455	0.7929	0.5829	0.3256

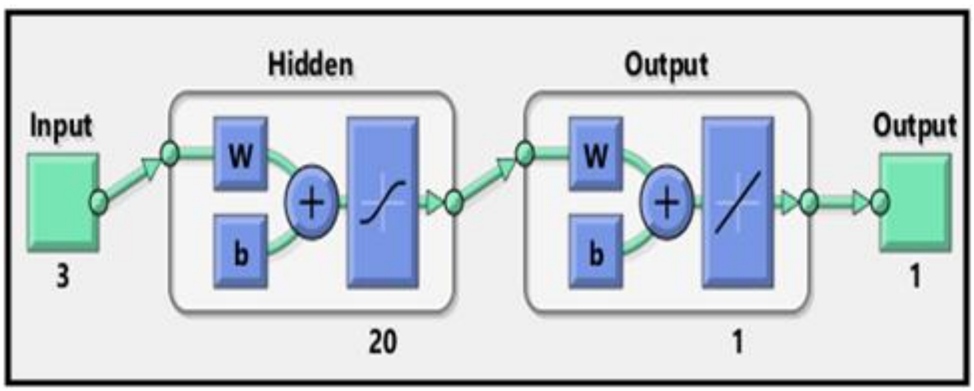

Fig. 5.1.1.1 Neural Network Architecture

When the network was trained using the Levenberg-Marquardt training function of MATLAB in this form, a corresponding output has been generated for each input. The training process is halted at iteration 6 due to the Mean Squared Error (MSE) reaching a value of 9.97×10^{-23}. Fig. (5.1.1.2) displays a graph depicting the training error, validation error and test error. This indicates that the outcome is plausible since the final Mean Square Error is very low and the training error and validation error exhibit comparable patterns and traits. Furthermore, there is no notable occurrence of overfitting by the third iteration, which is also when the highest validation performance is achieved. Fig. (5.1.1.3) illustrates the regression plot indicating the relationship between the network output and the related target during the validation phase. The regression analysis conducted between the network outputs and the associated targets, as shown in Fig. (5.1.1.3), reveals an overall Coefficient of Correlation of R= 0.79293, indicating a strong agreement. Further validation of the Network's performance is derived from the Error Histogram, which displays the extreme values where errors are concentrated around zero (meaning that, on a typical basis, the observed weights are near to the anticipated value) as seen in Fig. (5.1.1.4). A comparison is made between the outputs that were anticipated and the actual goals that were measured and the results of this comparison are graphically shown in Fig. (5.1.1.5). The point at

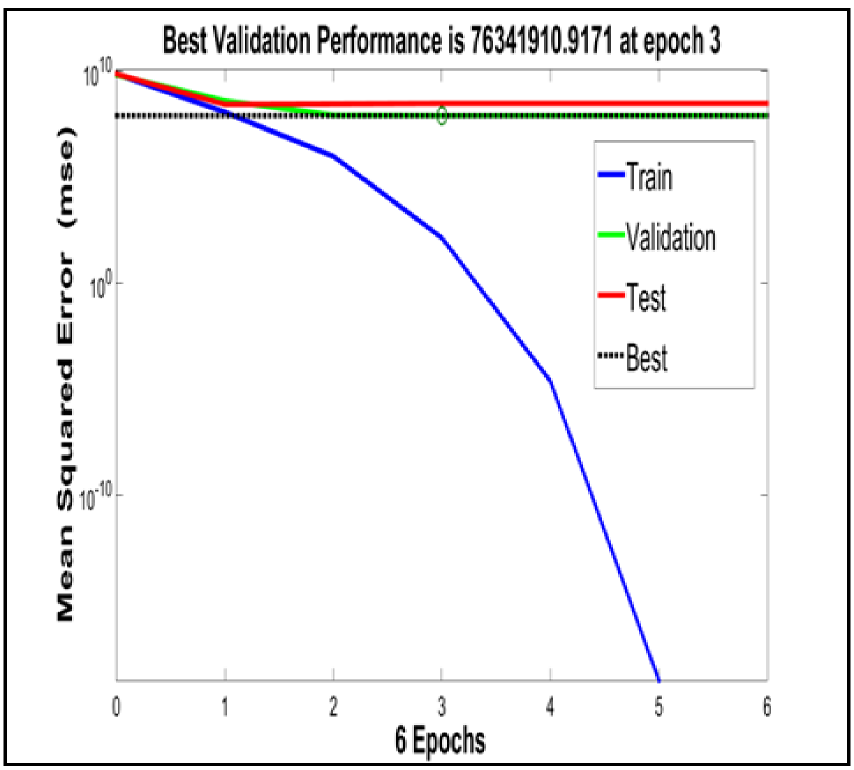

Fig. 5.1.1.2 Performance plot

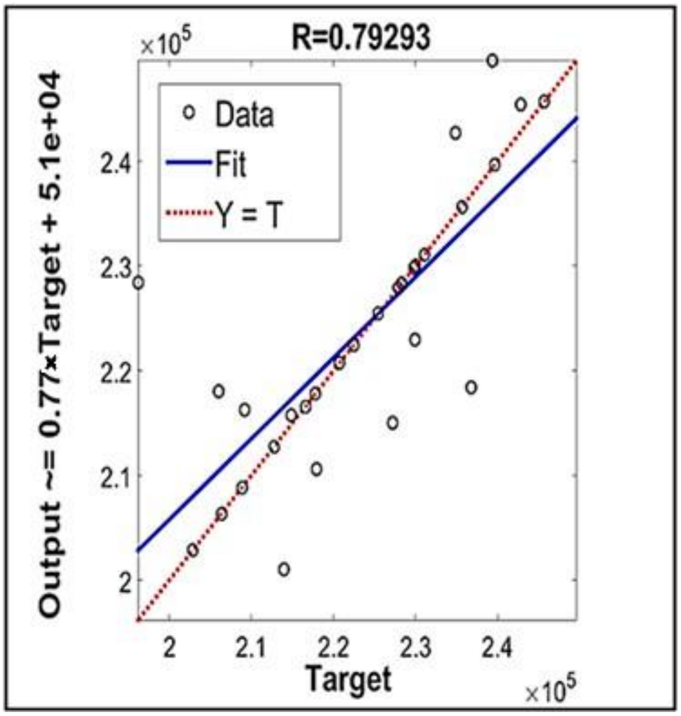

Fig. 5.1.1.3 Regression plot between output & target

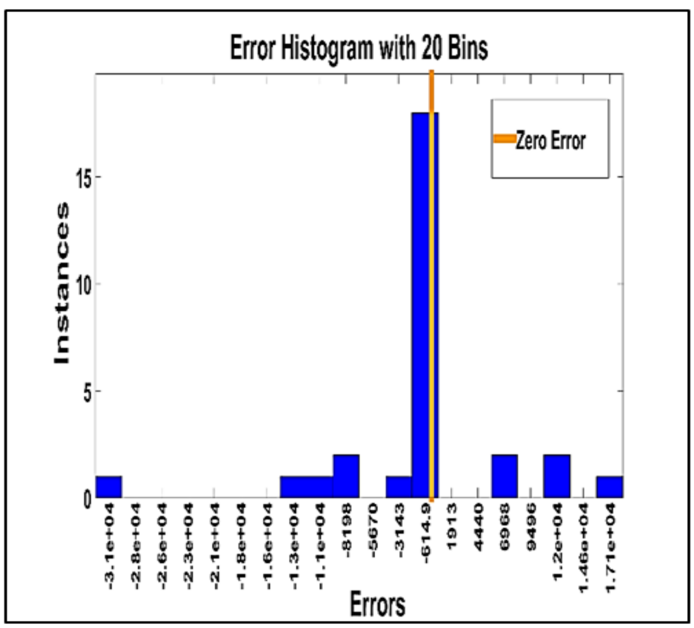

Fig. 5.1.1.4 Error Histogram

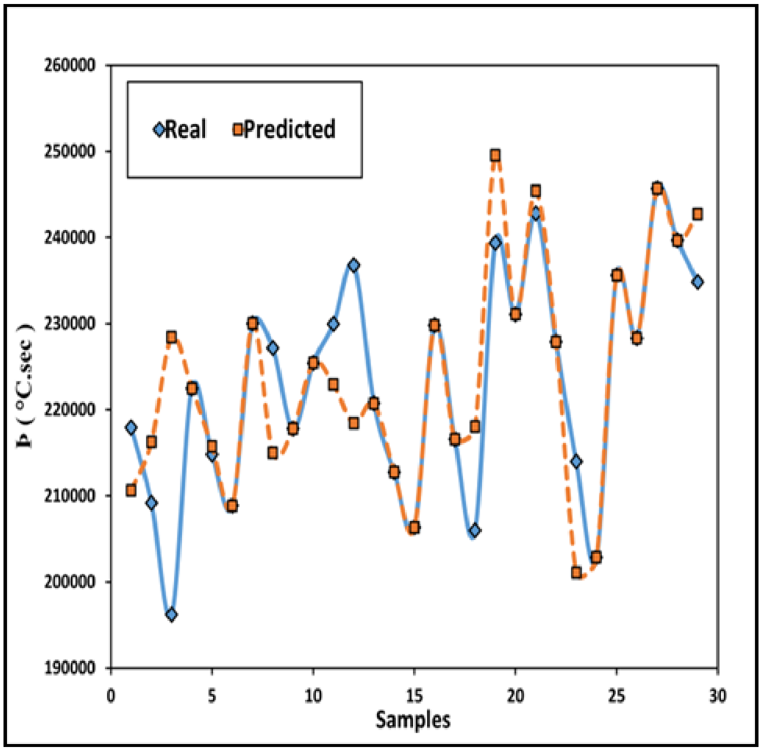

Fig. 5.1.1.5 Predicted output Vs Real measured target

which the curve overlaps by a large amount, which is an indication of how accurately the Artificial Neural Network performs. Hence, it can be concluded that employing the specified network for consistency verification of the experimental data is a favorable approach. This method not only enhances the reliability of the data but also lays a solid foundation for subsequent stages of the research, particularly in developing models to correlate the thermodynamic parameter with the independent experimental variables.

5.1.2 Consistency Analysis of Data Set 2

A study was conducted employing an Artificial Neural Network (ANN) to predict the cooling rate of a test specimen. The analysis considered the effects of variations in the convective heat transfer coefficient, the volumetric flow rate of cooling air, and the mean surface temperature of the heated plate on the cooling performance. During the second phase of data acquisition, the spacing between the upper and lower nozzle banks was held constant to ensure controlled conditions. To check the consistency and reliability of the experimental results, three distinct ANN methodologies were applied. In order to assess the effectiveness of the network, cooling rate versus convective heat transfer coefficient histories, together with their respective errors, were utilized. Fig. (5.1.2.1) demonstrates the relationship between the cooling rate (***q***) and the convective heat transfer coefficient (***h***) of network1. Based on Fig. (5.1.2.1), the overall coefficient of correlation (R) value for Network-1 is 0.9997. Fig. (5.1.2.2) depicts the error plot for Network-1, with an MSE value of 0.00025. The relationship between the cooling rate (***q***) and the convective heat transfer coefficient (***h***) of network 2 is shown in Fig. (5.1.2.3). The value of the Overall Coefficient of Correlation (R) is demonstrated to be 0.9993. A mean squared error (MSE) value of 0.00075 is used to illustrate the error plot for Network-2, which can be seen in Fig. (5.1.2.4). Fig. (5.1.2.5) illustrates the relationship that exists between the convective heat transfer coefficient (***h***) of network 3 and the corresponding cooling rate (***q***). Based on the data shown in Fig. (5.1.2.5), the overall value of the coefficient of correlation (R) for Network-3 is 0.9997. The error curve seen in Fig. (5.1.2.6) is for Network-3, which has a mean squared error value of 0.00045. Indicative of the consistency of the experimental arrangement and the data it provided, which may be used in the future to improve the cooling rate, the results of all three network models are pretty close to one another. This is an indicator of the consistency of the experimental design. It has been found that the 'R' values are much closer to unity in each and every plot. There is a significant degree of overlap between the predicted and experimental cooling rates, as seen in Fig. (5.1.2.1), Fig. (5.1.2.3) and Fig. (5.1.2.5), which is evidence that all of the neural training is precisely correct. It proved that Network-1 was the most appropriate choice among the three models because it showed a higher degree of correlation coefficient (R=0.9997) and a lower mean square error (MSE=0.00025). This indicates that Network-1 is the most suitable selection for training the experimental data in order to analyze the cooling rate in the subsequent phase of this study.

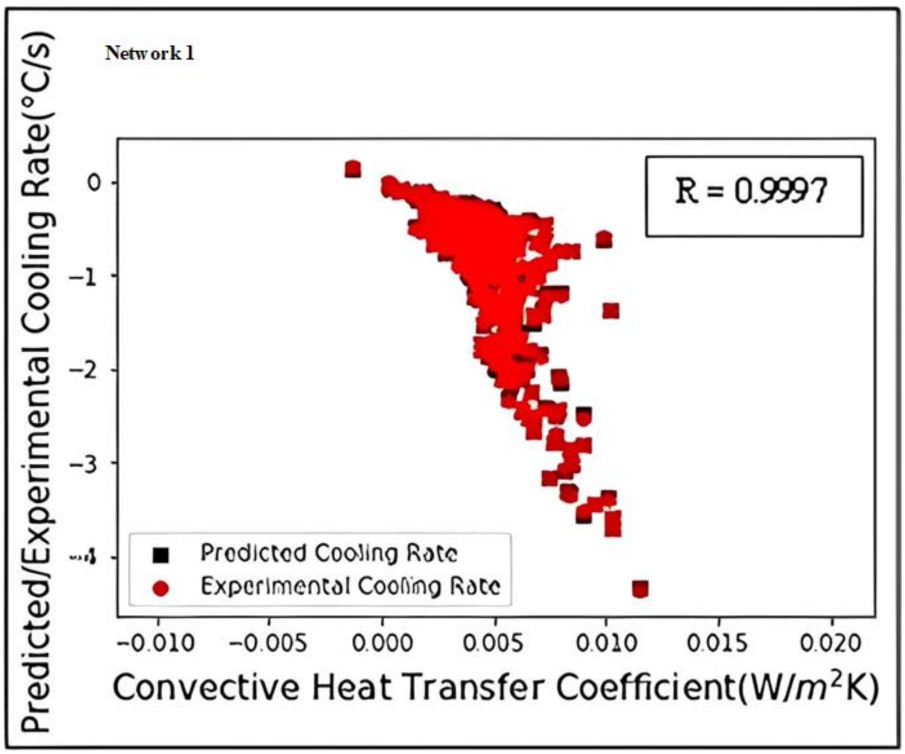

Fig. 5.1.2.1 Comparison between predicted and experimental cooling rate for Network-1

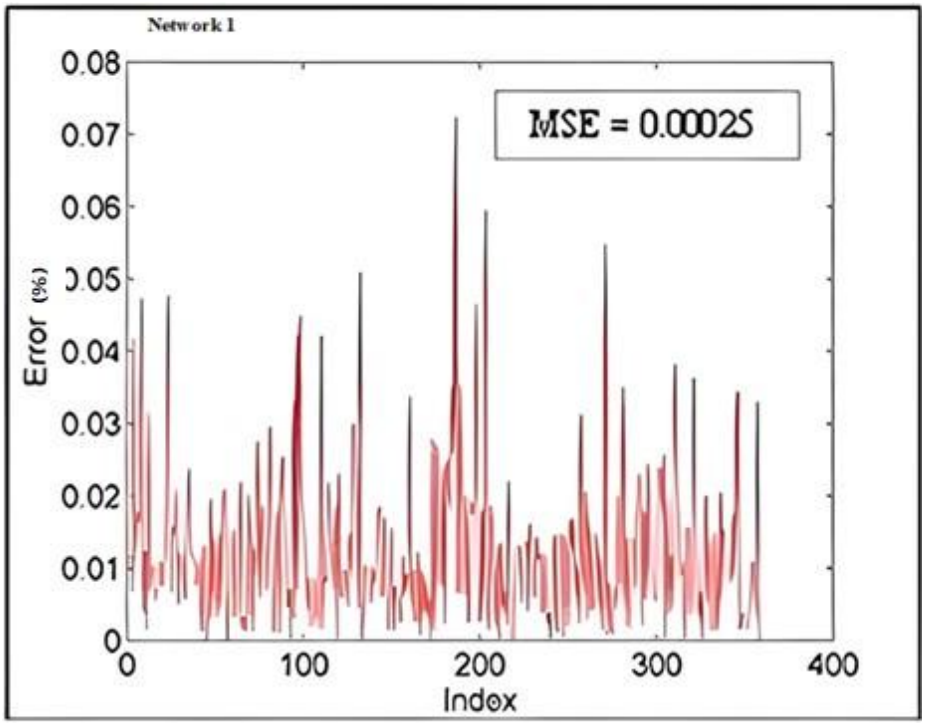

Fig. 5.1.2.2 Error plot for Network-1

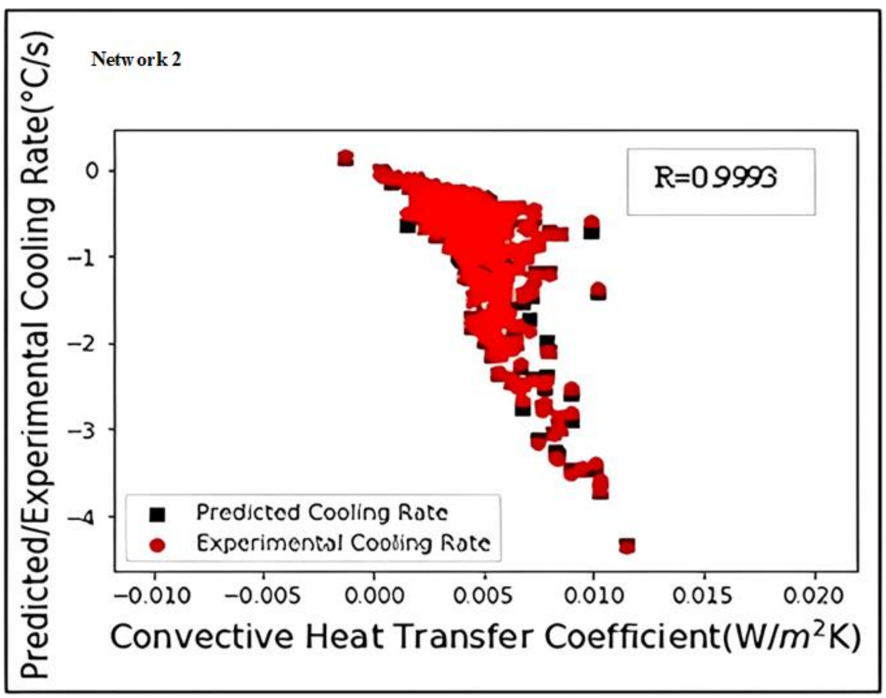

Fig. 5.1.2.3 Comparison between predicted and experimental cooling rate for Network-2

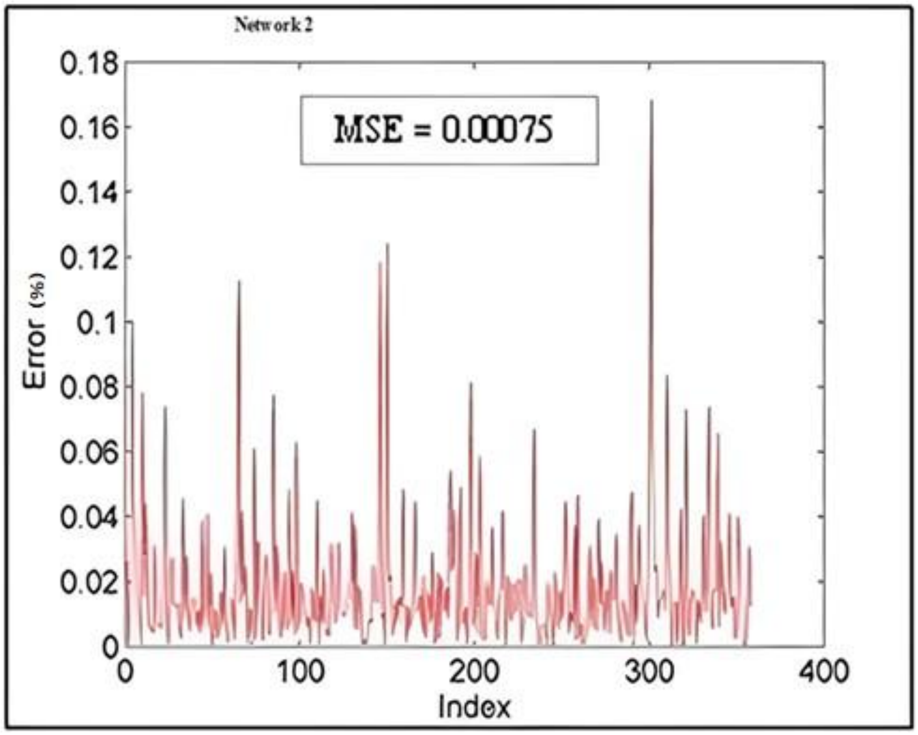

Fig. 5.1.2.4 Error plot for Network-2

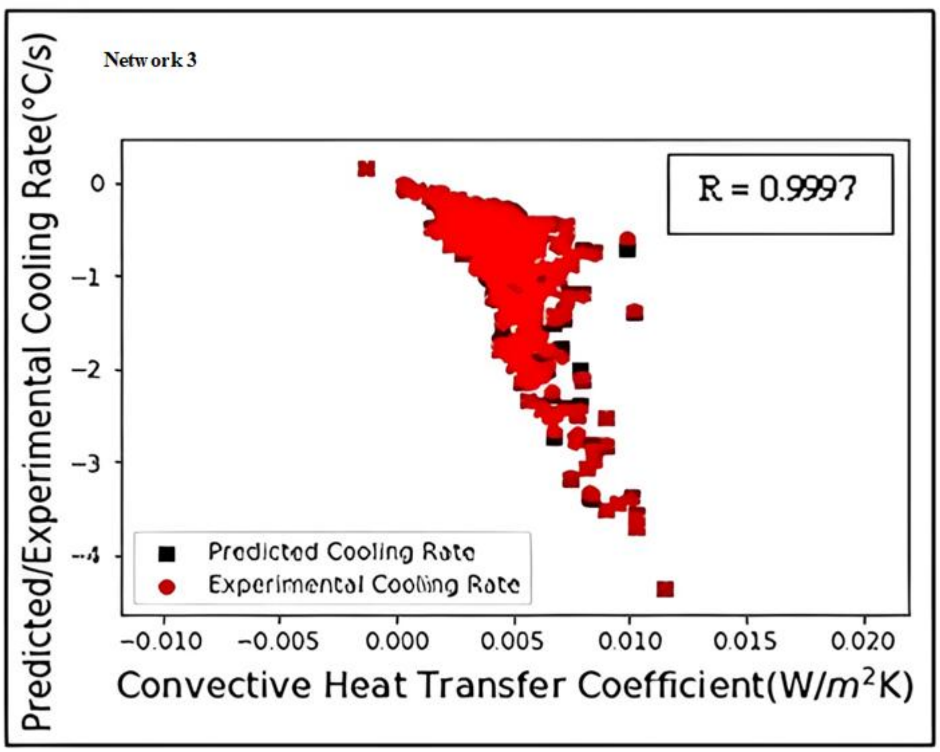

Fig. 5.1.2.5 Comparison between predicted and experimental cooling rate for Network-3

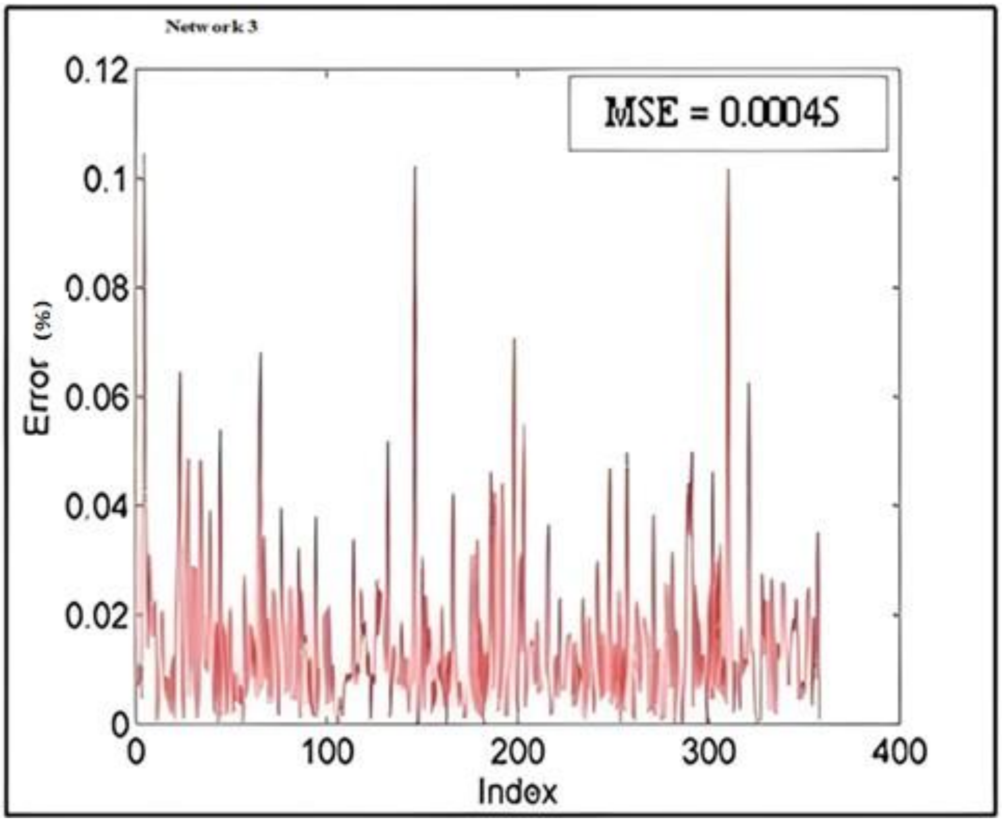

Fig. 5.1.2.6 Error plot for Network-3

5.2 Cooling Rate Study

In this section of the dissertation detailed the analysis of the generation wise cooling study. Throughout the course of twenty generations shown in Table 5.2.1, fundamental metrics such as the heat transfer coefficient ($\boldsymbol{h}$), the mean plate temperature ($\boldsymbol{T_{mf}}$), the volume flow rate ($\dot{\boldsymbol{v}}$), upper nozzle distance ($\boldsymbol{du}$), lower nozzle distance ($\boldsymbol{dl}$) and the cooling rate ($\boldsymbol{q}$) were tracked and recorded. An examination of the behaviour of cooling rate and standard deviation trends throughout generations was carried out and the results revealed that there have been considerable advancements made in subsequent iterations.

Experimental data was obtained throughout 20 generations, with each generation signifying an improvement in the cooling rate. The primary metrics monitored consist of the mean cooling rate ($\boldsymbol{q_{mean}}$), standard deviation (SD) and the range of values established by ‘ $\boldsymbol{q_{mean}}$ ± 2SD’. During the initial Generations (1-5), cooling rates shown relatively low values, accompanied by significant variability. During the mid-generations (6-15), there was a gradual increase in cooling rates. A significant decrease in variability was observed, indicated by the contraction of the standard deviation. During the final Generations (16-20), cooling rates reached their maximum and the variability experienced a slight increase once more. The mean values of the cooling rate indicate a trend towards optimal conditions of this study. The cooling rate shows an individual upward trend across generations. This section focuses on analyzing the influence of each independent parameter on the cooling rate.

During the initial Generations (1-5), cooling rates shown relatively low values, accompanied by significant variability. During the mid-generations (6-15), there was a gradual increase in cooling rates, which indicates progress of cooling rate. A significant decrease in variability was observed, indicated by the contraction of the standard deviation. During the final Generations

(16-20), cooling rates reached their maximum and the variability experienced a slight increase once more. The mean values of the cooling rate indicate a trend towards maximum value.

Table 5.2.1 Experimental Data on Cooling Rate

Generation	h (W/m^2-K)	T_{mf} (°C)	du (mm)	dl (mm)	$\dot{v}$ (m^3/h)	q (°C/Sec)
1	0.003552	120.0198	122	122	6	0.2684
1	0.003406	107.8621	124	124	7	0.2455
1	0.002739	121.0948	126	126	7	0.2288
1	0.003006	106.5281	128	128	7	0.2114
1	0.002217	129.9112	130	130	8	0.1782
1	0.001602	120.1903	132	132	6	0.1232
1	0.000771	180.0405	134	134	8	0.0943
1	0.000425	231.2053	136	136	6	0.07
1	0.000919	122.2506	138	138	6	0.0692
1	0.000359	222.4644	140	140	6	0.0553
2	0.004123	117.0611	116	116	8	0.3125
2	0.003764	121.5102	118	118	8	0.2935
2	0.00389	119.65	120	118	6	0.2891
2	0.003547	130.8934	120	120	8	0.2875
2	0.002858	144.5944	122	120	8	0.279
2	0.003552	120.0198	122	122	6	0.2684
2	0.003222	113.8374	122	124	7	0.2537
2	0.003406	107.8621	124	124	7	0.2455
2	0.002739	121.0948	126	126	7	0.2288
2	0.002217	129.9112	130	130	8	0.1782
3	0.002431	209.396	110	110	8	0.3452
3	0.002406	177.4932	110	112	7	0.3197
3	0.002769	155.0749	112	112	7	0.3177
3	0.003552	120.0198	114	114	6	0.2684
3	0.004123	117.0611	116	114	8	0.3125
3	0.004797	103.95	116	116	8	0.3044
3	0.004505	102.3859	118	116	7	0.3011
3	0.003764	121.5102	118	118	8	0.2935
3	0.00389	119.65	120	118	6	0.2891
3	0.003222	113.8374	122	124	7	0.2537

Generation	*h* (W/m²-K)	T_{mf} (°C)	*du* (mm)	dl (mm)	v̇ (m³/h)	*q* (°C/Sec)
4	0.004618	115.2279	110	106	7	0.3702
4	0.002917	163.2401	110	108	7	0.3594
4	0.004583	125.7218	110	114	8	0.352
4	0.004919	118.3017	108	108	7	0.3905
4	0.003288	159.233	110	108	8	0.3475
4	0.003764	121.5102	112	114	8	0.2935
4	0.004694	109.1151	110	109	7	0.337
4	0.002406	177.4932	110	112	7	0.3197
4	0.002769	155.0749	112	112	7	0.3177
4	0.004797	103.95	116	116	8	0.3044
5	0.003971	154.3074	104	104	8	0.4101
5	0.0033	190.7171	104	106	6	0.4097
5	0.00385	150.7443	106	106	7	0.4027
5	0.004919	118.3017	108	106	7	0.3905
5	0.003095	168.2976	108	108	7	0.3883
5	0.002769	155.0749	112	112	7	0.3177
5	0.003288	159.233	110	108	8	0.3475
5	0.004618	115.2279	110	106	7	0.3702
5	0.002917	163.2401	110	108	7	0.3594
5	0.004583	125.7218	110	114	8	0.352
6	0.004531	143.0108	96	96	8	0.4379
6	0.005761	125.235	96	98	8	0.4363
6	0.006165	115.3374	98	98	8	0.436
6	0.006292	110.3652	100	98	6	0.4334
6	0.00596	110.6741	100	100	7	0.4331
6	0.003666	160.0379	102	102	7	0.4308
6	0.005234	132.0773	102	104	8	0.4279
6	0.003971	154.3074	104	104	8	0.4101
6	0.0033	190.7171	104	106	6	0.4097
6	0.004618	115.2279	110	106	7	0.3702
7	0.005255	142.6262	88	88	6	0.505
7	0.004202	184.2187	90	90	8	0.4889
7	0.004795	153.3467	92	90	6	0.4881
7	0.004431	171.9708	92	92	6	0.4769
7	0.006146	123.9081	94	92	8	0.4743
7	0.004598	149.1832	94	94	8	0.4669
7	0.00332	210.0393	96	94	8	0.4658
7	0.004531	143.0108	96	96	8	0.4379
7	0.006292	110.3652	100	98	6	0.4334
7	0.00596	110.6741	100	100	7	0.4331

Generation	***h* (W/m²-K)**	**T_{mf} (°C)**	***du* (mm)**	***dl* (mm)**	**$\dot{v}$ (m³/h)**	***q* (°C/Sec)**
8	0.00411	215.7308	80	80	8	0.5846
8	0.004923	170.4825	82	80	8	0.5792
8	0.0054	164.8695	82	82	6	0.5778
8	0.004641	166.3234	84	82	7	0.5761
8	0.006103	140.397	84	84	6	0.5593
8	0.003443	209.8318	86	86	7	0.5381
8	0.005189	151.8884	86	88	6	0.5321
8	0.005255	142.6262	88	88	6	0.505
8	0.004202	184.2187	90	90	8	0.4889
8	0.004795	153.3467	92	90	6	0.4881
9	0.004243	213.1845	74	72	7	0.6669
9	0.004268	198.9271	74	74	7	0.6413
9	0.004183	195.6147	76	74	7	0.628
9	0.004994	186.25	76	76	6	0.6195
9	0.003674	222.8113	78	76	7	0.6088
9	0.003892	210.6698	78	78	7	0.6072
9	0.003686	221.9724	80	78	7	0.6042
9	0.00411	215.7308	80	80	8	0.5846
9	0.0054	164.8695	82	82	6	0.5778
9	0.004641	166.3234	84	82	7	0.5761
10	0.006003	177.0895	66	66	8	0.7373
10	0.004231	252.0653	68	66	8	0.7246
10	0.003694	282.487	68	68	8	0.7185
10	0.005131	211.9445	68	70	8	0.7154
10	0.004185	236.7993	70	70	6	0.7005
10	0.004247	233.3289	70	72	8	0.6902
10	0.003608	241.2612	72	72	7	0.6784
10	0.004243	213.1845	74	72	7	0.6669
10	0.004268	198.9271	74	74	7	0.6413
10	0.004183	195.6147	76	74	7	0.628
11	0.004899	230.2672	62	62	7	0.8316
11	0.00375	284.1905	62	64	7	0.8189
11	0.004142	291.046	64	64	8	0.8087
11	0.005414	221.3187	64	64	8	0.8001
11	0.007463	160.7105	64	66	8	0.79
11	0.003594	309.0175	66	66	6	0.7762
11	0.005304	218.9426	66	66	8	0.7757
11	0.006003	177.0895	66	66	8	0.7373
11	0.004231	252.0653	68	66	8	0.7246
11	0.004185	236.7993	70	70	6	0.7005

Generation	***h* (W/m^2-K)**	**T_{mf} (°C)**	***du* (mm)**	***dl* (mm)**	**$\dot{v}$ (m^3/h)**	***q* (°C/Sec)**
12	0.00339	373.3063	58	58	6	0.915
12	0.004447	262.7732	58	58	7	0.9061
12	0.003883	295.3372	58	58	7	0.8907
12	0.007411	179.0475	58	60	6	0.8862
12	0.005106	252.9121	60	60	6	0.8807
12	0.006948	197.6454	62	60	6	0.8728
12	0.003433	319.4184	62	62	7	0.8596
12	0.004899	230.2672	62	62	7	0.8316
12	0.00375	284.1905	62	64	7	0.8189
12	0.004142	291.046	64	64	8	0.8087
13	0.004383	296.7241	55	55	7	1.0116
13	0.004198	315.5326	56	56	7	1.0067
13	0.004479	319.3582	56	56	6	0.9624
13	0.003789	334.5951	57	58	7	0.9575
13	0.005231	239.1293	57	58	7	0.9572
13	0.004705	259.0375	56	58	7	0.9478
13	0.004784	289.9284	58	58	8	0.931
13	0.003998	334.3638	56	58	6	0.9197
13	0.00339	373.3063	58	58	6	0.915
13	0.004447	262.7732	58	58	7	0.9061
14	0.005007	326.3118	56	55	7	1.2665
14	0.007288	249.2251	56	56	8	1.2471
14	0.005212	312.3884	57	56	7	1.2471
14	0.005558	291.5733	56	56	7	1.2442
14	0.007971	220.5698	57	57	6	1.2083
14	0.005995	243.5884	57	56	7	1.1335
14	0.004435	331.827	56	55	7	1.1135
14	0.004383	296.7241	55	55	7	1.0116
14	0.004198	315.5326	56	56	7	1.0067
14	0.004479	319.3582	56	56	6	0.9624
15	0.004596	415.871	55	56	7	1.448
15	0.006869	309.6361	60	58	8	1.4458
15	0.004669	400.3625	57	56	7	1.4091
15	0.00487	418.5581	57	57	6	1.3929
15	0.01018	206.4053	55	56	6	1.3825
15	0.005842	339.2667	56	55	6	1.3465
15	0.004967	390.3042	56	56	8	1.3431
15	0.005081	403.7072	58	57	8	1.3417
15	0.005007	326.3118	56	55	7	1.2665
15	0.007288	249.2251	56	56	8	1.2471

Generation	h (W/m^2-K)	T_{mf} (°C)	du (mm)	dl (mm)	$\dot{v}$ (m^3/h)	q (°C/Sec)
16	0.007005	370.8113	55	54	8	1.874
16	0.004681	532.0874	58	57	7	1.8495
16	0.006289	394.4516	56	55	7	1.7989
16	0.005627	411.8121	56	57	7	1.7654
16	0.005169	466.8553	57	58	7	1.7573
16	0.005327	485.2531	58	58	6	1.7462
16	0.004596	415.871	57	57	7	1.448
16	0.006869	309.6361	60	58	8	1.4458
16	0.004669	400.3625	57	56	7	1.4091
16	0.00487	418.5581	57	57	6	1.3929
17	0.007645	530.8891	58	58	8	2.7785
17	0.007773	518.9824	56	57	6	2.7011
17	0.008973	422.8375	55	57	8	2.5186
17	0.006728	503.2687	57	55	7	2.5127
17	0.007853	441.1431	55	56	6	2.4233
17	0.006186	529.5497	56	57	7	2.4058
17	0.005633	582.5826	58	57	7	2.3382
17	0.007005	370.8113	55	54	8	1.874
17	0.007005	370.8113	55	54	8	1.874
17	0.004681	532.0874	58	57	7	1.8495
18	0.011418	553.2488	55	55	8	4.3485
18	0.010281	534.0146	56	55	6	3.7096
18	0.010298	511.7743	58	57	8	3.5802
18	0.008365	587.4482	54	56	6	3.3577
18	0.008255	577.4148	58	56	8	3.3309
18	0.008962	475.3329	56	57	8	2.8021
18	0.007645	530.8891	58	58	8	2.7785
18	0.007773	518.9824	56	57	6	2.7011
18	0.008973	422.8375	55	57	8	2.5186
18	0.006728	503.2687	57	55	7	2.5127

Generation	h (W/m2-K)	T_{mf} (°C)	du (mm)	dl (mm)	$\dot{v}$ (m^3/h)	q (°C/Sec)
19	0.011418	553.2488	55	55	8	4.3485
19	0.011418	553.2488	55	55	8	4.3485
19	0.011418	553.2488	55	55	8	4.3485
19	0.010281	534.0146	56	55	6	3.7096
19	0.010281	534.0146	56	55	6	3.7096
19	0.010281	534.0146	56	55	6	3.7096
19	0.010298	511.7743	58	57	8	3.5802
19	0.008365	587.4482	54	56	6	3.3577
19	0.008255	577.4148	58	56	8	3.3309
20	0.011418	553.2488	55	55	8	4.3485
20	0.011418	553.2488	55	55	8	4.3485
20	0.011418	553.2488	55	55	8	4.3485
20	0.011418	553.2488	55	55	8	4.3485
20	0.011418	553.2488	55	55	8	4.3485
20	0.011418	553.2488	55	55	8	4.3485
20	0.010281	534.0146	56	55	6	3.7096
20	0.010298	511.7743	58	57	8	3.5802
20	0.008365	587.4482	54	56	6	3.3577
20	0.008255	577.4148	58	56	8	3.3309

The cooling rate demonstrates a consistent increase across successive generations. The study contributed to improved stability in performance metrics during intermediate generations. An optimal balance was achieved among key factors, including heat transfer efficiency, coolant flow rate, upper and lower nozzle distances, and plate temperature.

5.2.1 Results and Analysis of Cooling Rate Study

In the first five generations, the cooling rates that were detected were rather modest, with averages ranging from 0.15 to 0.37. A significant improvement in cooling rates has been found, with averages ranging from 0.42 to 1.36 in the mid-generations (generations 6-15). This indicates that cooling rates have significantly improved. There was a major stabilization of the system over the middle generations, as shown by the decrease in variability between generations. By the 20th generation of the final generation (generations 16-20), peak cooling rates had been achieved, with values reaching 4.01 by the time the generation finished. Due to the significant reduction in variability, it may be concluded that the system has become more stable. There was a modest rise in the standard deviation, which indicates that there were some tiny variations around the ideal circumstances**.**

Over twenty generations, a consistent rise in the cooling rate has been observed, demonstrating the effectiveness of the cooling study, as shown in Fig. 5.2.1. The narrowing of confidence intervals ($\boldsymbol{q_{mean}}$ ± 2SD) during the middle generations reflects improved stability, while a slight widening is noted in later stages. Figures 5.2.2 and 5.2.3(a–e) further illustrate the upward trend in cooling rate ($\boldsymbol{q}$), with values progressively approaching the upper statistical threshold ($\boldsymbol{q_{mean}}$ + 2SD), where SD denotes the standard deviation.

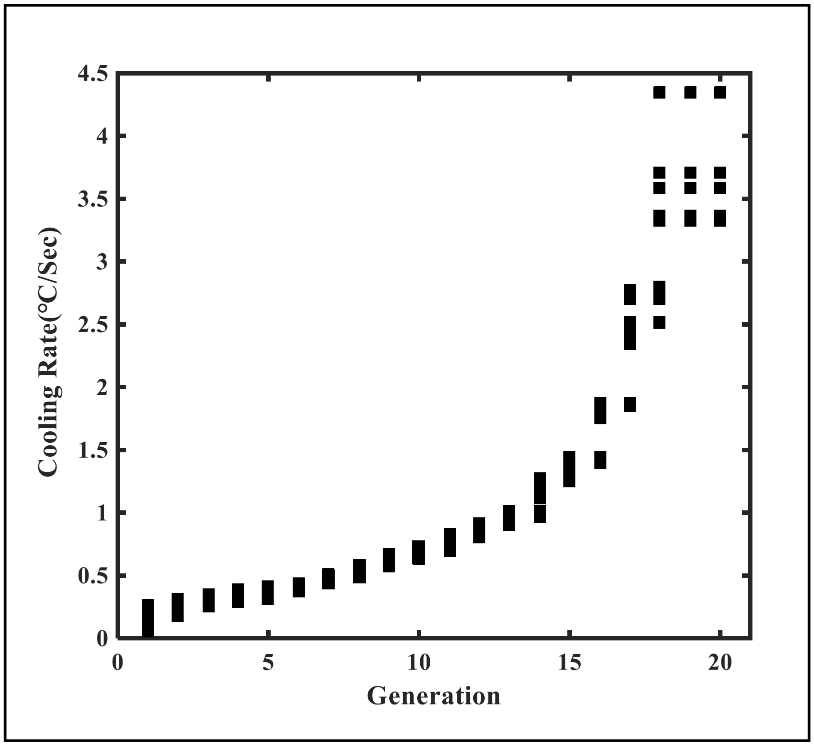

Fig. 5.2.1 Generation Vs Cooling Rate

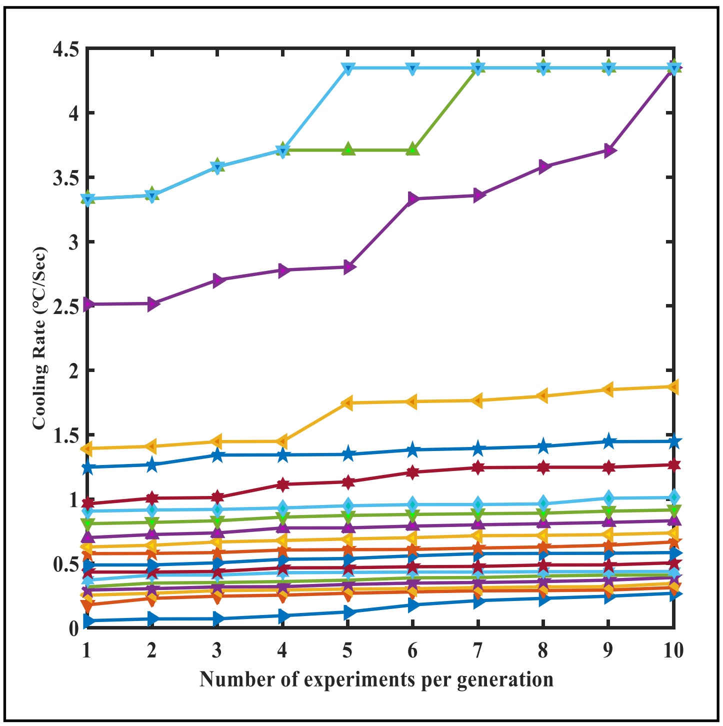

Fig. 5.2.2 Evolution of Cooling Rate over Successive Experimental Generations

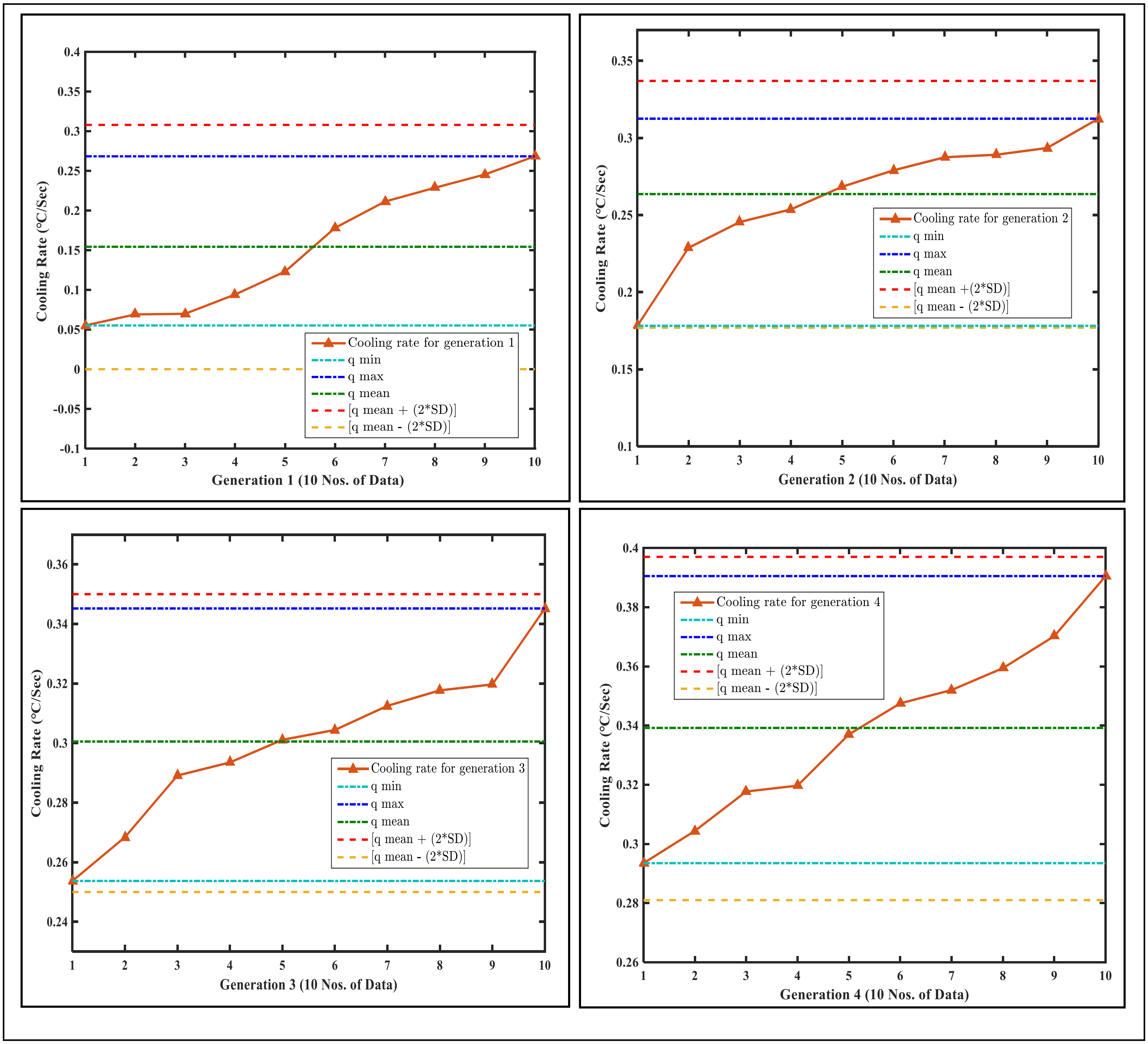

Cooling Rate (ºC/Sec)
Generation 1 (10 Nos. of Data)
Cooling rate for generation 1
q min
q max
q mean
[q mean + (2*SD)]
[q mean - (2*SD)]
Generation 2 (10 Nos. of Data)
Cooling rate for generation 2
[q mean +(2*SD)]
Generation 3 (10 Nos. of Data)
Cooling rate for generation 3
Generation 4 (10 Nos. of Data)
Cooling rate for generation 4

(a)

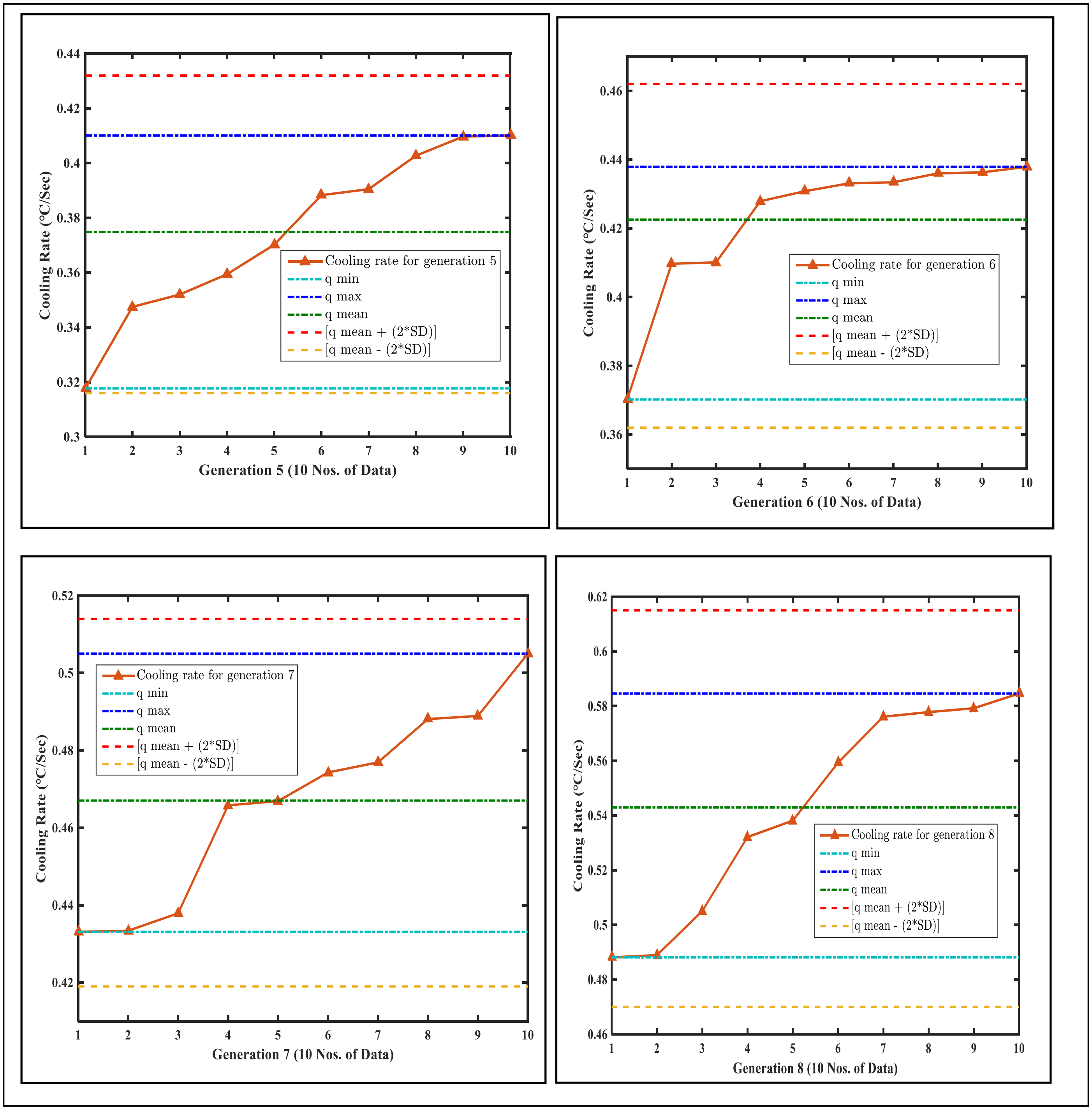
Cooling Rate (°C/Sec)
Generation 5 (10 Nos. of Data)
Cooling rate for generation 5
q min
q max
q mean
[q mean + (2*SD)]
[q mean - (2*SD)]
Generation 6 (10 Nos. of Data)
Cooling rate for generation 6
Generation 7 (10 Nos. of Data)
Cooling rate for generation 7
Generation 8 (10 Nos. of Data)
Cooling rate for generation 8

(b)

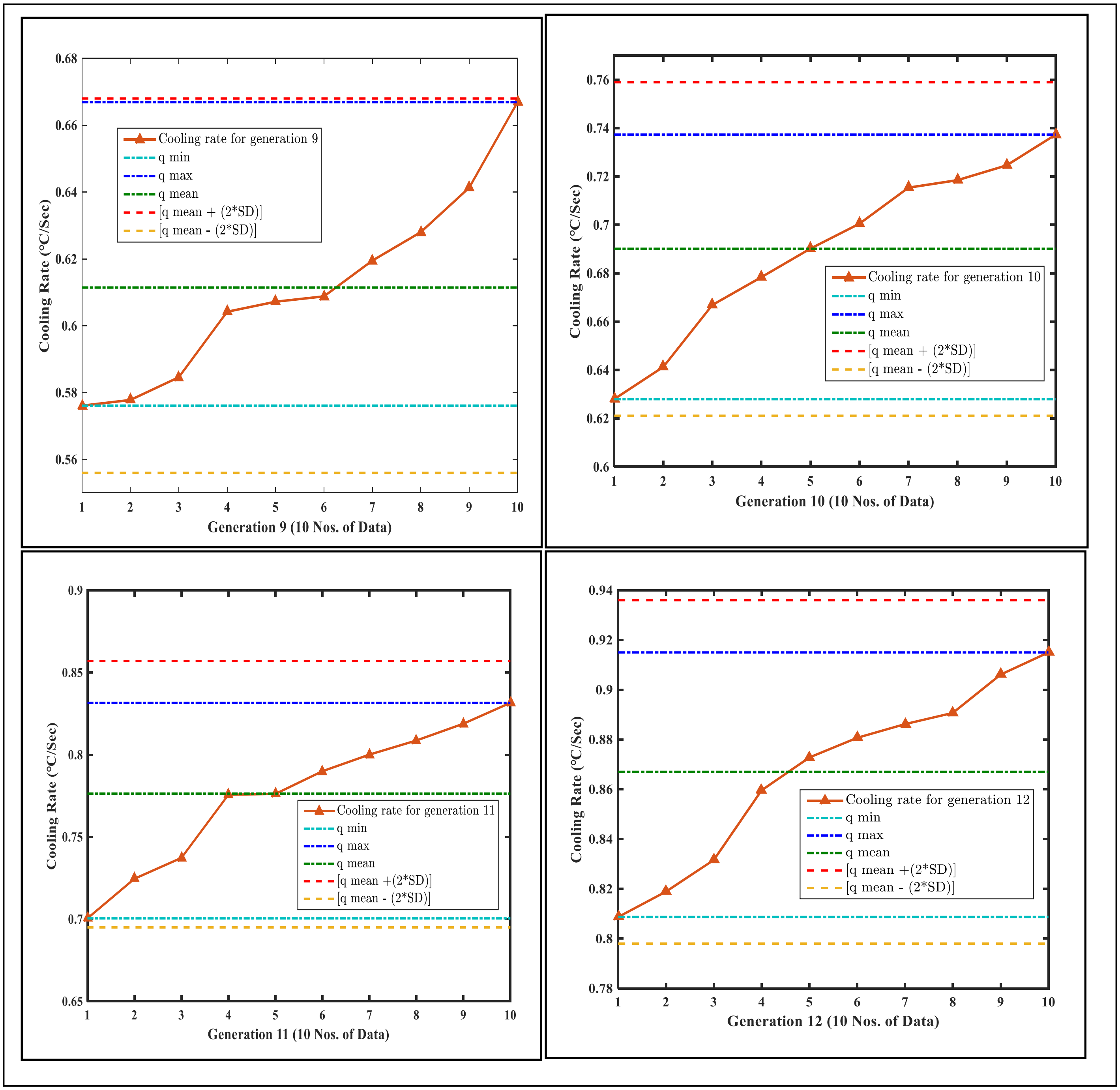
Cooling Rate (°C/Sec)
Generation 9 (10 Nos. of Data)
Cooling rate for generation 9
q min
q max
q mean
[q mean + (2*SD)]
[q mean - (2*SD)]
Generation 10 (10 Nos. of Data)
Cooling rate for generation 10
Generation 11 (10 Nos. of Data)
Cooling rate for generation 11
[q mean +(2*SD)]
Generation 12 (10 Nos. of Data)
Cooling rate for generation 12

(c)

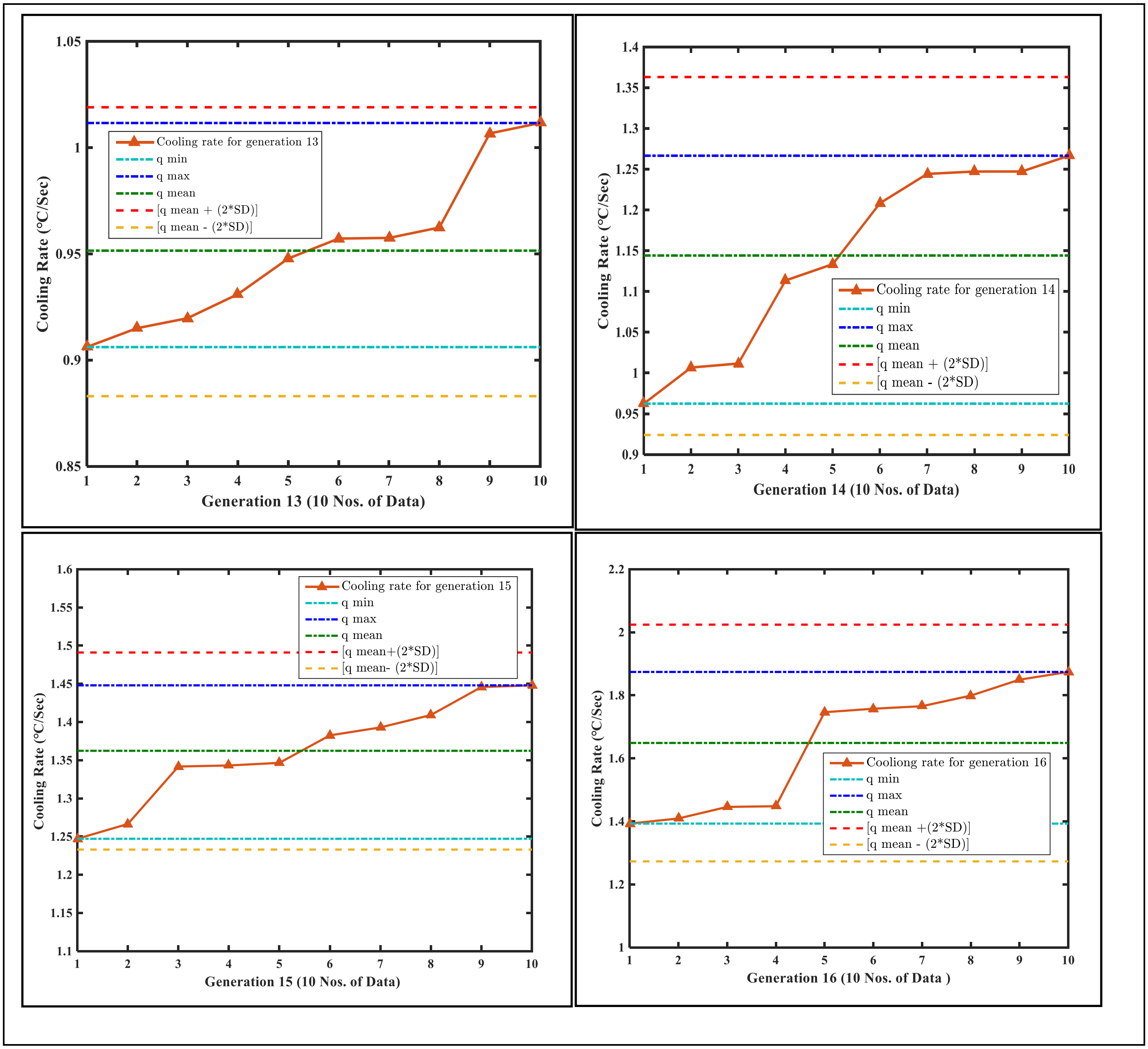
Cooling Rate (°C/Sec)
Generation 13 (10 Nos. of Data)
Cooling rate for generation 13
q min
q max
q mean
[q mean + (2*SD)]
[q mean - (2*SD)]
Cooling Rate (°C/Sec)
Generation 14 (10 Nos. of Data)
Cooling rate for generation 14
q min
q max
q mean
[q mean + (2*SD)]
[q mean - (2*SD)]
Cooling Rate (°C/Sec)
Generation 15 (10 Nos. of Data)
Cooling rate for generation 15
q min
q max
q mean
[q mean+(2*SD)]
[q mean- (2*SD)]
Cooling Rate (°C/Sec)
Generation 16 (10 Nos. of Data)
Cooliong rate for generation 16
q min
q max
q mean
[q mean +(2*SD)]
[q mean - (2*SD)]

(d)

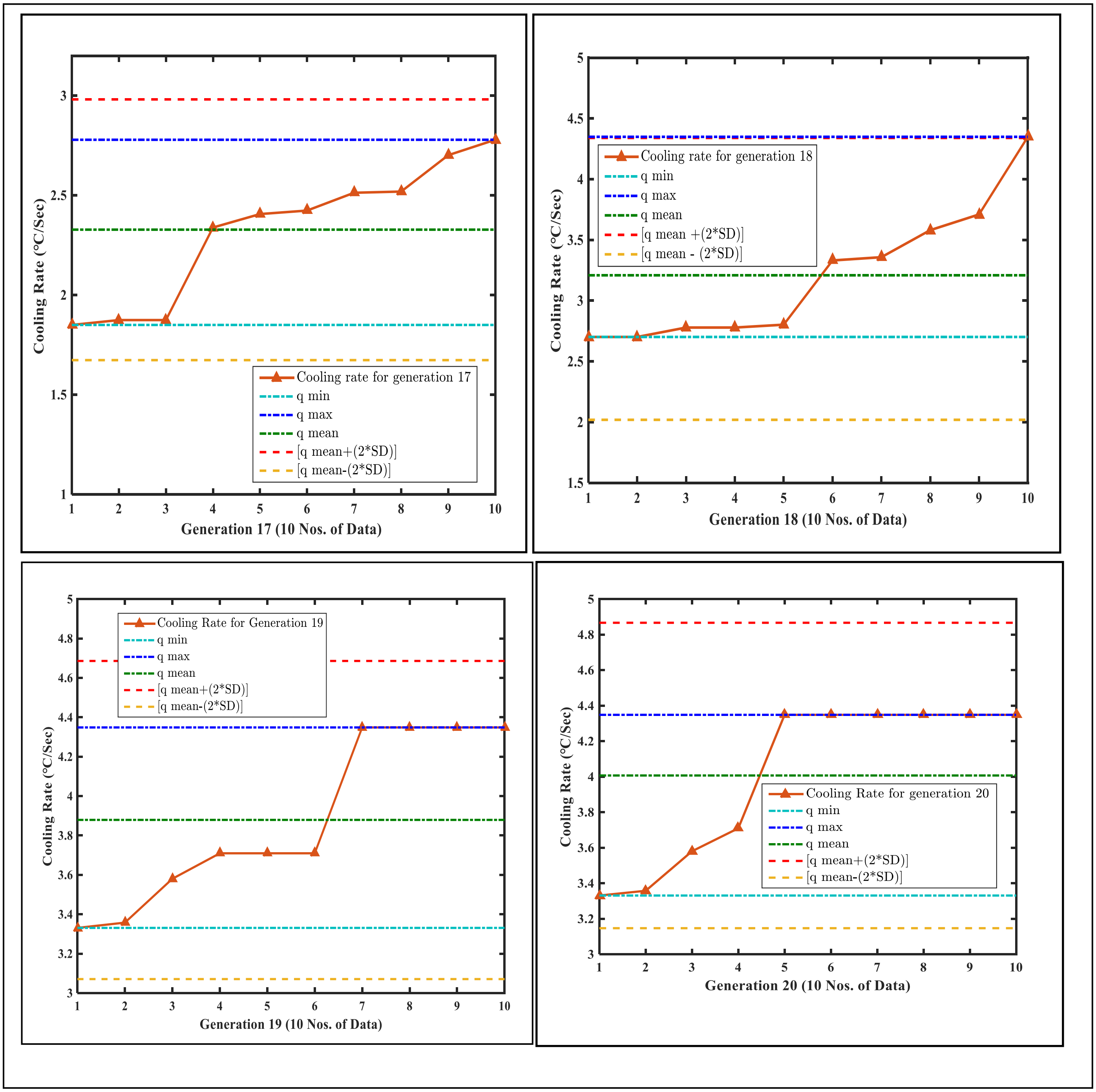

(e)

Fig. 5.2.3 Generation wise Cooling rate along with q_{mean} and Standard Deviation (SD), (a) Generation 1 to 4 ; (b) generation 5 to 8; (c) generation 9 to 12; (d) generation 13 to 16; (e) generation 17 to 20

Figure 5.2.4 provides insights into the variability of the results through the standard deviation plot, highlighting the stability achieved throughout the study. Meanwhile, Figure 5.2.5 illustrates a marked enhancement in the mean cooling rate. Collectively, these findings emphasize the potential for long-term stability and increased cooling efficiency of the experimental set-up. As shown in Fig. (5.2.6), the gap between (q_{mean} + 2SD) and (q_{mean} – 2SD) expands with the progression of generations, particularly after Generation 15. This widening reflects increased variability in cooling rate values, likely resulting from the exploration of diverse configurations within the cooling study. As this study is experimental in nature, a certain degree of variability is unavoidable due to measurement uncertainties, environmental influences, and material inconsistencies. The higher variability observed in later generations is likely due to the exploration of a wider design space, which enhances performance but also increases sensitivity to operating conditions. By Generation 20, the mean cooling rate begins to stabilize, indicating that although variability remains elevated, the upward trend persists. This suggests that the cooling study is effectively identifying configurations that yield higher cooling rates. The consistent improvement in the mean cooling rate highlights the success of the cooling study in enhancing performance. The sharp rise observed in later generation’s points to the successful identification and use of high-performance configurations. Overall, these results highlight the potential for sustained improvement and long-term stability in cooling performance. As illustrated again in Fig. (5.3.6), the increasing distance between (q_{mean} + 2SD) and (q_{mean} – 2SD) with generational progress especially beyond Generation 15 confirms rising variability, likely driven by the evaluation of various cooling study alternatives.

The cooling study is effectively identifying combinations that result in improved cooling rates. The continuous enhancement of the average cooling rate reflects the success of the cooling study approach. The significant increase observed in the later generations suggests that the study efficiently utilizes high-performance configurations. These findings indicate strong potential for sustained improvement and long-term stability in cooling rate performance of the experimental setup.

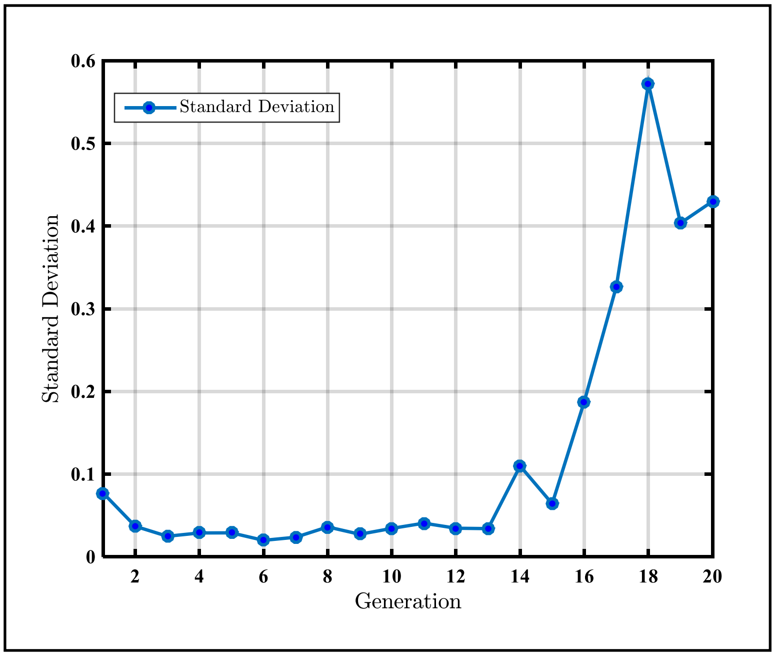

Fig. 5.2.4 Generation Vs Standard Deviation (SD)

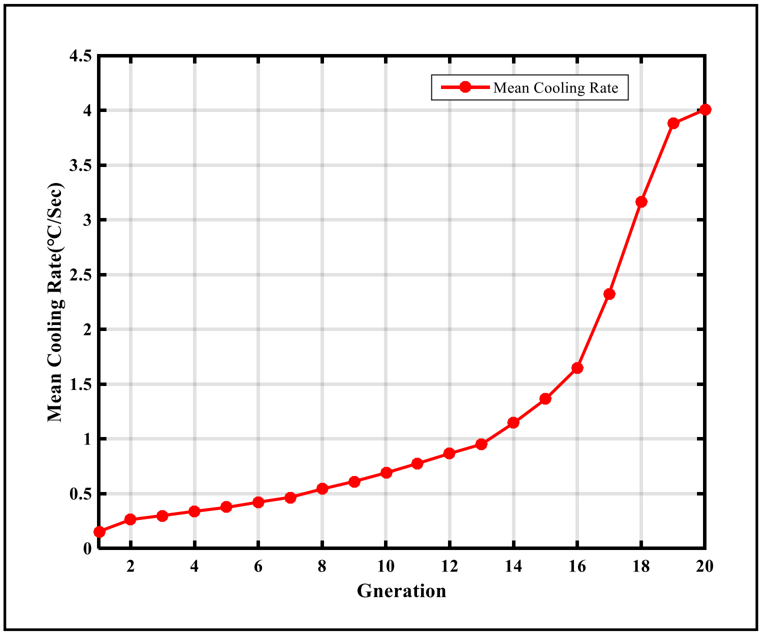

Fig. 5.2.5 Generation Vs Mean Cooling Rate

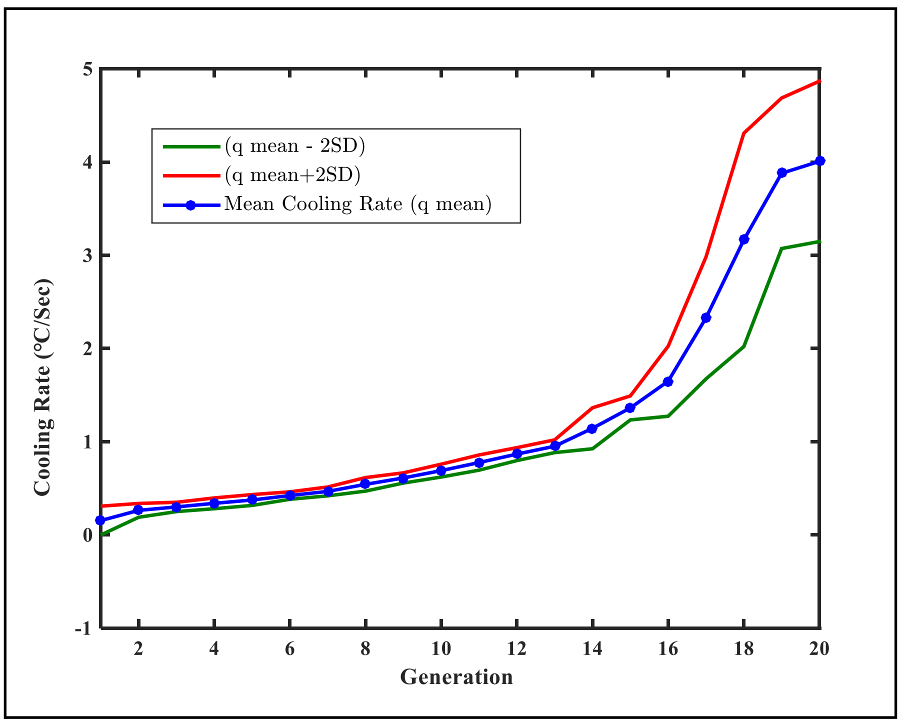

Fig. 5.2.6 Mean Cooling Curve along with (***q****mea*n+2SD) and (***q****mean* -2SD)

5.3 Modeling of Correlation by Regressions Analysis

Following consistency checking of the experimental data, two separate datasets were used to determine correlations between the thermodynamic parameter ($\mathbf{Þ} = \int_0^T \boldsymbol{T}\,\boldsymbol{dt}$) or cooling rate ($\boldsymbol{q}$) and independent observable data from the experimental setting by regression analysis.

5.3.1 Hypothesis for Regression Analysis of Data Set 1

The volumetric flow rate of the coolant that is travelling through the nozzle, in addition to the exact placement of the nozzle on the ROTs, both affect the cooling frequencies of the specimen. In this particular aspect of the study, the thermodynamic parameter (Þ) was selected since it has a considerable impact on the rate at which the specimen cools down on ROTs examinations. There are three factors that influence the thermodynamics parameter: the upper nozzle bank distance, the lower nozzle bank distance and the volume flow rate of the air that is used as a coolant. The upper nozzle bank distance, the lower nozzle bank distance and the rate of coolant flow are the parameters that have been chosen for the purpose of conducting an analysis of the impact that occurs throughout the cooling process. For the purpose of determining a statistical connection between the thermodynamic parameters and other independent factors that are essential for improving the cooling rate and obtaining specific characteristics in a material sample, regression analysis was used. In this portion of the research, experimental data were used to construct an empirical correlation between the independent factors and the dependent variables, resulting in a 94% level of accuracy.

As a result of the thermo-metallurgical phase change that occurs during the cooling process, the cooling rate is an essential component in the process of obtaining the appropriate metallurgical characteristics of steel. The purpose of this study is to investigate the relationship between the rate of cooling and a certain experimental parameter in order to fill a gap in the existing body of research. The findings of this study may be of assistance in regulating the rate of cooling during the actual work on ROTs. As was previously indicated, the objective is to establish a practical connection by making use of verified data, which is presented in the section titled "Consistency Checking of Experimental data," which has been gathered via experiments to improve the cooling rate. The best R square (coefficient of determination) and R values for establishing an empirical correlation have been determined via the evaluation of a number of different regression models. When compared to other approaches, the linear regression methodology is preferred because of its ease of use, effectiveness in terms of processing time and capacity to provide the greatest R and R square values.

5.3.1.1 Regression Model for Data Set 1

A collection of experimental data has been gathered from laboratory-scale ROTs. The dependent variable in this study is the thermodynamic parameter (**Þ**), which has an impact on the cooling rate. The independent variables include the upper nozzle distance (***du***), the lower nozzle distance (***dl***), and the volume flow rate of cooling air ($\dot{v}$). Controlling the rate of cooling and obtaining the desirable characteristics of the sample materials that are sought requires the establishment of a connection between the dependent and independent parameters. This relationship requires to be established through the context of this inquiry, the association in question was identified via the use of the multiple regression analysis techniques that are accessible inside SPSS. A presentation of the findings of this investigation may be found in the model summary. These findings are shown in Tables 5.3.1.1, 5.3.1.2 and 5.3.1.3 accordingly. Table 5.3.1.3 displays the R and R Square values for the linear regression model, while Tables 5.3.1.1 and 5.3.1.2 offer the values for the nonlinear regression model. However, the linear regression model is shown in Table 5.3.1.3. For the purpose of this inquiry, the linear regression model was used since, in

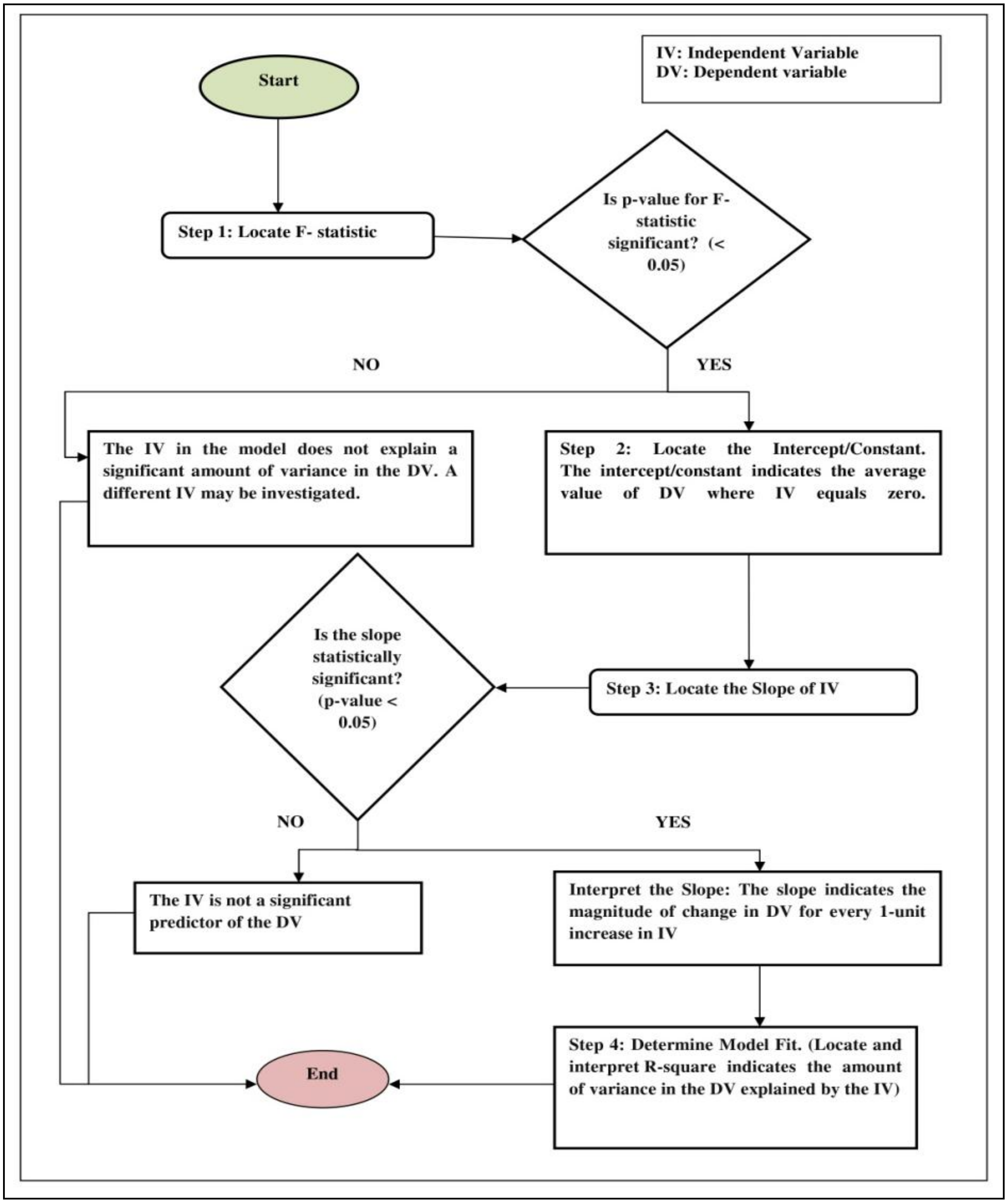

Fig. 5.3.1.1 Linear Regression Flow Diagram

comparison to non-linear regressions, it yielded consistently higher values for the same parameters. In addition, the computational simplicity of the linear regression model provides an advantage over the on-linear regression techniques in terms of the amount of time and effort required to calculate. This is due to the fact that the linear regression model is quicker and easier to calculate According to Table 5.3.1.3 of the linear regression model, the R Square and R value are respectively 0.940 and 0.955 in terms of their respective values. Based on the findings, it can be inferred that the independent factors account for around 94% of the variance in the dependent variable (Þ) and the correlation between the independent variables and the dependent variables is satisfactory, coming in at 95.5 percent. It has been found that the Adjusted R-Square for the present model is 0.947, which is a value that is pretty close to the traditional R-Square statistic. This was determined via the process of hypothesis testing. The proximity of these variables makes it more likely that the incorporation of predictors into the model will be incredibly relevant and meaningful. This is because of the tight relationship between the variables. It has been shown that a reduction in the standard error of the estimate is connected with an increase in the accuracy of predictive modeling. Latest estimations indicate that the present circumstance has a standard error that is somewhere in the range of 0.1503632. In addition to having a relatively low standard error associated with the estimate, which indicates that the model makes accurate predictions, the model has a high R Square value, which indicates that it is an outstanding fit for the actual data. The performance of the model is deemed to be satisfactory by both indicators.

An analysis of variance (ANOVA) is shown in Table 5.3.1.4, which is a table that contains the data. The relevance of the degree of connection between the set of forecasters (Constant, $\dot{v}$, ***du*** and ***dl***) and the dependent component (Þ) is outlined in this table. The sum of squares of the model has been determined to be 95.873 and the mean square has been calculated to be 35.035. Both of these numerical values have been verified. With regard to these values, there are four different degrees of freedom that are related to them. A larger F-value (1205.536) indicates that there is a stronger empirical relationship between the independent variable and the dependent variable. This is shown by the fact that the F-value measures the strength of the correlation. The P value (0.000[b]) of the model that is linked to the F evaluation demonstrates that there is a high degree of significance associated with the model for this study. This shows that the model is associated with the F evaluation. This theory is supported by a considerable amount of data, which may be derived from the sum of squares representing the residual row. The absolute t-value in the coefficient table (Table 5.3.1.5) reveals that this research displays a good degree of agreement. When the coefficient is statistically significant, a low p-value associated with each coefficient estimate, in combination with the constant, demonstrates that the coefficient is significant. This is the case in circumstances where the coefficient displays statistical significance. According to the p-values that were obtained, it can be concluded that all of the components exhibit statistical significance when it comes to predicting factors of the dependent parameter, which is represented by the letter 'Þ'. To represent the ultimate mathematical correlation that exists between a dependent variable and independent variables, one may use the equation (5.2) to express the relationship between the two. To do this, the value of the constant (C) and the coefficients (b_1, b_2 and b_3) from the coefficient table are substituted into the equation. The link between a dependent variable and independent variables is shown by equation (5.1), which makes use of a coefficient table to explain the relationship. This equation represents the correlation between the two variables.

$$\text{Þ} = -[\boldsymbol{C} + (\boldsymbol{b_1} \times, \boldsymbol{du}) + (\boldsymbol{b_2} \times \boldsymbol{dl}) + (\boldsymbol{b_3} \times \dot{\boldsymbol{v}})] \quad \textbf{(5.1)}$$

$$\text{Þ} = -[(-\mathbf{1.122}) + (\mathbf{181.093} \times \boldsymbol{du}) + (\mathbf{182.839} \times \boldsymbol{dl}) + (\mathbf{0.018} \times \dot{\boldsymbol{v}})] \quad \textbf{(5.2)}$$

Table 5.3.1.1 Model Summary (Logarithmic)

Model	R	R Square	Adjusted R Square	Std. Error of the Estimate
Logarithmic	0.913[a]	0.90163	0.9038	0.62201
a. Predictors: (Constant), $\dot{v}$, *dl*, *du*				

Table 5.3.1.2 Model Summary (Exponential)

Model	R	R Square	Adjusted R Square	Std. Error of the Estimate
Exponential	0.906[a]	0.89361	0.8854	0.5312
a. Predictors: (Constant), $\dot{v}$, *dl*, *du*				

Table 5.3.1.3 Model Summary (Linear)

Model	R	R Square	Adjusted R Square	Std. Error of the Estimate
Linear	0.955[a]	0.940	0.947	0.1503632
a. Predictors: (Constant), $\dot{v}$, *dl*,*du*				

Table 5.3.1.4 ANOVA Table (Linear)

ANOVA[a]						
Model		Sum of Squares	df	Mean Square	F	Sig.
Linear	Regression	95.873	4	35.035	1205.536	0.000[b]
	Residual	5.054	168	0.021		
	Total	102.160	169			
a. Dependent Variable: Þ = $\int_0^T \boldsymbol{T dt}$						
b. Predictors: (Constant), $\dot{v}$, *dl*, *du*						

Table 5.3.1.5 Coefficient Table (Linear)

Coefficients[a]						
Model		Unstandardized Coefficients		Standardized Coefficients	t	Sig.
		B	Std. Error	Beta		
Linear	(Constant)	-1.122	0.121		-8.917	0.000
	du	181.093	7.903	0.358	22.250	0.005
	dl	182.839	8.148	0.518	23.274	0.004
	$\dot{v}$	0.018	0.0025	0.713	33.523	0.001
a. Dependent Variable: Þ = $\int_0^T \boldsymbol{T dt}$						

5.3.1.2 Results and Analysis of Regression Model of Data Set 1

For the purpose of determining the relationship that exists between a dependent variable and the factors that are known to be independent of it, the regression method was utilized. The utilization of a neural network contributed to the validation of the data obtained from the studies, which ultimately led to the successful completion of this task. There is a significant degree of similarity between the experimentally measured dependent variable (Þ) and the corresponding computed (predicted) value included within the framework of the regression model. It is possible to draw the conclusion that the regression model that has been used in showing appropriate performance and is a reasonable fit for the data is a suitable fit for the data given the closeness that has been seen. An appropriate depiction of the connection that exists between the dependent variable (Þ) and the independent variables is provided by this. Fig. (5.3.1.2) illustrates the thermodynamic parameter that was derived from the experimental data as well as the model calculations acquired for the specimen that was under investigation. That the thermodynamic parameter (Þ) obtained from the experiment and the calculations made by the model are similar to one another is shown by the fact that this is the case. In addition, they often coincide with one another or come very close to aligning with one another, which is an indication that the model is accurate and might be accepted. Due to the fact that there is a discrepancy between the real data that corresponds to certain expected values of the thermodynamic parameter and the actual data that corresponds to such values, it is possible to deduce that there is a degree of ambiguity in the apparatus that was used for the experiment. In Fig. (5.3.1.3), an error plot is shown for the purpose of comparing the predictions made by the model with the actual results obtained from the experiment. Taking into consideration the fact that the error values that have been observed are quite low, it is possible to draw an argument that the predictions that the model has generated are extremely accurate and trustworthy.

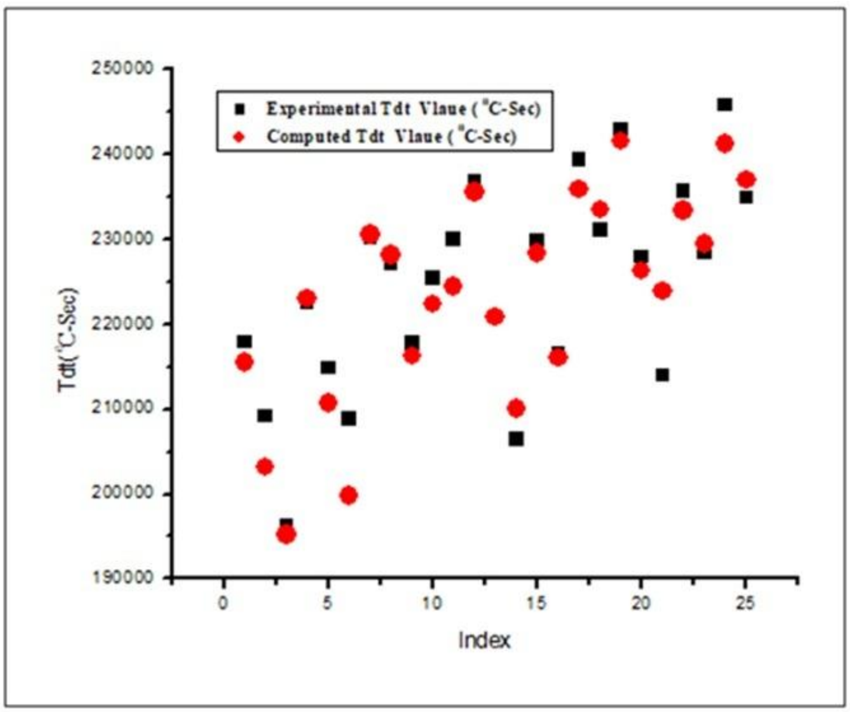

Fig 5.3.1.2 Experimental *Tdt* (Þ) Vs Computed *Tdt* (Þ)

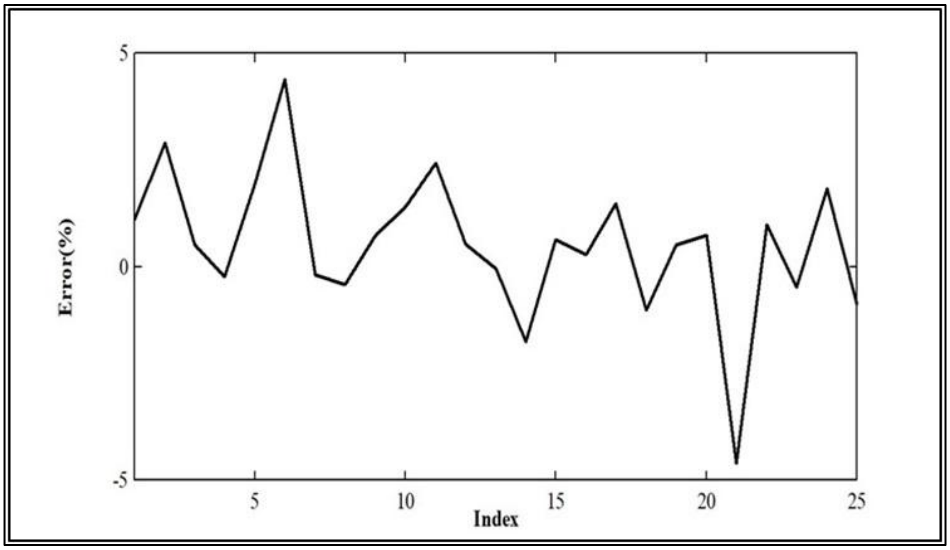

Fig 5.3.1.3 Error Plot

Based on the data shown in Fig. (5.3.1.2) and Fig. (5.3.1.3), it can be drawn that the model has a high degree of accuracy when it comes to forecasting and managing the rate at which the sample undergoes cooling. With the use of data taken from real-world scenarios, the model has been put through its paces and the findings demonstrate that the predictions made by the model are in excellent accord with the data that was measured. The model's correctness is shown by the minimum error values and the integration of both figures provides proof that the model regulates the cooling operation of the specimen in an effective manner. Equation 5.2 indicates that ***dl*** has the highest influence on the thermodynamic parameter **Þ**, followed closely by ***du***, whereas ***v*** exhibits the least contribution. This suggests that the cooling behavior and thermal history are predominantly controlled by ***du*** and ***dl***, while the influence of ***v*** remains comparatively minimal.

5.3.2 Hypothesis for Regression Analysis of Data Set 2

Various industries, such as transportation, aerospace, marine and medical, frequently utilize the cooling system due to its capacity for precise adjustments tailored to specific steel grades. The purpose of this study is to investigate the run-out table's (ROT) effective cooling parameters in a controlled laboratory environment. Both the precise location of the nozzle on the ROTs and the coolant flow rate has a significant impact on the specimen cooling rates. The specimen's temperature and the coolant flow rate greatly affect the mean film temperature surrounding the specimen plate and the heat transfer coefficient, which changes with the temperature of the heat transfer zone. Following variables has been chosen to assess the impact of the cooling process: heat transfer coefficient at a given nozzle bank location, mean film temperature and coolant flow rate. Essential for controlling the cooling rate and attaining certain steel properties, regression analysis establishes a statistical relationship between the cooling rate and several independent variables. An empirical correlation between the dependent and independent variables was constructed using validated experimental data in this portion of the research. Researchers found the correlation to be 95% accurate. Several regression models has been evaluated to identify the one with the highest R and R-square values. This study aimed to establish such an empirical connection. The researchers selected the linear regression approach as the method of choice over other alternatives due to its ability to provide the highest R and R square values, in addition to being straightforward and requiring less time to compute.

5.3.2.1 Regression Model for Data Set 2

A wide range of experimental data has been obtained from ROTs conducted on a laboratory scale. The cooling rate ($\boldsymbol{q}$) is the dependent variable, while the convective heat transfer coefficient ($\boldsymbol{h}$), mean film temperature ($\boldsymbol{T_{mf}}$) and volume flow rate of cooling air ($\dot{\boldsymbol{v}}$) are the independent factors considered in this study. In order to achieve the desired characteristics in the specimen materials and manage the cooling rate, it is essential to establish a connection between the components that are dependent and those that are independent. Within the scope of this investigation, SPSS utilized various regression analysis techniques to establish the aforementioned association, with the outcomes displayed in Table 5.3.2.1, Table 5.3.2.2 and Table 5.3.2.3. According to the model summary, Table 5.3.2.3 presents the R and R square values for the linear regression model. These values are greater when compared to the comparable values for the non-linear regression models that are shown in Tables 5.3.2.1 and 5.3.2.2. Consequently, as a result of the greater R and R square values that it has, linear regression analysis has been chosen as the technique of choice for this particular investigation. In addition, the linear regression model's computational simplicity definitely confers an advantage over the on-linear regression approaches in terms of the amount of time and effort required for computing. Because the R-square value for the regression model that is summarised in Table 5.3.2.3 is 0.950 and the R-value is 0.975, it can be deduced that the independent variables in the model are responsible for about 95.0% and 97.5% of the variation in the dependent parameter (***q***), respectively. It has been established that the adjusted R square for the current model is 0.949, which is a figure that is quite close to the conventional R-square statistic. Due to the close proximity of these variables, it is quite probable that the insertion of predictors into the model will be extremely relevant and meaningful. There is a correlation between a reduction in the standard error of the estimate and an increase in the accuracy of the model for making predictions. Based on the current circumstances, the standard error is projected to be somewhere around 0.1704645. The model has a high R-square value, which indicates that it provides a good fit to the data and a relatively low standard error of the estimate, which suggests that it provides accurate predictions. Both of these metrics demonstrate that the model has solid performance. An ANOVA table is shown in Table 5.3.2.4, which is a table that contains an analysis of variance. This analysis explains the significance of the link between the dependent variable ($\boldsymbol{q}$) and the set of predictors (Constant, $\dot{\boldsymbol{v}}$, $\boldsymbol{T_{mf}}$ and $\boldsymbol{h}$). It has been established that the sum of squares for the regression model is 96.123 and the mean square has been computed to be 32.041. This specific occurrence serves as an illustrative example of this concept. These values are associated with a total of three degrees of freedom. A closer empirical connection between the dependent variable and the predictors is shown by a bigger F-value (1102.647), which implies a stronger empirical link. Given that the p-value, which represents the significance level, is related to the F-statistic, it is seen that it is very low (shown as 0.000[b]), which indicates that the regression model has a high degree of significance. From the results of the regression analysis, it is clear that the sum of squares, degrees of freedom (df) and mean square value of residuals are all in striking agreement with one another.

The p-values for all coefficients in Table 5.3.2.5, including the constant, are significantly low, indicating their statistical significance. In brief, the coefficient table provides vital information on the estimated coefficients, standard errors, standardized coefficients, t-values and significance levels for all of the independent variables that are included in the context of the multiple linear regression models. All components, including the constant term, appear to be statistically significant predictors of the variable 'q' under study based on the obtained p-values. Equation (5.4) is used to represent the final mathematical correlation between a dependent variable and independent variables. This is accomplished by inserting the value of the constant (C) and the coefficients (b_4, b_5 and b_6) from the coefficient table. The coefficient table is used to express the correlation between a dependent variable and independent variables and equation (5.3) is used to illustrate this correlation.

$$\boldsymbol{q} = -[\boldsymbol{C} + (\boldsymbol{b_4} \times, \boldsymbol{h}) + (\boldsymbol{b_5} \times \boldsymbol{T_{mf}}) + (\boldsymbol{b_6} \times \ \dot{\boldsymbol{v}}\ )] \qquad \textbf{(5.3)}$$

$$\boldsymbol{q} = -[(-\mathbf{1.113}) + (\mathbf{183.429} \times \boldsymbol{h}) + (\mathbf{0.004} \times \boldsymbol{T_{mf}}) + (\mathbf{0.017} \times \dot{\boldsymbol{v}}\ )] \qquad \textbf{(5.4)}$$

Table 5.3.2.1 Model Summary (Logarithmic)

Model	R	R Square	Adjusted R Square	Std. Error of the Estimate
Logarithmic	.935[a]	0.93171	0.9238	0.52201
a. Predictors: (Constant), $\dot{v}$, T_{mf}, h				

Table 5.3.2.2 Model Summary (Exponential)

Model	R	R Square	Adjusted R Square	Std. Error of the Estimate
Exponential	.926[a]	0.92361	0.9154	0.4312
a. Predictors: (Constant), $\dot{v}$, T_{mf}, h				

Table 5.3.2.3 Model Summary (Linear)

Model	R	R Square	Adjusted R Square	Std. Error of the Estimate
Linear	0.975[a]	0.950	0.949	0.1704645
a. Predictors: (Constant), $\dot{v}$, T_{mf}, h				

Table 5.3.2.4 ANOVA Table (Linear)

Model		Sum of Squares	df	Mean Square	F	Sig .(P- Value)
Linear	Regression	96.123	3	32.041	1102.647	0.000[b]
	Residual	5.027	173	0.029		
	Total	101.150	176			
a. Dependent Variable: q						
b. Predictors: (Constant), $\dot{v}$, T_{mf}, h						

Table 5.3.2.5 Coefficient Table (Linear)

Coefficients[a]						
Model		Unstandardized Coefficients		Standardized Coefficients	t	Sig.
		B	Std. Error	Beta		
Linear	(Constant)	-1.113	.123		-9.042	0.000
	h	183.429	8.268	0.432	22.185	0.000
	$\dot{v}$	0.004	0.000	0.693	35.652	0.000
	T_{mf}	0.017	0.017	0.017	1.004	0.037
a. Dependent Variable: q						

5.3.2.2 Results and Analysis of Regression Model of Data Set 2

Following the validation of the experimental data via the use of a neural network, regression analysis has been utilized in order to determine the link between a dependent variable and the independent variables. This was done in order to determine the relationship between the parameters. The regression model indicates that there is a significant level of similarity between the experimental dependent variable (***q***) and its corresponding calculated (predicted) value. This is the case since the two variables are quite similar. According to the proximity that was noticed, the regression model that was used demonstrates good performance and is a reasonable fit for the data. It is also able to adequately represent the link between the dependent variable (***q***) and the independent factors. Fig. (5.3.2.1) is a graphical representation that depicts the cooling rates that were determined from both the actual experiment (experimental) and the calculations that were carried out using the model (computed) for the specimen that was being analyzed. This shows that the cooling rates obtained from the experiment and the calculations made by the model are similar to one another. Furthermore, they often match or nearly coincide with one another, which is an indication of the model's correctness and acceptability. The goal of the graphical representation of the error values associated with a regression model, as is shown in Fig. (5.3.2.2), is to facilitate the comparison of the projected outcomes of the model with the actual experimental results. In light of the fact that the observed error values are quite low, it can be concluded that the predictions made by the model are highly accurate and reliable. It is feasible to reach a consensus that the model exhibits a high degree of accuracy in its ability to forecast and regulate the pace at which the specimen cools. This conclusion can be reached on the basis of the information that is shown in Fig. (5.3.2.1) and (5.3.2.2). Adjusting the model parameters serves as a straightforward and effective approach to control the cooling rate required to achieve the desired properties in the test plate. For the purpose of providing a concise summary, the model has been subjected to testing using empirical data, and the results suggest that there is a significant concordance between the model's predictions and the measurements that have been observed. Both of these statistics give support to the argument that the model successfully regulates the cooling rate of the specimen. The low error values demonstrate that the model is accurate and the combination of the two numbers provides evidence that the model is accurate.

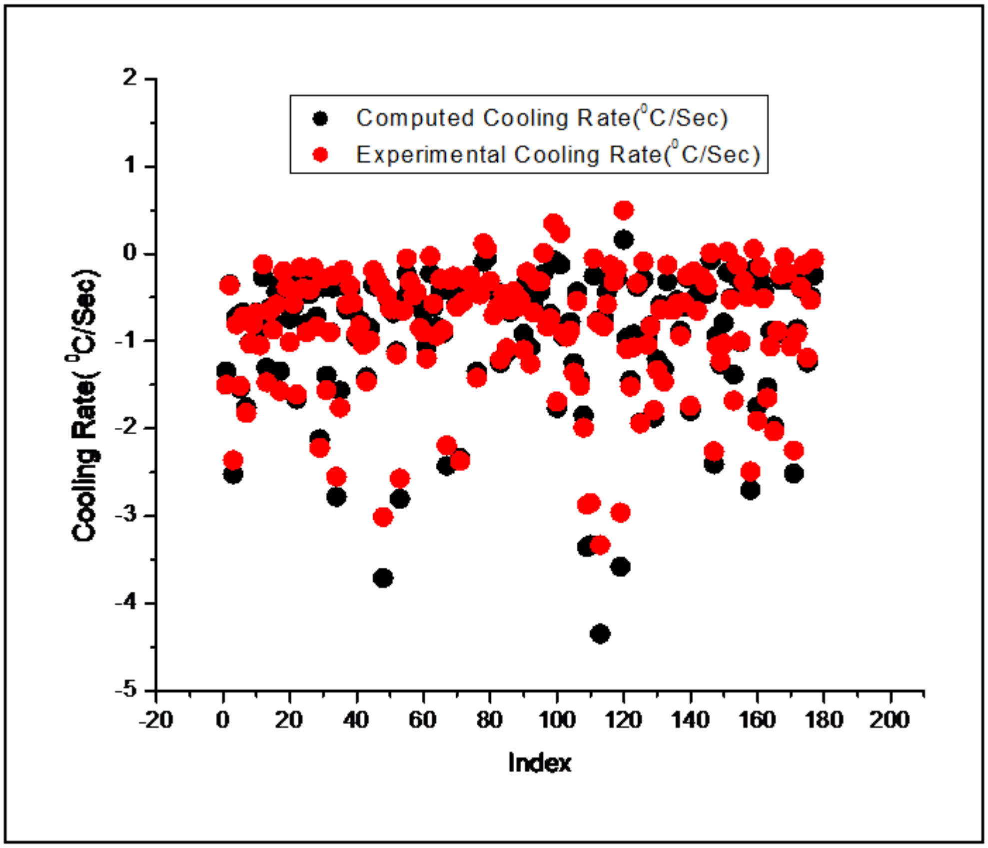

Fig 5.3.2.1 Experimental Cooling Rate Vs Computed Cooling Rate

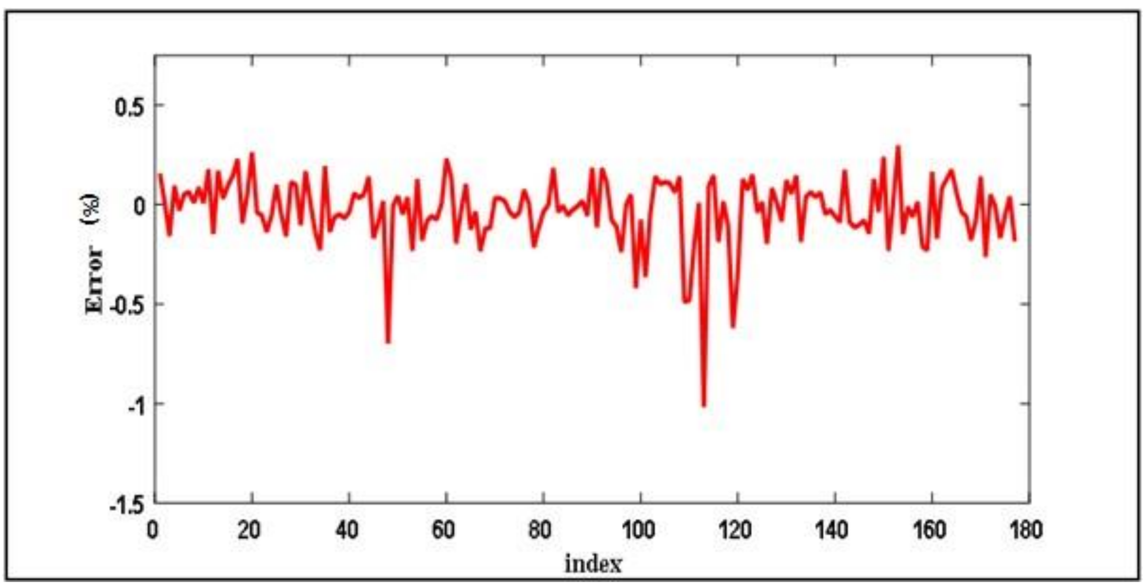

Fig 5.3.2.2 Error Plot

SUMMERY & CONCLUSION

The conclusion part of the dissertation presents a summary of the research results, analysis, and arguments offered throughout the body of the work. Additionally, an attempt has been made in this chapter to highlight both the future scope of this work and the constraints of this research.

6.1 Organization of the Thesis

The study provided an in-depth literature review, emphasizing the gathered insights and recent developments related to the Run-Out Table and the numerical modeling of cooling rates derived from experimental data. The research reviewed the usage of air-jet impingement for cooling in the steel industry throughout the previous decades, focusing on methodology, equipment, experimental parameters and their impact on achieving target steel quality. Laboratory Scale Run Out Tables (ROTs) of the Hydraulic Laboratory at Jadavpur University, designed with financial support from M/s Tata Steel as part of TEQIP Phase II, were used for this research work. In order to gather information that would be invaluable for the development of this research project, a number of experiments were conducted under a variety of conditions. In order to check the consistency of the experimental data, two distinct Artificial Neural Network (ANN) models were created with the assistance of MATLAB. A generation-wise iterative approach was implemented to analyze the cooling rate, making use of experimental data throughout the process. Following the confirmation of the two separate experimental data sets, the decision was made to use regression analysis in order to establish correlations between the thermodynamic parameter (Þ) or the cooling rate ($\boldsymbol{q}$) and independent observable data.

6.2 Conclusion from the Study

6.2.1 Consistency of the Experimental Data

The following conclusions have been drawn from the artificial neural network (ANN) modeling that was employed to validate two distinct data sets:

i) Figure 5.1.1.5 makes it evident that the first set of observed data and the data calculated by the model are not only very close to one another but also greatly overlap with one another. The parameter (Þ) is the dependent variable, whereas the other parameters (***du***, ***dl***, and $\dot{v}$) are the independent variables for the first set of data under consideration. The better performance of the ANN model suggests that the working setup's uncertainty is limited, allowing the verified data to be utilised to establish the correlation between the dependent and independent variables.

ii) An Artificial Neural Network study was conducted to predict the cooling rate in the second set of data. The study focused on varying the convective heat transfer coefficient, volume flow rate of cooling air and mean film temperature around the heated plate at fixed upper and lower nozzle bank distances. Figures 5.1.2.1, 5.1.2.3 and 5.1.2.5 show the contrast between the cooling rates calculated by the three artificial neural network (ANN) models and the actual experimental cooling rate. The close alignment of results from all three network models for the second dataset suggests the reliability of the experimental setup and the data generated. This consistency might be used in the future to enhance the cooling process. Network-1 (Fig. 5.1.2.1) was identified as the best appropriate choice among the three models because of its high correlation coefficient (R=0.9997) and lower mean square error (MSE=0.00025) illustrated in Fig. 5.1.2.2. Therefore, checking consistency of the experimental data using network-1 is recommended for the future improvement of the job, namely numerical modeling of cooling rates using verified experimental data.

6.2.2 Cooling Rate Study

i) Enhancement across generations: Cooling rates markedly improved from earlier to later generations, demonstrating a distinct increasing trajectory.
ii) Generations 6-15 indicated significant enhancements in cooling rates (0.42 to 1.36) with less variability, indicating a stabilization of the system.
iii) The increasing average cooling rates signify the effective discovery of high-performance setups during this study.

6.2.3 Modeling of Correlation by Regression Analysis

A regression analysis was conducted on an experimental data set to establish the relationship between the thermodynamic parameter (Þ) and the effective cooling parameters affecting the cooling process of laboratory-scale ROTs. Linear regression analysis is favored over nonlinear regression analysis due to its simplicity and superior accuracy. Linear regression analysis is the preferred approach for conducting experimental sets. The linear model used is considered effective due to its high coefficient of determination (0.955) and R-Square (0.940) values shown in Table 5.3.1.3, which indicate strong performance. The model has good predictive capability with a 94% confidence level. The visual representation of the congruence between experimental and computational findings validates the dependability and consistency of the present study. According to Table 5.3.1.5, the nozzle distance (***du***, ***dl***) has a greater impact on the specimen's cooling rate compared to the volume flow rate of the air ($\dot{v}$) as a cooling medium. Figures 5.3.1.2 and 5.3.1.3 depict the model's accuracy and error value, making them suitable for practical use.

Using a data set that was collected via experimentation, a regression analysis was performed to determine the link that exists between the cooling rate (***q***) and the effective cooling parameters that have an influence on the cooling process of laboratory-sized ROTs at the laboratory scale. It has been shown that linear regression analysis is preferable to nonlinear regression analysis in terms of its ease of use and high level of accuracy. As a result, linear regression analysis is the preferred method for executing experimental setups. It is determined that the model that was used is adequate because of its good performance, which is shown by its high R and R-Square values of 0.975a and 0.950, respectively, which are displayed in Table 5.3.2.3. This indicates that the model has strong predictive power with a confidence level of 95%. As seen in Table 5.3.2.4, the trustworthiness of the model as well as the results it produces have been shown by the presence of a high F-value and a low p-value. The congruence between the conclusions obtained via experimentation and those obtained by computation has been visually displayed, which substantiates the reliability and consistency of the current work.

6.3 . Limitation

During the course of this investigation, the following limitations were observed:

i) Only from upper and lower side there is a provision to supply of the cooling medium.

ii) On account of this research, each and every nozzle has been left open.

6.4 Future Scope

i) Conduct a comprehensive series of tests on this configuration using water and mist for the purpose of cooling.

ii) It is possible to examine the impact of plate velocity by transferring the plate using the EHAS.

iii) Studying the impact on cooling may be achieved by altering the quantity and layout of open nozzles.

iv) Investigating the effect of the cooling media on the specimen from all angles is possible in the future.

REFERENCES

Aamir, M., Liu, Q., Zhu, X., Wang, H., & Zubair, M. (2014). Ultra Fast Spray Cooling and Critical Droplet Daimeter Estimation from Cooling Rate. Journal of Power and Energy Engineering, 02(04), 259–270. https://doi.org/10.4236/jpee.2014.24037

Atici, U. Prediction of the strength of mineral admixture concrete using multivariable regression analysis and an artificial neural network. Expert Systems With Applications 2011; 38(8), 9609–9618.

Bhattacharya, P., Samanta, A., & Chakraborty, S. (2009). Spray evaporative cooling to achieve ultra fast cooling in runout table. International Journal of Thermal Sciences, 48(9), 1741–1747. https://doi.org/10.1016/j.ijthermalsci.2009.01.015

Chen, S., & Tseng, A. A. (1992). Spray and jet cooling in steel rolling. International Journal of Heat and Fluid Flow, 13(4), 358–369. https://doi.org/10.1016/0142-727x(92)90006-u

Cai, X., Liu, C., & Liu, Z. (2014). Process design and prediction of mechanical properties of dual phase steels with prepositional ultra fast cooling. Materials in Engineering, 53, 998–1004. https://doi.org/10.1016/j.matdes.2013.07.071

Cho, H., Cho, Y., Kim, D., Kim, S. J., Lee, W., & Han, H. N. (2014). Finite Element Investigation for Edge Wave Prediction in Hot Rolled Steel during Run Out Table Cooling. Isij International, 54(7), 1646–1652. https://doi.org/10.2355/isijinternational.54.1646

Cho, M. J., Thomas, B. G., & Lee, P. J. (2008). Three-Dimensional numerical study of impinging water jets in runout table cooling processes. Metallurgical and Materials Transactions B-process Metallurgy and Materials Processing Science, 39(4), 593–602. https://doi.org/10.1007/s11663-008-9160-8

Dhua, S. K., & Sarkar, P. P. (2013). Development of ultrafine grains in C–Mn steel plates through hot-rolling and air-cooling. Materials Science and Engineering: A, 575, 177–188. https://doi.org/10.1016/j.msea.2013.03.052

Gomez, C., Van Der Geld, C., Kuerten, J. G., Bsibsi, M., & Van Esch, B. (2020). Quench cooling of fast moving steel plates by water jet impingement. International Journal of Heat and Mass Transfer, 163, 120545. https://doi.org/10.1016/j.ijheatmasstransfer.2020.120545

Guemo, G. G., Prodanovic, V., & Militzer, M. (2018). Simulation of runout table cooling. Steel Research International, 90(4). https://doi.org/10.1002/srin.201800361

Guo, F., Zhao, X., Wang, L., Wu, D., Wang, G., & Ning, Z. (2013). Effect of controlled cooling on microstructure and mechanical properties of H-Beam. Journal of Iron and Steel Research International, 20(8), 60–65. https://doi.org/10.1016/s1006-706x(13)60142-9

Golhar, A., Choudhari, N., & Patil, A. Prediction of aluminium content in a metal using SPSS based linear regression analysis. Journal of Physics Conference Series, (2021), 1913(1), 012002.

Han, H. N., Lee, J. K., Kim, H. J., & Jin, Y. (2002). A model for deformation, temperature and phase transformation behavior of steels on run-out table in hot strip mill. Journal of Materials Processing Technology, 128(1–3), 216–225. https://doi.org/10.1016/s0924-0136(02)00454-5

Hassan, A. M., Alrashdan, A., Hayajneh, M. T., & Mayyas, A. (2009). Prediction of density, porosity and hardness in aluminum–copper-based composite materials using artificial neural network. Journal of Materials Processing Technology, 209(2), 894–899. https://doi.org/10.1016/j.jmatprotec.2008.02.066

Horský, J., Raudenský, M., & Kotrbáček, P. (1998). Experimental study of long product cooling in hot rolling. Journal of Materials Processing Technology, 80–81, 337–340. https://doi.org/10.1016/s0924-0136(98)00191-5

Hou, Y., Liu, X., Liu, J., Li, M., & Pu, L. (2013). Experimental study on phase change spray cooling. Experimental Thermal and Fluid Science, 46, 84–88. https://doi.org/10.1016/j.expthermflusci.2012.11.023

Islamoglu, Y. (2003). A new approach for the prediction of the heat transfer rate of the wire-on-tube type heat exchanger—use of an artificial neural network model. Applied Thermal Engineering, 23(2), 243–249. https://doi.org/10.1016/s1359-4311(02)00155-2

Jambunathan, K., Hartle, S., Ashforth-Frost, S., & Fontama, V. (1996). Evaluating convective heat transfer coefficients using neural networks. International Journal of Heat and Mass Transfer, 39(11), 2329–2332. https://doi.org/10.1016/0017-9310(95)00332-0

Jha, J. M., Ravikumar, S. V., Sarkar, I., Pal, S. K., & Chakraborty, S. (2015). Ultrafast cooling processes with surfactant additive for hot moving steel plate. Experimental Thermal and Fluid Science, 68, 135–144. https://doi.org/10.1016/j.expthermflusci.2015.04.004

Jha, J. M., Ravikumar, S. V., Tiara, A., Sarkar, I., Pal, S. K., & Chakraborty, S. (2015). Ultrafast cooling of a hot moving steel plate by using alumina nanofluid based air atomized spray impingement. Applied Thermal Engineering, 75, 738–747. https://doi.org/10.1016/j.applthermaleng.2014.10.005

Jang, H., & Topal, E. Optimizing overbreak prediction based on geological parameters comparing multiple regression analysis and artificial neural network. Tunnelling and Underground Space Technology 2013; 38, 161–169.

K. Ermis, A. Erek, I. Dincer, 'Heat transfer analysis of phase change process in a finned-tube thermal energy storage system using artificial neural network', International Journal of Heat and Mass Transfer, 50(15-16), 3163–3175. https://doi.org/10.1016/j.ijheatmasstransfer.2006.12.017

Li, H., Xu, J., Wang, G., Shi, L., & Xiao, Y. (2010). Development of strip flatness and crown control model for hot strip mills. Journal of Iron and Steel Research International, 17(3), 21–27. https://doi.org/10.1016/s1006-706x(10)60067-2

Lim, H. S., & Kang, Y. T. (2018). Estimation of finish cooling temperature by artificial neural networks of backpropagation during accelerated control cooling process. International Journal of Heat and Mass Transfer, 126, 579–588. https://doi.org/10.1016/j.ijheatmasstransfer.2018.06.022

Liu, E., Liang-Gui, P., Yuan, G., Wang, Z., Zhang, D., & Wang, G. (2012). Advanced run-out table cooling technology based on ultra fast cooling and laminar cooling in hot strip mill. Journal of Central South University, 19(5), 1341–1345. https://doi.org/10.1007/s11771-012-1147-6

Mohapatra, S., Chakraborty, S., & Pal, S. K. (2012). Experimental studies on different cooling processes to achieve Ultra-Fast cooling rate for hot steel plate. Experimental Heat Transfer, 25(2), 111–126. https://doi.org/10.1080/08916152.2011.582567

Mohapatra, S., Ravikumar, S. V., Jha, J. M., Singh, A. K., Bhattacharya, C., Pal, S. K., & Chakraborty, S. (2013). Ultra fast cooling of hot steel plate by air atomized spray with salt solution. Heat and Mass Transfer, 50(5), 587–601. https://doi.org/10.1007/s00231-013-1260-6

Mukhopadhyay, A., & Sikdar, S. (2005). Implementation of an on-line run-out table model in a hot strip mill. Journal of Materials Processing Technology, 169(2), 164–172. https://doi.org/10.1016/j.jmatprotec.2005.04.039

Nasab, M. H., & Serajzadeh, S. (2015). Thermal stresses and kinetics of phase transformation on the run-out table after hot strip rolling of low-carbon steels. The International Journal of Advanced Manufacturing Technology, 83(9–12), 1725–1736. https://doi.org/10.1007/s00170-015-7604-2

Nobari, A. H., Prodanovic, V., & Militzer, M. (2016). Heat transfer of a stationary steel plate during water jet impingement cooling. International Journal of Heat and Mass Transfer, 101, 1138–1150. https://doi.org/10.1016/j.ijheatmasstransfer.2016.05.108

Nayak, S. K., Mishra, P. C., & Parashar, S. K. S. (2016). Influence of spray characteristics on heat flux in dual phase spray impingement cooling of hot surface. Alexandria Engineering Journal, 55(3), 1995–2004. https://doi.org/10.1016/j.aej.2016.07.015

Pacheco-Vega, A., Sen, M., Yang, K. T., & McClain, R. L. (2001). Neural network analysis of fin-tube refrigerating heat exchanger with limited experimental data. International Journal of Heat and Mass Transfer, 44(4), 763–770. https://doi.org/10.1016/s0017-9310(00)00139-3

Padhy, S. M., Kambli, A., Ukamanal, M., & Mishra, P. C. (2018). Cooling mechanisms on run out table: A technical review. Materials Today: Proceedings, 5(9), 18162–18169. https://doi.org/10.1016/j.matpr.2018.06.152

Padhy, S. M., Mishra, P. C., & Mishra, R. (2018). Nozzle positioning for ultra-fast cooling of steel strips in a run out table. Materials Today: Proceedings, 5(9), 18656–18663. https://doi.org/10.1016/j.matpr.2018.06.211

Patel, M., Shettigar, A. K., Krishna, P., & Parappagoudar, M. B. (2017). Back propagation genetic and recurrent neural network applications in modelling and analysis of squeeze casting process. Applied Soft Computing, 59, 418–437. https://doi.org/10.1016/j.asoc.2017.06.018

Pavlenko, I., Piteľ, J., Ivanov, V., Berladir, K., Mižáková, J., Kolos, V., & Trojanowska, J. Using regression analysis for automated material selection in smart manufacturing. Mathematics 2022; 10(11), 1888.

Qin, Q., Li, X., Zang, Y., & Wu, D. (2016). Research on the mechanism of spray cooling of H-beam after rolling. Advances in Mechanical Engineering, 8(10), 168781401667254. https://doi.org/10.1177/1687814016672540

Ozden, M. G., Liu, X., Wilkinson, T. J., Üstün-Yavuz, M. S., & Morley, N. A. Predictive modelling of laser powder bed fusion of Fe-based nanocrystalline alloys based on experimental data using multiple linear regression analysis. Heliyon 2024; 10(15), e35047.

Ravikumar, S. V., Haldar, K., Jha, J. M., Chakraborty, S., Sarkar, I., Pal, S. K., & Chakraborty, S. (2015). Heat transfer enhancement using air-atomized spray cooling with water–Al2O3 nanofluid. International Journal of Thermal Sciences, 96, 85–93. https://doi.org/10.1016/j.ijthermalsci.2015.04.012

Ravikumar, S. V., Jha, J. M., Mohapatra, S., Pal, S. K., & Chakraborty, S. (2013). Influence of ultrafast cooling on microstructure and mechanical properties of steel. Steel Research International, 84(11), 1157–1170. https://doi.org/10.1002/srin.201200346

Ravikumar, S. V., Jha, J. M., Mohapatra, S., Sinha, A., Pal, S. K., & Chakraborty, S. (2013). Experimental study of the effect of spray inclination on ultrafast cooling of a hot steel plate. Heat and Mass Transfer, 49(10), 1509–1522. https://doi.org/10.1007/s00231-013-1190-3

Ravikumar, S. V., Jha, J. M., Sarkar, I., Pal, S. K., & Chakraborty, S. (2014). Enhancement of heat transfer rate in air-atomized spray cooling of a hot steel plate by using an aqueous solution of non-ionic surfactant and ethanol. Applied Thermal Engineering, 64(1–2), 64–75. https://doi.org/10.1016/j.applthermaleng.2013.12.008

Ravikumar, S. V., Jha, J. M., Tiara, A., Pal, S. K., & Chakraborty, S. (2014). Experimental investigation of air-atomized spray with aqueous polymer additive for high heat flux applications. International Journal of Heat and Mass Transfer, 72, 362–377. https://doi.org/10.1016/j.ijheatmasstransfer.2014.01.024

Serajzadeh, S. (2003). Prediction of temperature distribution and phase transformation on the run-out table in the process of hot strip rolling. Applied Mathematical Modelling, 27(11), 861–875. https://doi.org/10.1016/s0307-904x(03)00085-4

Serajzadeh, S. (2004). Modelling of temperature history and phase transformations during cooling of steel. Journal of Materials Processing Technology, 146(3), 311–317. https://doi.org/10.1016/j.jmatprotec.2003.11.010

Serajzadeh, S. (2006). Prediction of temperature variations and kinetics of austenite phase change on the run-out table. Materials Science and Engineering: A, 421(1–2), 260–267. https://doi.org/10.1016/j.msea.2006.01.071

Sharma, A. K., & Sahu, S. K. (2019). The thermal and rewetting behavior of hot moving surface by water jet impingement. Applied Thermal Engineering, 159, 113950. https://doi.org/10.1016/j.applthermaleng.2019.113950

Suebsomran, A., & Butdee, S. (2013). Cooling process on a run-out table by the simulation method. Case Studies in Thermal Engineering, 1(1), 51–56. https://doi.org/10.1016/j.csite.2013.07.002

Sun, C. G., Han, H. N., Lee, J. K., Jin, Y., & Hwang, S. (2002). A finite element model for the prediction of thermal and metallurgical behavior of strip on run-out-table in hot rolling. Isij International, 42(4), 392–400. https://doi.org/10.2355/isijinternational.42.392

Suwanpinij, P., Prahl, U., Bleck, W., & Kawalla, R. (2012). Fast algorithms for phase transformations in dual phase steels on a hot strip mill run-out table (ROT). Archives of Civil and Mechanical Engineering, 12(3), 305–311. https://doi.org/10.1016/j.acme.2012.06.004

Tan, C., Ward, J., Wilcox, S. J., & Payne, R. (2009). Artificial neural network modelling of the thermal performance of a compact heat exchanger. Applied Thermal Engineering, 29(17–18), 3609–3617. https://doi.org/10.1016/j.applthermaleng.2009.06.017

Wang, X., Li, F., & Jiang, Z. (2012). Thermal, Microstructural and Mechanical Coupling Analysis Model for flatness Change Prediction during Run-Out Table cooling in hot strip rolling. Journal of Iron and Steel Research International, 19(9), 43–51. https://doi.org/10.1016/s1006-706x(13)60007-2

Wang, X., Li, F., Yang, Q., & He, A. (2013). FEM analysis for residual stress prediction in hot rolled steel strip during the run-out table cooling. Applied Mathematical Modelling, 37(1–2), 586–609. https://doi.org/10.1016/j.apm.2012.02.042

Wang, X., Yang, Q., & He, A. (2008). Calculation of thermal stress affecting strip flatness change during run-out table cooling in hot steel strip rolling. Journal of Materials Processing Technology, 207(1–3), 130–146. https://doi.org/10.1016/j.jmatprotec.2007.12.076

Weisz-Patrault, D., & Koedinger, T. (2018). Residual stress on the run out table accounting for multiphase transitions and transformation induced plasticity. Applied Mathematical Modelling, 60, 18–33. https://doi.org/10.1016/j.apm.2018.02.026

Wu, H., Sun, J., Lü, X., Wen, P., Wang, Q., & Zhang, D. (2022). Predicting stress and flatness in hot-rolled strips during run-out table cooling. Journal of Manufacturing Processes, 84, 815–831. https://doi.org/10.1016/j.jmapro.2022.10.053

Wiranto, G., Lubis, S. Y., & Rosehan, N. Multiple linear regression analysis on effect of time variations and voltage variations on spot welding against shear strength of AA5083 material using IBM SPSS application. IOP Conference Series Materials Science and Engineering 2020; 1007(1), 012062.

Xie, G., Wang, Q., Zeng, M., & Luo, L. Q. (2007). Heat transfer analysis for shell-and-tube heat exchangers with experimental data by artificial neural networks approach. Applied Thermal Engineering, 27(5–6), 1096–1104. https://doi.org/10.1016/j.applthermaleng.2006.07.036

Xie, H., Jiang, Z., Liu, X., Wang, G., & Tieu, A. K. (2006). Prediction of coiling temperature on run-out table of hot strip mill using data mining. Journal of Materials Processing Technology, 177(1–3), 121–125. https://doi.org/10.1016/j.jmatprotec.2006.04.089

Yuasa, Y., Yamane, T., Saitô, M., Yoshino, M., Miyai, Y., & Shimizu, R. (1990). New temperature control system for hot strip mill run out table. IFAC Proceedings Volumes, 23(8), 143–148. https://doi.org/10.1016/s1474-6670(17)51410-x

Zhao, Y., Huang, X., Yu, B., Yuan, X., & Li, X. (2017). Effect of coiling temperature on microstructure, properties and resistance to Fish-Scaling of hot rolled enamel steel. Materials, 10(9), 1012. https://doi.org/10.3390/ma10091012

Zhou, Z. Q., Thomson, P. F., Lam, Y. C., & Yuen, D. D. (2003). Numerical analysis of residual stress in hot-rolled steel strip on the run-out table. Journal of Materials Processing Technology, 132(1–3), 184–197. https://doi.org/10.1016/s0924-0136(02)00850-6

Prabir Biswas
01/07.26